DISSERTATION

EVIDENCE FOR ACUTE INFLAMMATION IN THE PATHOGENESIS OF DIFFERENT MOUSE MODELS OF POST-TRAUMATIC OSTEOARTHRITIS

Submitted by

Ariel E Timkovich

Department of Microbiology, Immunology, and Pathology

In partial fulfillment of the requirements

For the Degree of Doctor of Philosophy

Colorado State University

Fort Collins, Colorado

Fall 2022

Doctoral Committee:

Advisor: Kelly Santangelo

Christine Olver
Julie Moreno
Laurie Goodrich

ABSTRACT

EVIDENCE FOR ACUTE INFLAMMATION IN THE PATHOGENESIS OF DIFFERENT MOUSE MODELS OF POST-TRAUMATIC OSTEOARTHRITIS

Post-traumatic osteoarthritis (PTOA) is a debilitating, degenerative condition affecting more than 5.6 million people in the United States. Following injury to the knee, a person is 4.2 times more likely to develop PTOA in that joint, compared to an uninjured joint. PTOA is characterized by clinical symptoms such as pain, swelling, and decreased range of motion of the knee or affected joint. As a leading cause of pain and disability, PTOA is a major contributor to a decreased quality of life. Notably, loss of mobility associated with PTOA can increase the risk of a multitude of other ailments including heart disease and diabetes.

PTOA due to traumatic joint injury can result in damage to intra-articular structures, such as menisci, ligaments, cartilage, and subchondral bone. Despite current treatment options, many of these joint injuries progress to end-stage PTOA within 10 to 20 years. Rupture of the most commonly injured knee ligament, the anterior cruciate ligament (ACL), typically occurs in athletes and people who are physically active, with the majority of ACL tears occurring in patients who are less than 30 years old. The detrimental pathways driving PTOA remain loosely defined and little progress has been made in predicting, preventing, and treating the disease.

The goal of this work was to further our understanding of PTOA mouse models through both development and characterization of models, as well as through the

testing of therapeutics in pre-established PTOA mouse models. In the first part of this work (Chapter 2), we created and characterized a novel full and partial ACL rupture model. This work is the first published partial ACL rupture model to date and provides a novel platform to use as a preclinical model for testing of potential therapeutics and to further our understanding of PTOA following ACL rupture.

Chapter 3 evaluates the therapeutic potential of a toll-like receptor 4 (TLR4) antagonist on a full depth PTOA model. We found that short term treatment with a systemic TLR4 antagonist significantly improved relevant gait parameters, and improved cartilage structural metrics and modified Mankin PTOA scores, implying improvement of clinical signs.

Chapter 4 addresses the therapeutic potential of intra-articular bone marrow aspirate concentrate (BMAC), for treatment of PTOA in a well characterized meniscus degeneration model, compared to red blood cell (RBC) depleted BMAC or no injection controls. These results suggest that RBC-depleted BMAC improved treatment of PTOA in an animal model and may have translational therapeutic potential for humans suffering from similar disease processes.

Finally, Chapter 5 sought to: (1) Identify transcriptional sex differences in knee joint tissue from naïve animals; and (2) Identify compensatory gene expression changes related to sex that are specific to animals receiving DMM surgery as compared to a naïve animal when taking into account surgery changes (i.e., sham surgery).

The work described in this dissertation has improved our understanding of the mouse knee joint during PTOA progression and potential therapeutics and targets for clinical treatment of PTOA.

ACKNOWLEDGEMENTS

It’s hard to believe that I’ve finally made it to this milestone, which has always seemed so far off. I wouldn’t be here if not for the guidance and support of so many, and I apologize in advance that I won’t remember everyone to thank. First, thank you Mom and Dad for supporting me through the highs and lows, all the trips to Fort Collins and back, and always being there when I needed some encouragement or to vent. Dr. Kelly Santangelo has been with me for this entire journey, from being my undergraduate advisor when I first started at CSU, to taking me back as her graduate student after a year away at the University of Texas. Her mentorship and guidance have enabled me to be successful and I’ve learned so much from the example and standards she set. Thanks to my roommate and fellow PhD student Emily “Fitz” Fitzmeyer and her trusted feline Chloe for forcing me to take Netflix breaks and reminding me that there is more to life than just graduate school. Along those same lines, thanks to all the wonderful equestrians at The Great Escape and Windfall Equestrian, who have watched me learn with my first horse Ozzie and now push me to excel with my future big show jumper, Marvin. I also need to give a special thanks to my “dad’s” two cats, Peach, and Schnapps, who have been waking me up every morning for the past several weeks so that I could finish my dissertation. Thanks to Dr. Katie Sikes for being there to help me with my project and answering so many questions. And, finally, thanks to the bestest dog in the whole wide world, Shadow the wonder puppy, for always being so happy to see me, for all the cuddles, and for making me smile no matter what.

TABLE OF CONTENTS

LIST OF TABLES

LIST OF FIGURES

Chapter 1: Introduction

1.1 Importance of Osteoarthritis

Osteoarthritis (OA), particularly of the knee, is a leading cause of physical disability worldwide and a major reason for a decreased quality of life[1]. Additionally, OA is the most common joint disorder both in the United States of America and around the world[2], with estimates suggesting that at least 250 million people are affected[3]. This multifaceted and heterogeneous disease has a wide array of underlying pathways that lead to joint destruction[4], and is commonly characterized by joint space narrowing, inflammation and loss of articular cartilage[5].

Osteoarthritis is commonly categorized into two categories, primary OA and post-traumatic (also known as secondary) OA. Primary OA has no known causal event and is often referred to as spontaneous or idiopathic OA[6]. Post-traumatic OA (PTOA) occurs following traumatic injury to the joint and is believed to account for approximately 12% of all symptomatic OA cases[7], with weight bearing joints, such as the knee, being most at risk[8]. Chronic changes seen are similar between primary OA and PTOA, with PTOA having an explicit inciting incident[9]. Primary OA tends to effect older individuals while PTOA is commonly seen in younger populations, athletes, and military personnel[9,10].

Pain and loss of mobility are the major complaints from people suffering from PTOA[3]. To date, there is no cure for this disease, which highlights a critical need for novel therapies to mitigate the progression of pathology of OA after injury. Current treatments for PTOA, such as nonsteroidal anti-inflammatory drugs (NSAIDs) and corticosteroids, do not change the progression of the disease but help to alleviate

symptoms. Unfortunately, long-term administration of these drugs is associated with severe adverse side effects[11]. Therefore, there is a critical need to understand and utilize animal models to further our understanding of PTOA and for development of future therapeutics to treat PTOA.

It is believed that PTOA occurs in 21% of patients that receive an ACL transection injury, with that number increasing to 48% with accompanying meniscal injury[12]. Importantly, most ACL tears occur in patients who are <30 years old, with many <20 years[13]. Surgical reconstruction of the ACL is the gold standard treatment; however, re-injury and/or contralateral ACL rupture may still occur. Collectively, these complications result in decreased mobility and quality of life. As disease-modifying therapies are lacking, understanding the relationship between PTOA initiation post-ACL rupture using clinically relevant models is paramount for developing intervention strategies to mitigate injury progression.

A variety of animal models exist to study PTOA including mice, rats, rabbits, guinea pigs, dogs, pigs, and horses[14]. Mice are a common animal model to study OA as their musculoskeletal system develops quickly[15,16], which allows for animals to be raised and tested on in a short period of time. Additionally, mice are a relatively cheap animal model and are commonly used as a first line of testing for drugs and other therapeutics testing[14].

Mouse models of PTOA are typically grouped into two categories: induced (invasive) models and non-invasive models[17], which will be described in depth later and are laid out visually in **Figure 1.1**.

1.2 Surgically Induced Models of PTOA

Induced models of PTOA are often initiated through surgery and were initially developed to study therapeutic effects on the PTOA disease process as this causes rapid induction of joint degeneration and studies can therefore be completed in shorter timeframes. Surgically induced models of PTOA can be highly advantageous as they are reproducible based on expertise, progress rapidly and can be easily used to cause a specific lesion. Conversely, some disadvantages to surgically induced models are they require highly trained personnel, they allow additional blood into the joint and often require opening the joint capsule which may upset the natural environment[6]. Additionally, as with any surgery, there is an increased risk of infection and the type of injury induced is not fully applicable to human injury, as OA in human patients typically is not induced through surgery.

A large variety of surgically induced models exist in mice and can be induced in a variety of ways including: meniscal injury, medial and/or collateral ligament injury, transection of the cruciate ligament (anterior or posterior), patellectomy and articular groove[18]. One of the first surgical models was the ACL transection model (ACLT), which was first described in dogs in 1973[19]. Following the development of this model it has subsequently been utilized and described in dogs, rats, rabbits, cats, guinea pigs, sheep and mice[6].

Another commonly utilized model for induction of surgical PTOA involves the partial or total removal of the medial meniscus. Additionally, ACLT and meniscectomy have been combined, to view an injury combination seen commonly clinically[20,21]. Destabilization of the medial meniscus (DMM) is one of the most common surgical

mouse models for studying PTOA in mice. Results from this model tend to be reproducible and generate similar results within male animals[5]. Interestingly, male mice develop PTOA more severely and consistently within the DMM model than female mice[22].

A variety of other surgical defect models also exist for study, including the joint surface defect model. This model was developed because following arthroscopic procedures, joint surface defects are seen in 60% of cases and have been associated with cartilage loss leading to PTOA progression[23]. These models are often utilized as a method to study joint surface restoration. Importantly, large animal joint surface defect models have demonstrated spontaneous repair[24-26]. This implies there may be intrinsic repair methods which can help repair full surface cartilage defects and if we understood the cellular and molecular mechanisms behind this repair they could potentially be harnessed as a treatment for PTOA.

1.3 Chemically Induced Models of PTOA

Another subset of induced/invasive models of PTOA are those that are induced through injection of a degrative agent into the joint system. These models involve the injection of a chemical agent intra-articularly into the joint space. A variety of chemicals have been utilized including monosodium iodoacetate (MIA)[27,28], papain[29], collagenase[30], and quinolone, along with cytokines such as tumor necrosis factor (TNF)[31], transforming growth factor β, and interleukin-1. These methods can be advantageous for studying joint changes following a specific biological process but are

questionably translational to human injury and therefore information gathered through these methods may only be relevant in very specific circumstances.

1.4 Non-invasive models of PTOA

Non-invasive models of PTOA utilize a mechanical force that produce an external insult to the joint of study which negates the need of surgical or chemical induction. These models are advantageous as they have rapid induction, are consistent within a laboratory, are clinically relevant to human injury and do not require surgical expertise to perform. The major cons to this induction method are that the equipment to produce the injury is not universally available and, within the literature, there is variability in injury induction. A variety of non-invasive mechanical models of PTOA have been developed and can be used to study specific aspects of human injury including cartilage damage, bone fracture, or soft tissue rupture.

1.5 Intra-articular tibial plateau fracture

The earliest non-invasive mouse model is the intra-articular tibial plateau fracture (IATPF) model[32]. This model initiates injury through an indenter which adds force to the knee and causes a closed fracture of the joint. Importantly, the amount of force applied by the indenter can be modified to modulate the severity of joint changes and the severity of lesions[17]. The injury generated in this model can be representative of acute injuries occurred during high-energy impact injuries, such as during an automobile accident[6]. As such, it is an ideal model for studying pathological changes following

acute injury and can be used to follow the early inflammatory effects of PTOA[33]. The fracture creating success rates with this model are anywhere from 87%[32] to 95%[33].

1.6 Cyclic articular cartilage tibial compression

The cyclic articular cartilage tibial compression (CACTC) model cyclically applies an axial load through the ankle and knee joint and produces articular cartilage lesions[34]. This model is highly advantageous for the study of chronic overuse injury and subsequent PTOA development[17]. Joint damage has also been shown to increase with longer duration of loading[35]. While this model typically utilizes many cycles periodically over a series of weeks, a study demonstrated that after a single session mice demonstrated acute injury pathology consistent with severe injury[36]. The highly adjustable nature of the CACTC model is a major benefit of this model as the severity of subsequent joint degradation can be controlled[6]. Importantly, joint degradation achieved with this model is typically mild when there is no confounding ligament injury. To attempt to achieve severe OA progression limbs must be loaded with a high force for several weeks and is therefore highly time consuming. Interestingly, a recent study found that low level cyclical loading of knees that underwent DMM surgery, attenuated DMM-induced cartilage degradation, and osteophyte formation[37]. This implies that there may be an amount of cyclical repeated movement following injury that improves knee health and repair, but overuse of the knee, either following injury or with a healthy joint, could increase or cause OA progression.

1.7 Tibial compression overload

The mechanical tibial compression overload model, which was first described for use in rabbits[38] and then subsequently for use in mice[39], creates an acute injury in mice by rupturing the anterior cruciate ligament (ACL). These models aim to create an injury seen clinically, though can result in divergence of ACL rupture locations, either mid-substance or an avulsion fracture. Notably, the majority of ACL injuries in humans involve a mid-substance tear rather than an avulsion fracture; the latter is usually observed in children/adolescents with immature bone[40]. Additionally, loads obtained from published mechanical models differ (range 3N-12N[34,39,41-44]) and demonstrate relatively rapid PTOA progression, with histologic evidence of PTOA as early as 7 days post injury[39].

It is important to note that the age of mice at time of tibial displacement may play a role in the ability to achieve a mid-substance ACL rupture versus an avulsion fracture. Historically, mice at time of rupture are typically 8[34], 10[39,42], 12[43], or 16 weeks[44] of age. Importantly, age, sex, and weight have all been shown to effect avulsion fractures and mid-substance tear success rates in an alternate non-surgical ACL injury model[45]. As age and skeletal maturity at time of injury may affect rupture outcomes, future studies should consider these factors more overtly in study design.

Additionally, most current ACL rupture models exclusively produce a full rupture; of note, partial ACL ruptures account for 10-27% of total injuries clinically, and treatment of partial ACL rupture can differ from that of a full rupture[46]. Recently a mechanical partial ACL rupture model was developed[47], which will provide an important model for

the study of partial ACL tear progression to full rupture and testing of therapeutics following a partial rupture.

1.8 Considerations of the contralateral limb

Many PTOA mouse models focus exclusively on the injured limb. As such, clinical considerations, and treatment primarily – and understandably – focus on the injured limb, with relatively little attention given to the compensatory leg. Interestingly, mouse models of PTOA have utilized the contralateral limb in a variety of ways, including naïve internal controls, sham surgery internal controls, or bilateral surgery. To date, comprehensive evaluations of contralateral limb changes following knee injury have been minimally investigated in animal models of PTOA. Importantly, systemic inflammatory and bone turnover exists following injury[39,48], and may ultimately confound results when the contralateral limb is used as the control. Interestingly, human ACL rupture patients showed elevated concentrations of aggrecan, cartilage oligomeric matrix protein (COMP) fragments, stromelysin-1 also known as matrix metalloproteinase-3 (MMP-3) in the contralateral uninjured limb immediately after injury when compared to healthy controls[49]. Additionally, following total joint replacement, a marker of end stage OA, the contralateral lower extremity is at an elevated risk of joint degeneration and subsequent total joint replacement[50-52]. This increased risk may be due to nonstandard joint loading, a known cause of OA initiation, which may promote quicker joint degradation[53-55]. Importantly, it has been shown that excessive loads on cartilage can cause structural deterioration[56], though biomechanical changes alone may not be the driving cause of contralateral OA progression[57]. For this reason, chapter 5 of

this dissertation aims to characterize inflammatory gene changes in the contralateral knees of mice following DMM surgery.

1.9 Conclusions

When designing a study, model choice and limb controls should be evaluated to determine the appropriate choice to answer the overarching study questions. Non-invasive mouse models are a major step forward in the study of PTOA. These models are able to initiate the progression of PTOA without the confounding factor of interrupting the joint capsule, and as such are more closely representative of human injuries[6]. Further research still needs to be conducted before we can truly translate novel insights from these non-invasive mouse PTOA models to human disease and treatments. Investigators of future studies should be conscious of inherent sex difference and biological differences between male and female animals and should design their studies to reflect that. Additionally, when selecting/designating use of contralateral controls for mouse PTOA studies, the potential for compensatory limb changes should be carefully considered during conceptualization of the experimental design.

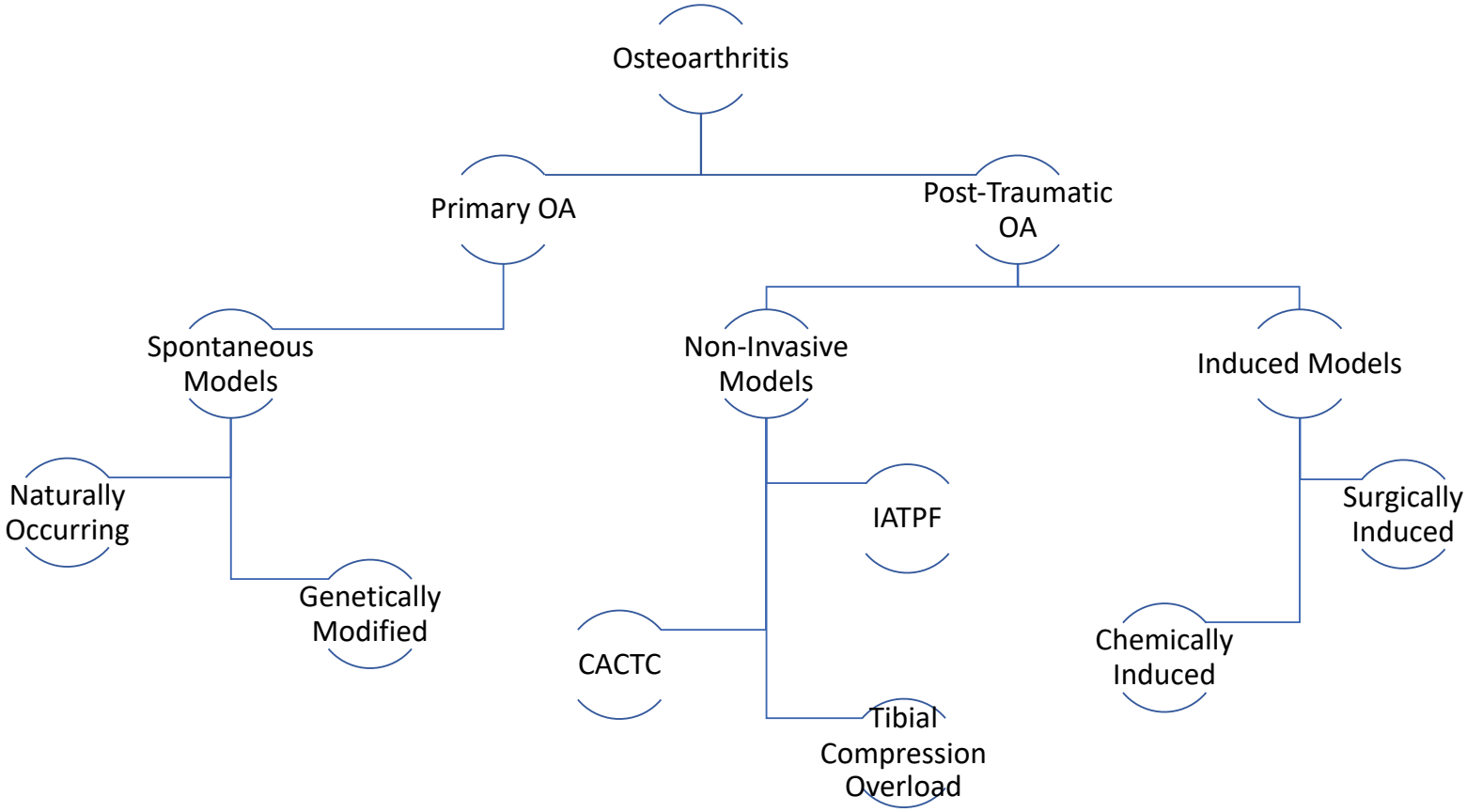

Figure 1.1 Classification of osteoarthritis mouse models with a subset of examples. *OA* osteoarthritis, *IATPF* intra-articular tibial plateau fracture, *CACTC* cyclic articular cartilage tibial compression. Figure adapted from Kuyinu *et al*. (2016)[17].

1.10 References

1. March L, Smith EU, Hoy DG, et al. Burden of disability due to musculoskeletal (MSK) disorders. *Best Pract Res Clin Rheumatol*. Jun 2014;28(3):353-66. doi:10.1016/j.berh.2014.08.002

2. Felson DT. Epidemiology of hip and knee osteoarthritis. *Epidemiol Rev*. 1988;10:1-28. doi:10.1093/oxfordjournals.epirev.a036019

3. Hunter DJ, Bierma-Zeinstra S. Osteoarthritis. *Lancet*. 04 27 2019;393(10182):1745-1759. doi:10.1016/S0140-6736(19)30417-9

4. Deveza LA, Loeser RF. Is osteoarthritis one disease or a collection of many? *Rheumatology (Oxford)*. 05 01 2018;57(suppl_4):iv34-iv42. doi:10.1093/rheumatology/kex417

5. Glasson SS, Blanchet TJ, Morris EA. The surgical destabilization of the medial meniscus (DMM) model of osteoarthritis in the 129/SvEv mouse. *Osteoarthritis Cartilage*. Sep 2007;15(9):1061-9. doi:10.1016/j.joca.2007.03.006

6. Christiansen BA, Guilak F, Lockwood KA, et al. Non-invasive mouse models of post-traumatic osteoarthritis. *Osteoarthritis Cartilage*. Oct 2015;23(10):1627-38. doi:10.1016/j.joca.2015.05.009

7. Jiménez G, Cobo-Molinos J, Antich C, López-Ruiz E. Osteoarthritis: Trauma vs Disease. *Adv Exp Med Biol*. 2018;1059:63-83. doi:10.1007/978-3-319-76735-2_3

8. He Y, Li Z, Alexander PG, et al. Pathogenesis of Osteoarthritis: Risk Factors, Regulatory Pathways in Chondrocytes, and Experimental Models. *Biology (Basel)*. Jul 29 2020;9(8)doi:10.3390/biology9080194

9. Punzi L, Galozzi P, Luisetto R, et al. Post-traumatic arthritis: overview on pathogenic mechanisms and role of inflammation. *RMD Open*. 2016;2(2):e000279. doi:10.1136/rmdopen-2016-000279

10. Brown TD, Johnston RC, Saltzman CL, Marsh JL, Buckwalter JA. Posttraumatic osteoarthritis: a first estimate of incidence, prevalence, and burden of disease. *J Orthop Trauma*. 2006 Nov-Dec 2006;20(10):739-44. doi:10.1097/01.bot.0000246468.80635.ef

11. Gómez R, Villalvilla A, Largo R, Gualillo O, Herrero-Beaumont G. TLR4 signalling in osteoarthritis--finding targets for candidate DMOADs. *Nat Rev Rheumatol*. Mar 2015;11(3):159-70. doi:10.1038/nrrheum.2014.209

12. Thomas AC, Hubbard-Turner T, Wikstrom EA, Palmieri-Smith RM. Epidemiology of Posttraumatic Osteoarthritis. *J Athl Train*. Jun 2017;52(6):491-496. doi:10.4085/1062-6050-51.5.08

13. Lohmander LS, Englund PM, Dahl LL, Roos EM. The long-term consequence of anterior cruciate ligament and meniscus injuries: osteoarthritis. *Am J Sports Med*. Oct 2007;35(10):1756-69. doi:10.1177/0363546507307396

14. Bapat S, Hubbard D, Munjal A, Hunter M, Fulzele S. Pros and cons of mouse models for studying osteoarthritis. *Clin Transl Med*. Nov 21 2018;7(1):36. doi:10.1186/s40169-018-0215-4

15. Lorenz J, Grässel S. Experimental osteoarthritis models in mice. *Methods Mol Biol*. 2014;1194:401-19. doi:10.1007/978-1-4939-1215-5_23

16. Malfait AM, Little CB. On the predictive utility of animal models of osteoarthritis. *Arthritis Res Ther*. Sep 14 2015;17:225. doi:10.1186/s13075-015-0747-6

17. Kuyinu EL, Narayanan G, Nair LS, Laurencin CT. Animal models of osteoarthritis: classification, update, and measurement of outcomes. *J Orthop Surg Res*. Feb 02 2016;11:19. doi:10.1186/s13018-016-0346-5

18. Lampropoulou-Adamidou K, Lelovas P, Karadimas EV, et al. Useful animal models for the research of osteoarthritis. *Eur J Orthop Surg Traumatol*. Apr 2014;24(3):263-71. doi:10.1007/s00590-013-1205-2

19. Pond MJ, Nuki G. Experimentally-induced osteoarthritis in the dog. *Ann Rheum Dis*. Jul 1973;32(4):387-8. doi:10.1136/ard.32.4.387

20. Kamekura S, Hoshi K, Shimoaka T, et al. Osteoarthritis development in novel experimental mouse models induced by knee joint instability. *Osteoarthritis Cartilage*. Jul 2005;13(7):632-41. doi:10.1016/j.joca.2005.03.004

21. Karahan S, Kincaid SA, Kammermann JR, Wright JC. Evaluation of the rat stifle joint after transection of the cranial cruciate ligament and partial medial meniscectomy. *Comp Med*. Dec 2001;51(6):504-12.

22. Ma HL, Blanchet TJ, Peluso D, Hopkins B, Morris EA, Glasson SS. Osteoarthritis severity is sex dependent in a surgical mouse model. *Osteoarthritis Cartilage*. Jun 2007;15(6):695-700. doi:10.1016/j.joca.2006.11.005

23. Hjelle K, Solheim E, Strand T, Muri R, Brittberg M. Articular cartilage defects in 1,000 knee arthroscopies. *Arthroscopy*. Sep 2002;18(7):730-4. doi:10.1053/jars.2002.32839

24. Breinan HA, Hsu HP, Spector M. Chondral defects in animal models: effects of selected repair procedures in canines. *Clin Orthop Relat Res*. Oct 2001;(391 Suppl):S219-30.

25. Convery FR, Akeson WH, Keown GH. The repair of large osteochondral defects. An experimental study in horses. *Clin Orthop Relat Res*. 1972 Jan-Feb 1972;82:253-62.

26. Shapiro F, Koide S, Glimcher MJ. Cell origin and differentiation in the repair of full-thickness defects of articular cartilage. *J Bone Joint Surg Am*. Apr 1993;75(4):532-53. doi:10.2106/00004623-199304000-00009

27. Barve RA, Minnerly JC, Weiss DJ, et al. Transcriptional profiling and pathway analysis of monosodium iodoacetate-induced experimental osteoarthritis in rats: relevance to human disease. *Osteoarthritis Cartilage*. Oct 2007;15(10):1190-8. doi:10.1016/j.joca.2007.03.014

28. Ogbonna AC, Clark AK, Gentry C, Hobbs C, Malcangio M. Pain-like behaviour and spinal changes in the monosodium iodoacetate model of osteoarthritis in C57Bl/6 mice. *Eur J Pain*. Apr 2013;17(4):514-26. doi:10.1002/j.1532-2149.2012.00223.x

29. Marcelon G, Cros J, Guiraud R. Activity of anti-inflammatory drugs on an experimental model of osteoarthritis. *Agents Actions*. Feb 1976;6(1-3):191-4. doi:10.1007/BF01972207

30. van Osch GJ, van der Kraan PM, Vitters EL, Blankevoort L, van den Berg WB. Induction of osteoarthritis by intra-articular injection of collagenase in mice. Strain and sex related differences. *Osteoarthritis Cartilage*. Jul 1993;1(3):171-7. doi:10.1016/s1063-4584(05)80088-3

31. Malfait AM, Tortorella M, Thompson J, et al. Intra-articular injection of tumor necrosis factor-alpha in the rat: an acute and reversible in vivo model of cartilage proteoglycan degradation. *Osteoarthritis Cartilage*. May 2009;17(5):627-35. doi:10.1016/j.joca.2008.10.005

32. Furman BD, Strand J, Hembree WC, Ward BD, Guilak F, Olson SA. Joint degeneration following closed intraarticular fracture in the mouse knee: a model of posttraumatic arthritis. *J Orthop Res*. May 2007;25(5):578-92. doi:10.1002/jor.20331

33. Lewis JS, Hembree WC, Furman BD, et al. Acute joint pathology and synovial inflammation is associated with increased intra-articular fracture severity in the mouse knee. *Osteoarthritis Cartilage*. Jul 2011;19(7):864-73. doi:10.1016/j.joca.2011.04.011

34. Poulet B, Hamilton RW, Shefelbine S, Pitsillides AA. Characterizing a novel and adjustable noninvasive murine joint loading model. *Arthritis Rheum*. Jan 2011;63(1):137-47. doi:10.1002/art.27765

35. Ko FC, Dragomir C, Plumb DA, et al. In vivo cyclic compression causes cartilage degeneration and subchondral bone changes in mouse tibiae. *Arthritis Rheum*. Jun 2013;65(6):1569-78. doi:10.1002/art.37906

36. Wu P, Holguin N, Silva MJ, Fu M, Liao W, Sandell LJ. Early response of mouse joint tissue to noninvasive knee injury suggests treatment targets. *Arthritis Rheumatol*. May 2014;66(5):1256-65. doi:10.1002/art.38375

37. Holyoak DT, Chlebek C, Kim MJ, Wright TM, Otero M, van der Meulen MCH. Low-level cyclic tibial compression attenuates early osteoarthritis progression after joint injury in mice. *Osteoarthritis Cartilage*. 10 2019;27(10):1526-1536. doi:10.1016/j.joca.2019.06.005

38. Killian ML, Isaac DI, Haut RC, Déjardin LM, Leetun D, Donahue TL. Traumatic anterior cruciate ligament tear and its implications on meniscal degradation: a preliminary novel lapine osteoarthritis model. *J Surg Res*. Dec 2010;164(2):234-41. doi:10.1016/j.jss.2009.03.006

39. Christiansen BA, Anderson MJ, Lee CA, Williams JC, Yik JH, Haudenschild DR. Musculoskeletal changes following non-invasive knee injury using a novel mouse model of post-traumatic osteoarthritis. *Osteoarthritis Cartilage*. Jul 2012;20(7):773-82. doi:10.1016/j.joca.2012.04.014

40. Bengtson H, Giangarra C. Osteochondral avulsion fracture of the anterior cruciate ligament femoral origin in a 10-year-old child: a case report. *J Athl Train*. 2011 Jul-Aug 2011;46(4):451-5. doi:10.4085/1062-6050-46.4.451

41. Duan X, Rai MF, Holguin N, et al. Early changes in the knee of healer and non-healer mice following non-invasive mechanical injury. *J Orthop Res*. 03 2017;35(3):524-536. doi:10.1002/jor.23413

42. Lockwood KA, Chu BT, Anderson MJ, Haudenschild DR, Christiansen BA. Comparison of loading rate-dependent injury modes in a murine model of post-traumatic osteoarthritis. *J Orthop Res*. Jan 2014;32(1):79-88. doi:10.1002/jor.22480

43. Gilbert SJ, Bonnet CS, Stadnik P, Duance VC, Mason DJ, Blain EJ. Inflammatory and degenerative phases resulting from anterior cruciate rupture in a non-invasive murine model of post-traumatic osteoarthritis. *J Orthop Res*. Feb 2018;doi:10.1002/jor.23872

44. Chang JC, Sebastian A, Murugesh DK, et al. Global molecular changes in a tibial compression induced ACL rupture model of post-traumatic osteoarthritis. *J Orthop Res*. Mar 2017;35(3):474-485. doi:10.1002/jor.23263

45. Blaker CL, Little CB, Clarke EC. Joint loads resulting in ACL rupture: Effects of age, sex, and body mass on injury load and mode of failure in a mouse model. *J Orthop Res*. 08 2017;35(8):1754-1763. doi:10.1002/jor.23418

46. Temponi EF, de Carvalho Júnior LH, Sonnery-Cottet B, Chambat P. Partial tearing of the anterior cruciate ligament: diagnosis and treatment. *Rev Bras Ortop*. 2015 Jan-Feb 2015;50(1):9-15. doi:10.1016/j.rboe.2015.02.003

47. Timkovich AE, Sikes KJ, Andrie KM, et al. Full and Partial Mid-substance ACL Rupture Using Mechanical Tibial Displacement in Male and Female Mice. *Ann Biomed Eng*. Sep 07 2022;doi:10.1007/s10439-022-03065-1

48. Satkunananthan PB, Anderson MJ, De Jesus NM, Haudenschild DR, Ripplinger CM, Christiansen BA. In vivo fluorescence reflectance imaging of protease activity in a mouse model of post-traumatic osteoarthritis. *Osteoarthritis Cartilage*. Oct 2014;22(10):1461-9. doi:10.1016/j.joca.2014.07.011

49. Dahlberg L, Roos H, Saxne T, et al. Cartilage metabolism in the injured and uninjured knee of the same patient. *Ann Rheum Dis*. Dec 1994;53(12):823-7. doi:10.1136/ard.53.12.823

50. Shakoor N, Block JA, Shott S, Case JP. Nonrandom evolution of end-stage osteoarthritis of the lower limbs. *Arthritis Rheum*. Dec 2002;46(12):3185-9. doi:10.1002/art.10649

51. Sayeed SA, Trousdale RT, Barnes SA, Kaufman KR, Pagnano MW. Joint arthroplasty within 10 years after primary charnley total hip arthroplasty. *Am J Orthop (Belle Mead NJ)*. Aug 2009;38(8):E141-3.

52. Husted H, Overgaard S, Laursen JO, et al. Need for bilateral arthroplasty for coxarthrosis. 1,477 replacements in 1,199 patients followed for 0-14 years. *Acta Orthop Scand*. Oct 1996;67(5):421-3. doi:10.3109/17453679608996660

53. Andriacchi TP, Mündermann A. The role of ambulatory mechanics in the initiation and progression of knee osteoarthritis. *Curr Opin Rheumatol*. Sep 2006;18(5):514-8. doi:10.1097/01.bor.0000240365.16842.4e

54. Wilson DR, McWalter EJ, Johnston JD. The measurement of joint mechanics and their role in osteoarthritis genesis and progression. *Rheum Dis Clin North Am*. Aug 2008;34(3):605-22. doi:10.1016/j.rdc.2008.05.002

55. Foucher KC, Wimmer MA. Contralateral hip and knee gait biomechanics are unchanged by total hip replacement for unilateral hip osteoarthritis. *Gait Posture*. Jan 2012;35(1):61-5. doi:10.1016/j.gaitpost.2011.08.006

56. Maly MR, Acker SM, Totterman S, et al. Knee adduction moment relates to medial femoral and tibial cartilage morphology in clinical knee osteoarthritis. *J Biomech*. Sep 18 2015;48(12):3495-501. doi:10.1016/j.jbiomech.2015.04.039

57. Aljehani MS, Christensen JC, Snyder-Mackler L, Crenshaw J, Brown A, Zeni JA. Knee biomechanics and contralateral knee osteoarthritis progression after total knee arthroplasty. *Gait Posture*. 01 2022;91:266-275. doi:10.1016/j.gaitpost.2021.10.020

Chapter 2: Full and Partial Mid-substance ACL Rupture using Mechanical Tibial Displacement in Male and Female Mice[1]

2.1 Overview

The anterior cruciate ligament (ACL) is the most commonly injured knee ligament. Surgical reconstruction is the gold standard treatment for ACL ruptures, but 20-50% of patients develop post-traumatic osteoarthritis (PTOA). ACL rupture is thus a well-recognized etiology of PTOA; however, little is known about the initial relationship between ligamentous injury and subsequent PTOA. The goals of this project were to: (1) develop both partial and full models of mid-substance ACL rupture in male and female mice using non-invasive mechanical methods by means of tibial displacement; and (2) to characterize early PTOA changes in the full ACL rupture model. A custom material testing system was utilized to induce either partial or full ACL rupture by means of tibial displacement at 1.6 or 2.0mm, respectively. Mice were euthanized either (i) immediately post-injury to determine rupture success rates or (ii) 14 days post-injury to evaluate early PTOA progression following full ACL rupture. Our models demonstrated high efficacy in inciting either full or partial ACL rupture in male and female mice within the mid-substance of the ACL. These tools can be utilized for preclinical testing of potential therapeutics and to further our understanding of PTOA following ACL rupture.

[1] A version of this manuscript has been published in the Annals of Biomedical Engineering: Timkovich AE, Sikes KJ, Andrie KM, et al. Full and Partial Mid-substance ACL Rupture Using Mechanical Tibial Displacement in Male and Female Mice [published online ahead of print, 2022 Sep 7]. *Ann Biomed Eng*. 2022;10.1007/s10439-022-03065-1. doi:10.1007/s10439-022-03065-1

2.2 Introduction

The anterior cruciate ligament (ACL) is the most commonly injured knee ligament, with damage typically occurring in professionally or occupationally active patients[1,2]. Between 100,000 to 200,000 people in the United States are affected by ACL ruptures annually[3], with a 10-fold higher instance in military service members relative to the general population[4,5]. The majority of ACL tears occur in patients who are <30 years old, with many <20 years[6]. Surgical reconstruction of the ACL is the gold standard treatment; however, re-injury and/or contralateral ACL rupture may still occur. Further, 20-50% of patients develop post-traumatic osteoarthritis (PTOA). Indeed, after ACL rupture a person is 4.2 times more likely to develop PTOA in that knee[7,8]. Collectively, these complications result in decreased mobility and quality of life. As disease-modifying therapies are lacking, understanding the relationship between PTOA initiation post-ACL rupture using clinically relevant models is paramount for developing intervention strategies to mitigate injury progression.

Mouse models of PTOA associated with ACL rupture are typically grouped into two categories: induced (invasive) models and non-invasive models[9]. Induced models of ACL rupture are often initiated through surgery (e.g. manual ACL transection)[10]. Two disadvantages to surgically-induced models include: variability in disease progression post-operatively, which may be partially dictated by surgeon experience and technique; and compromise to the joint capsule during exposure, which adds compounding variables absent during a typical clinical injury[10]. Recently, researchers have utilized non-invasive models via custom-designed systems to cause injury through an applied

load[11-16]. Non-invasive models are advantageous as they are more reproducible, have minimal infection risks, and are more translatable to human injury.

Current non-invasive ACL rupture models in mice typically induce ACL rupture through tibial displacement. These models employ various mechanical methods to induce ACL injury (cyclic[12,13] vs. single compressive loading[11,14-16]) and can result in a divergence of rupture locations (mid-substance, avulsion fracture[11], or not reported[12-14,16]). Notably, the majority of ACL injuries in humans involve a mid-substance tear rather than an avulsion fracture; the latter is usually observed in children/adolescents with immature bone[17]. Loads obtained from published mechanical models differ (range 3N-12N[11-16]) and demonstrate relatively rapid PTOA progression, with histologic evidence of PTOA as early as 7 days post injury[11]. Further, these rupture models aim to incite full ACL ruptures. Interestingly, partial ACL tears have been observed in 10% to 27% of isolated ACL injuries, and thus should be considered during injury model development[18-20]. Finally, most ACL rupture models utilize male animals; however, in people, females have a higher prevalence of ACL ruptures[21,22]. Cumulatively, this highlights a need to study ACL rupture in both sexes and investigate if males and females differ in their injury rates and response to non-invasive ACL rupture.

The current study had two main goals. First, we sought to develop non-invasive ACL rupture models in male and female mice for both partial and full mid-substance tears such that future studies could recapitulate multiple scenarios. To our knowledge, this is the first non-invasive partial ACL rupture model. To ensure reproducible methods, we

hypothesized that preconditioning prior to ACL rupture would improve ACL rupture success rates. Additionally, we utilized output loading curves following injury induction to develop diagnostic capabilities in our model.

Second, we studied early PTOA progression following full ACL rupture. Specific features of our model that improved previous protocols included the use of a fixture to allow for overhang of the tibia relative to the femur, preconditioning, and application of a lower loading force. Given this, we anticipated that our models would result in less severe PTOA (relative to existing models of mouse mechanical tibial displacement) up to 14 days post-injury, as measured via animal movement and knee histopathology. Overall, our models can be used to further our understanding of mechanistic changes following full and partial ACL ruptures and allow for testing of therapeutics.

2.3 Materials and Methods

Animals

Procedures were approved by the University's Institutional Animal Care and Use Committee and were performed in accordance with the NIH Guide for the Care and Use of Laboratory Animals. C57BL/6Nci wild-type (WT) male and female mice were purchased from Charles River Laboratories (Wilmington, MA) at 63 days of age and allowed to acclimate for 21 days prior to experimentation. Thus, animals were 12 weeks old at time of injury for historical data comparability[15]. Animals were housed together by sex in groups of five in solid bottom cages with corncob bedding and allowed ad libitum

water and standard rodent chow. They were maintained at 22–24°C on a 12-h light/dark cycle and were assessed daily with body weights monitored weekly.

Experimental Design

Seventy mice were used for this study **(Figure 2.1)** and were split into two experimental phases – (1) Phase 1: ACL Rupture Model Development and (2) Phase 2: Early PTOA Progression. Phase 1 utilized 40 mice that were randomly assigned to receive either pre-conditioning or no pre-conditioning to induce tibial displacement. Following pre-conditioning, or lack thereof, one limb of each animal was randomly assigned to receive either 1.6mm displacement or 2.0mm displacement to incite a partial mid-substance ACL rupture or a full mid-substance ACL rupture, respectively; the contralateral limb received the alternative option. Animals were immediately euthanized following injury induction via CO_2 inhalation with confirmatory cervical dislocation. Following euthanasia, both legs received a manual cranial drawer test and were also macroscopically imaged and assessed for ACL status.

Phase 2 utilized 30 mice to evaluate early PTOA progression using the full ACL rupture protocol: the right limb of all animals received preconditioning followed by 2.0mm of tibial displacement to incite a full rupture. The left limb remained as an unmanipulated contralateral sham. All mice received a subcutaneous injection of 1mg/kg slow-release buprenorphine for pain control immediately prior to injury. Sustained-release buprenorphine provides pain relief (but no anti-inflammatory activity) for up to 3 days post injection[23]. Animals were randomly assigned by cage into groups and euthanized

at either 3-, 7-, or 14-days post-injury (n=5 per group per sex), with the 14-day animals receiving *ANY-maze*^{TM} cage monitoring at days 0, 1, 3, 7 and 14. Following euthanasia, knees were assessed for ACL status macroscopically via imaging. Limbs were then processed for histology.

Non-invasive ACL rupture

For both full and partial ACL ruptures, animals were anesthetized via 2% isoflurane inhalation, and placed in a custom material testing system with an actuator (Ultra Motion Series A1; 3in stroke capacity, 0.01% accuracy) and load cell (Interface Model 1210; 300 lbf maximum, 0.04% accuracy) controlled using NI instrumentation in LabView. For placement, the femur was positioned in a bottom groove with the tibia overhanging by 1mm with the knee at 90° of flexion; the foot was secured in a custom 3D printed cup with the ankle at 10° of flexion (**Figure 2.2A and B**). Given this arrangement, long bones were not able to rotate or translate beyond the vertical direction of applied force. With respect to the chosen displacements for both preconditioning and tibial displacement to induce ACL rupture, non-destructive laxity testing of cadaveric mouse limbs has historically been tested using a displacement on average of less than 0.50mm with no ACL ruptures or injuries to the limb noted[24-26].

The custom loading protocol (LabView) was initiated as follows: 1) manual preload to 0.7N; 2) preconditioning at 0.4mm displacement for 200 cycles at 1Hz (sinusoidal waveform; to replicate physiologic preconditioning, as pilot studies indicated 200 cycles allowed for equilibrium force to be achieved) (**Figure 2.2C**); 3) tibial displacement at

either 1.6mm or 2.0mm displacement (square wave; relatively instantaneous loading); and 4) post-injury displacement test at 0.4mm displacement for 1 cycle at 1Hz (sinusoidal waveform).

The post-injury displacement test, which is a single sinusoidal cycle utilizing our pre-conditioning parameters, provides a confirmatory measure of the presence or absence of joint stability and ACL integrity. This motion was recapitulated in the fixture by moving the tibia past the femur, with the presence of zero change in load indicating a positive test (i.e., ruptured ACL). For all testing, output curves (**Figure 2.2C, Left**) were generated. A representative curve for a control mouse (from n=5 tested) receiving the loading protocol without tibial displacement (only preload, preconditioning, and post-injury displacement test) is also provided (**Figure 2.2C, Right**).

ANY-maze™ Cage Monitoring

Behavior/mobility assessment data were recorded using *ANY-maze™* software (Wood Dale, IL). Animals were placed singly in their resident cage with their environmental enrichment hut (hidden zone). Animals were acclimated twice with each baseline measurement taken in duplicate prior to the start of the study. Cage monitoring occurred on days 1, 3, 7 and 14. Animals were recorded for 10 consecutive minutes/time-point. Training and data collection were performed during the same period of the day (8 AM to 12 PM) and involved the same handlers. Mobility parameters for time spent freezing, modulated time spent in resident environmental enrichment hut, time on top of

environmental enrichment hut, and time mobile were automatically collected; see **Supplemental Table 2.1** at https://doi.org/10.7910/DVN/BJE7C9 for a full list**.**

Magnetic Resonance Imaging

At day 3 post-injury, a subset of three male mice were transported to the University of Colorado Animal Imaging Shared Resource. In-vivo Magnetic Resonance Imaging (MRI) was performed on anesthetized mice (2.5% isoflurane) using a 9.4 Tesla BioSpec animal MRI scanner (Bruker Medical, Billerica, MA). First, a localizer scan was obtained for the knee by placing animal injured and collateral limbs in the center of phase-array rat head coil. Then, a multi-sequential MR protocol was obtained based on optimized T1- and proton density (PD)-weighted RARE (rapid acquisition with relaxation enhancement) sequences as well as a set of DIXON-type sequences (water-only, fat-only, and out-of-phase). All images were obtained in coronal and sagittal planes; all sequence parameters are included in **Supplemental Table 2.3.** Total acquisition time for all sequences was 23 min 29 sec. The animals were monitored during the scan for appropriate body temperature and respiratory rate.

The joint space was quantified by placing a hand-drawn region of interest (ROI) on representative sagittal PD- and T1-weigted sagittal slices for the right and left knees[27-30], summing and multiplying by the slice thickness (reported in mm^3) using Bruker ParaVision NEO360 v2.0 software. The extent of the knee edema was also quantitatively assessed (in mm^3) in the right limb by placing hand-drawn ROIs on water-only DIXON images. Edema in the contralateral sham left limb was not discernable and

therefore not assessed. The total limb volume was also determined from PD-RARE coronal scans. All images analysis was performed by an MRI physicist (NJS) with >15 years of experience.

Macroscopic Imaging

Images for both experimental Phases were taken using a VWR Trinocular inverted microscope with a Moticam X wireless camera and the Motic Live Imaging Module (Richmond, BC). Macroscopic imaging prior to tissue processing was utilized along with the manual cranial drawer test immediately post-injury (Phase 1) or euthanasia (Phase 2) to confirm ACL status.

Histologic assessment of knee joints

Limbs from Phase 2 were coronally sectioned at mid-joint. Knee joints were fixed in 10% neutral buffered formalin for 24 hours and transferred to phosphate buffered saline. Limbs were then submerged for 7 days in 14% EDTA at a pH of 7 for decalcification. Samples were paraffin embedded and sections (5 μm) were stained with toluidine blue. One independent pathologist (KMA), blinded to identifying data, performed histological grading based on recommended OARSI OA scoring guidelines in mice[31]. No osteophytes were observed; however, enthesophytes located at bone/ligament interfaces were scored as per the osteophyte grading scheme. Additional findings included the presence of: (1) blood, (2) joint space deposits, (3) further ACL remnant deterioration, (4) PCL degeneration or injury, (5) joint capsule expansion, and (6)

meniscal injury. Each of these additional findings were graded based on severity on a scale of 0-3.

Statistical Analysis

For Phase 1, loading curve parameters were analyzed by a One-Way ANOVA with Tukey's multiple comparisons test; preconditioning was not considered as a factor. All groups were normality distributed and passed tests for equal variance. A receiver operating characteristic (ROC) curve was generated for each of the loading curve parameters (preconditioning peak force, tibial displacement peak force, and post-injury displacement peak force) using the Wilson/Brown method; sensitivity and specificity were reported as percentages. The experimental sample size for Phase 2 (5 animals per sex per time-point) was calculated using GPower Version 3.1.1[32]. Specifically, an *a-priori* power analysis was conducted using peak tibial displacement data generated during Phase 1. This power analysis resulted in a power of 99%, using mean group tibial displacement peak forces of -1.65 N and -0.78 N and a standard deviation of 0.31 N for both groups. For Phase 2 *ANY-maze*^{TM} parameter comparisons, a mixed effects model was utilized, and p-values were calculated for timepoint (0, 1, 3, 7, and 14 days) using Tukey's multiple comparison tests. Originally, statistics were run to stratify sex; however, no significant differences were seen ($p>0.05$). Therefore, the sexes were combined (10 animals per time-point), leaving time as the main factor of interest. For correlations between parameters, a Pearson Correlation Analysis was conducted. For Phase 2 histological grading, a mixed effects model was utilized, and p-values were calculated for timepoint (3, 7, 14 days) using Tukey's multiple comparison tests.

Significance was set to $p<0.05$ for all comparisons. All post-hoc statistics were conducted in GraphPad Prism v8.4.1 (San Diego, CA).

2.4 Results

Full and Partial ACL Rupture Success Rates

For Phase 1, **Figure 2.3** shows success rates based on macroscopic assessment following loading protocols. Of note, only 9 female mice were tested with preconditioning due to a LabView code malfunction during tibial displacement leading to one animal being excluded. Consistent with our hypothesis, 1.6mm displacement caused a majority of partial ACL ruptures, and 2.0mm displacement showed a majority of full ACL ruptures for both sexes. Of note, all ruptures appeared to be in the mid-substance region of the ACL with no avulsion fractures noted macroscopically. Further, pre-conditioning prior to tibial displacement was either equivalent to or improved attainment of appropriate ACL status compared to animals that did not receive pre-conditioning **(Figure 2.3A)**. Specifically, males and females receiving preconditioning prior to full rupture resulted in a 30% or 28% increase in success rate compared to mice without preconditioning, respectively. Success rates of partial ruptures for males with preconditioning were equivalent to mice without preconditioning; however, female mice demonstrated a 39% increase in success rate for partial rupture with preconditioning. Representative images of an intact, partial, and full ACL rupture are shown in **Figure 2.3B**.

Predictive Capacity of ACL Rupture Loading Curves

For Phase 1, we aimed to determine if the loading curves could be used to distinguish between an intact leg, partial rupture, or full rupture. Model specificity and sensitivity were analyzed by ROC testing. Based on the tibial displacement peak force, we can distinguish between either a partial vs. intact ACL (ROC Cutoff of -1.136N) or full vs. intact ACL (ROC Cutoff of -1.134N) with greater than 97% sensitivity and 100% specificity in each scenario **(Figure 2.4A).**

To distinguish between a partial vs. full rupture, we considered tibial displacement peak force and post-injury displacement peak force, stratified by sex. In males with pre-conditioning, we saw that tibial displacement peak force (ROC Cutoff of -1.495N) is capable of distinguishing between a partial and full rupture with a sensitivity of 76.92% and specificity of 100% **(Figure 2.4B)**. Conversely, in females with pre-conditioning, the post-injury displacement peak force is superior to the tibial displacement peak force. For distinguishing between a full and partial rupture in females, we see a specificity of 90% and sensitivity of 75% at a ROC Cutoff -0.0655N when looking at the post-injury displacement peak force **(Figure 2.4C)**. Taken together, (i) tibial displacement peak force (higher than 1N of compressive force), (ii) post-injury displacement peak force (greater than 80% reduction relative to tibial displacement peak force), and (iii) translocation of the hip during preconditioning followed by the lack of hip movement during the post-injury displacement peak force, allowed for the qualitative evaluation of whether rupture occurred in real-time.

For Phase 2, all mice passed predictive capabilities during ACL injury induction. Notably, there were no statistical differences ($p>0.05$) between loading curve parameters for male and female mice, except for the post-injury displacement peak force ($p=0.04$, data not shown), reiterating slight variations in loading outputs based on sex, comparable to the ROC analysis. Interestingly, female mice experienced significantly decreased percent relaxation during preconditioning ($p=0.04$; **Supplemental Figure 2.1**). At necropsy,14 days later, all animals had a positive manual cranial drawer.

In Vivo Magnetic Resonance Imaging

No abnormalities were seen in contralateral left sham joints on MRI **(Figure 2.5A-C**). The joint space volume in the left uninjured knee was 3.2 +/- 0.2 mm^3 (n=3), which supports previous data obtained by ultrasound imaging[28]. For all mice, the injury to the right knee 3 days prior to MRI led to an 12-19% difference in joint space when compared to the left knee **(Figure 2.5C-D)**. Quantitative image analysis of water fraction in DIXON images revealed dramatic water accumulation in the right injured knee relative to the left contralateral limb **(Figure 2.5C)**. Quantitatively, the gross increase in total limb volume (due to the water accumulation and swelling of soft tissue) was persistently up to 20% in the right limb day 3 post-injury compared to the left uninjured limb, as calculated from 3D PD-MRI **(Figure 2.5B).**

Histopathology and OARSI Grading

Histologically, all animals' knees appeared to have ruptured ACLs and some concurrent PCL and meniscal tearing; no subjective differences were observed between male and female mice. Notably, mild cartilage lesions were seen on tibial plateaus (**Figure 2.6I-L**) and femoral condyles (**Figure 2.6E-H**) by day 3 but these did not progress in severity through day 14 (**Supplemental Figure 2.2A-F**). Statistically significant early PTOA differences post-injury were most often associated with soft tissue structures and were characterized by: enthesophyte formation (**Figure 2.6M-P**; **Figure 2.7A**, 3d vs 7d ($p=0.0027$), 3d vs 14d ($p<0.0001$), 7d vs 14d ($p=0.0419$); joint capsule expansion (**Figure 2.6Q-T; Figure 2.7B**, 3d vs 7d ($p=0.0002$), 3d vs 14d ($p=0.0005$)); synovial hypertrophy and hyperplasia (**Figure 2.6U-X; Supplemental Figure 2.2I**), meniscal degeneration (**Figure 2.6Y-BB**; **Figure 2.7C;** 3d vs 7d ($p=0.0018$), 3d vs 14d ($p=0.0048$); anterior cruciate ligament rupture and/or degeneration (**Figure 2.6CC-FF; Supplemental Figure 2.2H**); and mild subchondral bone thickening (**Figure 2.7D;** 3d vs 14d ($p=0.0097$), 7d vs 14d ($p=0.0262$)). Notably, histopathology parameters were not statistically correlated to the tibial displacement peak force obtained during injury induction (p values >0.05; **Supplemental Table 2.2**).

Overhead Enclosure Monitoring

Phase 2 utilized *ANY-maze*^{TM} cage monitoring as a behavior/mobility assessment. Observed differences relative to pre-rupture baseline were characterized by: (1) decreased time spent freezing (**Figure 2.8A;** 1d ($p=0.0234$)); (2) modulated time spent

in their resident environmental enrichment hut with time increased at 1 day post rupture and decreased starting at 6 days post rupture (**Figure 2.8B;** 1d (p=0.0113), 6d (p=0.0206), 14d (p=0.0453)); and (3) decreased time on top of their environmental enrichment hut (**Figure 2.8C;** 1d (p=0.015)). Mice showed a significant increase in time mobile by 6 days post injury, which remained increased through the duration of the study (**Figure 2.8D;** 6d (p=0.036), 14d (p=0.021)).

2.5 Discussion

This study developed a non-invasive ACL rupture injury model for partial and full mid-substance ACL ruptures; both sexes were included. We demonstrated that preconditioning, repetitive cyclical loading under physiological displacement to remove tissue laxity prior to rupture was either equivalent or improved accuracy of appropriate ACL status. Preconditioning has previously been shown to cause ligaments and tendons to have higher tensile properties[33,34], and increased the reproducibility of ACL rupture during ex-vivo mechanical testing in bovine ACL. Cyclic preconditioning has also previously been demonstrated to decrease tissue laxity and, as such, it is anticipated that including pre-conditioning in our protocols decreased the variation in limb loading during tibial displacement, leading to increased rupture consistency. Additionally, as the majority of ACL injuries occur during physical activity, preconditioning is suggested to recapitulate movement and activity prior to injury, and therefore, produces a more clinically relevant injury and result.

Decreased severity compared to previous models

We demonstrated clinical signs of ACL rupture via *in-vivo* MRI 3 days post-injury, including swelling and increased joint space. While future work will include a higher sample size that includes both sexes, this proof-of-principle approach: was able to highlight that it is possible to capture usable MRI data in mice post-ACL rupture; and show that, shortly after ACL rupture, immediate soft tissue swelling are present in our model that are translatable to the human condition.

We also documented early histologic PTOA differences in full ACL rupture mice by 14 days post injury. Previous models have shown PTOA progression in other mouse models of mechanical tibial displacement as early as 7 days post injury[11], with total OARSI scores of approximately 11 by day 7, average tibia scores of approximately 4.5 and average femur scores of approximately 3 by day 14[35] post-ACL rupture. Our model demonstrates a relatively decreased PTOA progression with mean total OARSI scores of 5.8 at day 7, and an average tibia score of 1.04 and average femur score of 2.89 by day 14 post rupture. Overall, our model does not appear to incite PTOA onset at the same rate post-injury as current published models. Most importantly, our model demonstrates PTOA progression similar to that seen clinically in humans post-ACL rupture. These similarities include bony pathology such as increased flattening (less convexity) of the femur[36], a feature of early OA changes[37,38], and early degenerative changes such as enthesophytes/osteophytes, which are present in about 40% of post-ACL patients by 2 years post-injury[39].

Previous non-invasive ACL rupture models demonstrate loads that range from 3N-12N[11-16]. These higher loads may have led to avulsion fractures seen in some ACL rupture models, as well as account for earlier histopathologic PTOA evidence. Our model demonstrates loads during tibial displacement of ~1.0-2.5N for both partial and full ACL rupture. This potentially accounts for why our model produces mid-substance tears without avulsion fractures[40]. This also allows our model to be clinically relevant, as avulsion fractures occur in less than 10% of patients following an ACL rupture[41]. However, it should be recognized that other studies have pointed to the rate of displacement[14], as well as position of the animal and/or joint[10,42], along with age, sex and body mass[43] as additional factors dictating whether mid-substance tears versus avulsion fractures occur. It is important to note that variations in loading, both knee flexion angles, and direction of tibial loading, will also affect the load seen during ACL rupture[11-16].

Other Etiologies

The status of the meniscus following ACL injury has been shown to be important factor for the development of PTOA in patients[44]. We observed meniscal degeneration and tears (**Figure 2.6Y-BB**) which is translatable to humans as meniscal injury and meniscectomy are the most common risk factors for PTOA in people post ACL rupture[45]. We showed through correlative analysis that there were no associations between the degree of loading at the time of injury and the presence of meniscal tears. Therefore, we anticipate that meniscal tears in our model are arising from rotational

instability post-rupture, which is observed clinically[46], and not due to initial damage at the time of injury, which utilizes uniaxial loading. Further study is warranted to determine the progression of such meniscal tears post-ACL rupture to assist in clinical management of whole joint health.

Functional Mobility

The chief complaint for patients with PTOA is loss of mobility and painful locomotion[47]. To date, relatively few pre-clinical PTOA models track behavior and mobility alterations, and, to the authors' knowledge, few mechanical models of ACL rupture used mobility as an outcome[48]. Historically, PTOA progression has been assessed primarily by histological and radiographical changes, although severity of joint pathology does not always correlate to the degree of clinical symptoms presented by the patient. Phase 2 of the current study utilized *ANY-maze*^{TM} cage monitoring as a behavior and mobility assessment provided longitudinal assessment of individual animals throughout the course of disease progression. We demonstrated that, at 1-day post ACL rupture, mice exhibited altered mobility, implying a potential pain or physical response not addressed by buprenorphine. Interestingly, mice returned to pre-surgery movement levels by the conclusion of the study (day 14). As unmanipulated sham mice were not evaluated for this study, however, there is the possibility that day 1 changes seen may also be due to pre-operative analgesics, anesthesia, or handling procedures. Of note, a different mechanical ACL rupture model also reported no differences between sham and ACL-ruptured mice in open field mobility testing up to 14 days post-injury[48]. Given that 14-days is still an early timepoint post ACL rupture, and that mice are quadrupeds, it was

expected that we would not see significant differences in an outcome that assesses overall voluntary animal movement. Future work will focus on utilization of methods able to detect outcomes such as gait symmetry. Indeed, previous studies have demonstrated that a loss of this symmetry can indicate pain associated with knee OA[49].

Sex Differences

Our model demonstrated consistency in inciting both full and partial ACL ruptures in male (full: 100%, partial: 67%) and female (full: 78%, partial: 89%) mice with pre-conditioning. This is important as females have a higher incidence of ACL rupture clinically[21,22] but historically tend to be underutilized in animal models of PTOA. From a clinical perspective, females have a greater anterior knee joint laxity than males[50,51], which we hypothesize could account for the differences seen in the sensitivity and specificity determined by the ROC cutoffs. Additionally, our data demonstrates female mice had significantly less relaxation during preconditioning (calculated as a ratio of the peak force during preconditioning relative to the equilibrium force at the end of preconditioning) than male mice, which would correspond to increased female knee laxity discussed above.

Age Considerations with ACL Rupture

It is important to note that the age of mice at time of tibial displacement may play a role in the ability to achieve a mid-substance ACL rupture versus an avulsion fracture. Historically, mice at time of rupture are typically 8[12], 10[11,14], 12[15], or 16 weeks[16] of age. For this study, we used mice that were 12 weeks at time of injury. Importantly, age, sex

and weight have all been shown to effect avulsion fractures and mid-substance tear success rates in an alternate non-surgical ACL injury model[43]. As age and skeletal maturity at time of injury may affect rupture outcomes, future studies should consider these factors more overtly in study design.

Importance of Partial ACL Rupture Model Development

Partial ACL ruptures account for 10-27% of total injuries clinically, and treatment of partial ACL rupture can differ from that of a full rupture[52]. Importantly, to the authors' knowledge, this is the first non-invasive mouse partial ACL rupture model. Due to the positioning of the knee in flexion during injury, we anticipate that the anteromedial band of the mouse ACL is ruptured, while the posterolateral band remains intact. Specifically, we anticipate this to be the case because the anteromedial band is tensed in knee flexion (as opposed to the posterolateral band in extension)[53]. However, further validation, including optimization of soft tissue MR imaging protocols for detection of ACL rupture status, are warranted to track ACL status over time. Notably, for partial ruptures, the anteromedial bundle is the most commonly injured clinically, with the majority of tears involving 50-75% of the ACL (e.g., one bundle) progressing to full rupture. Our newly developed partial rupture model allows for the study of partial ACL tear progression to full rupture and testing of therapeutics following a partial rupture. As this study only assessed our ability to initially produce partial ACL ruptures, future studies will characterize PTOA development following partial ACL rupture in rodents.

Predictive Capabilities

Utilizing the loading curves obtained during testing allowed for real-time assessment of ACL status following rupture. First, based on tibial displacement peak force (N), we are able to distinguish between an intact limb following tibial displacement (which would be an unintended outcome demonstrating a failed test) versus a full or partial rupture for both sexes. Indeed, using the Phase 1 data, we calculated a specificity, or true negative rate, of 100% and a sensitivity, or true positive rate, upwards of 97% for both loading cutoffs for intact versus rupture status. Second, rupture status of male and female animals could be discerned based on different loading curve parameters (e.g., tibial displacement peak force or post-injury displacement peak force). Finally, distinguishing between a partial rupture versus a full rupture was more difficult due to the lower loads achieved with each rupture state using our model. Prospective work would need to be completed to confirm use of these ROC cutoffs moving forward. A benefit of this assessment is that it allows for more reliable determination of ante mortem ACL rupture than manual cranial drawer testing. This will give us more confidence during ACL rupture, allowing for animals with incorrect ACL status to be removed from study continuation.

Study Caveats and Summary

One limitation of this study not already addressed above is that our Phase 2 full-rupture animals were only taken out to 14 days and, as such, we were not able to document longer-term effects of our model. Future studies will include both full and partial rupture animals at later time-points to more comprehensively characterize PTOA progression.

Additional work will also consider whether long bone size or weight may factor into rupture success, as it was noted that male and female mice had significantly difference masses. Finally, randomization of time-points within cages will be utilized moving forward.

In summary, the results from this study demonstrated development of both non-invasive full and partial ACL rupture in mice of both sexes. Both rupture types occurred within the mid-substance of the ligament, with no avulsion fractures noted macroscopically. Following full ACL rupture, we noted signs of early PTOA progression by 14 days post injury with behavioral changes at 1 day post injury that were minimized by 14 days post injury. Importantly, this clinically relevant model provides a unique way to study both full and partial mid-substance ACL ruptures in male and female mice and can be used to tease out potential mechanisms that could be utilized for therapeutic intervention.

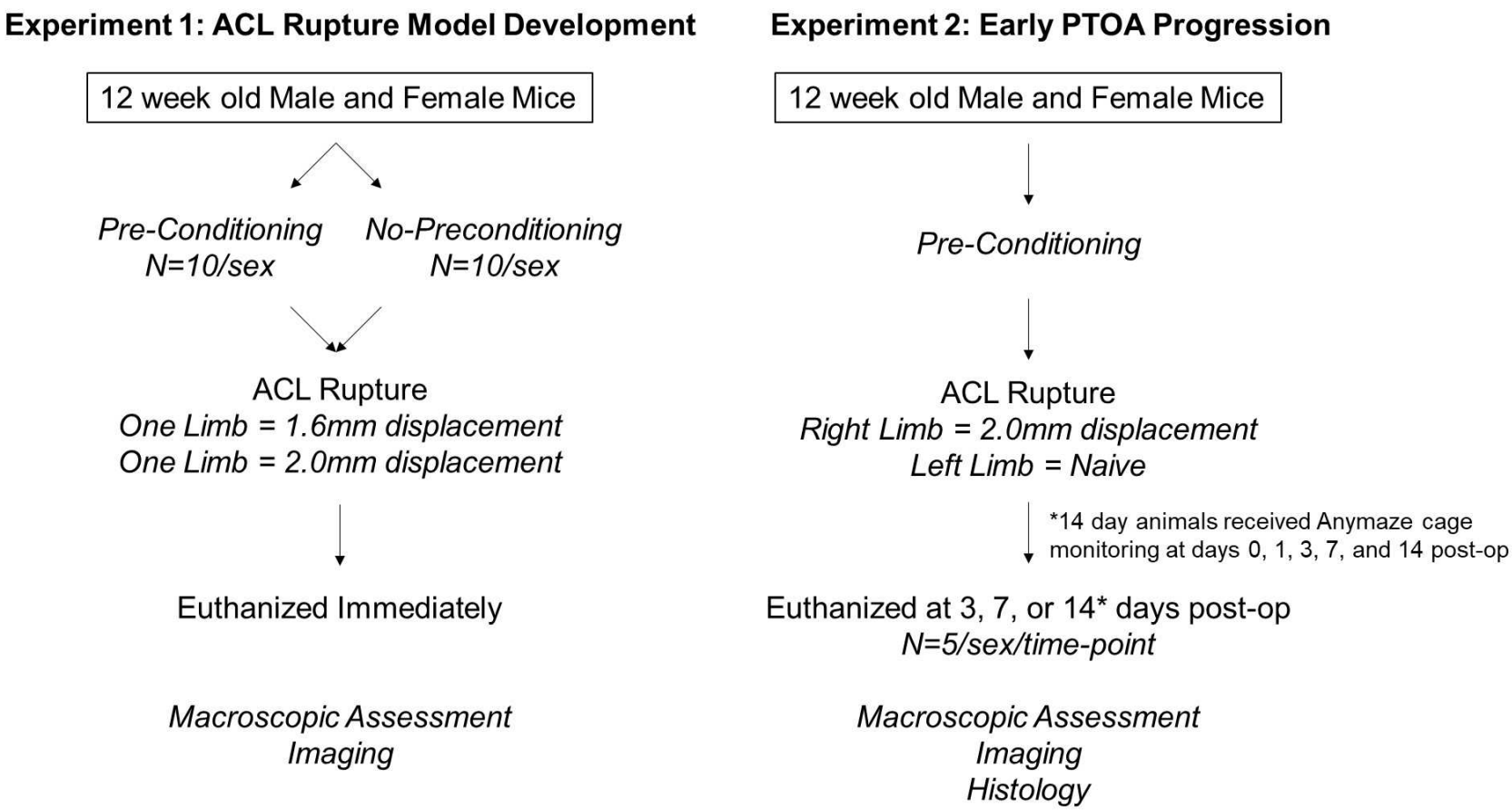

Figure 2.1 Schematic of the noninvasive rupture model development experimental design. Animals were split into two experimental phases; (Left) Phase 1: ACL Rupture Model Development and (Right) Phase 2: Early PTOA Progression. Phase 1 animals received either pre-conditioning, or no pre-conditioning (n=10/sex) and limbs were randomly assigned to either 1.6mm displacement of 2.0mm displacement. Animals were euthanized immediately and assessed macroscopically and imaged. Phase 2 animals all received 2.0mm displacement, following pre-conditioning, on their right legs. Animals were euthanized at 3-, 7-, or 14-days post injury (n=5/sex/time-point) with animals in the 14 days post injury group receiving *ANY-maze*^{TM} cage monitoring on days 0, 1, 3, 7, and 14 post injury. Following euthanasia knee joints were assessed macroscopically, imaged, and evaluated histologically.

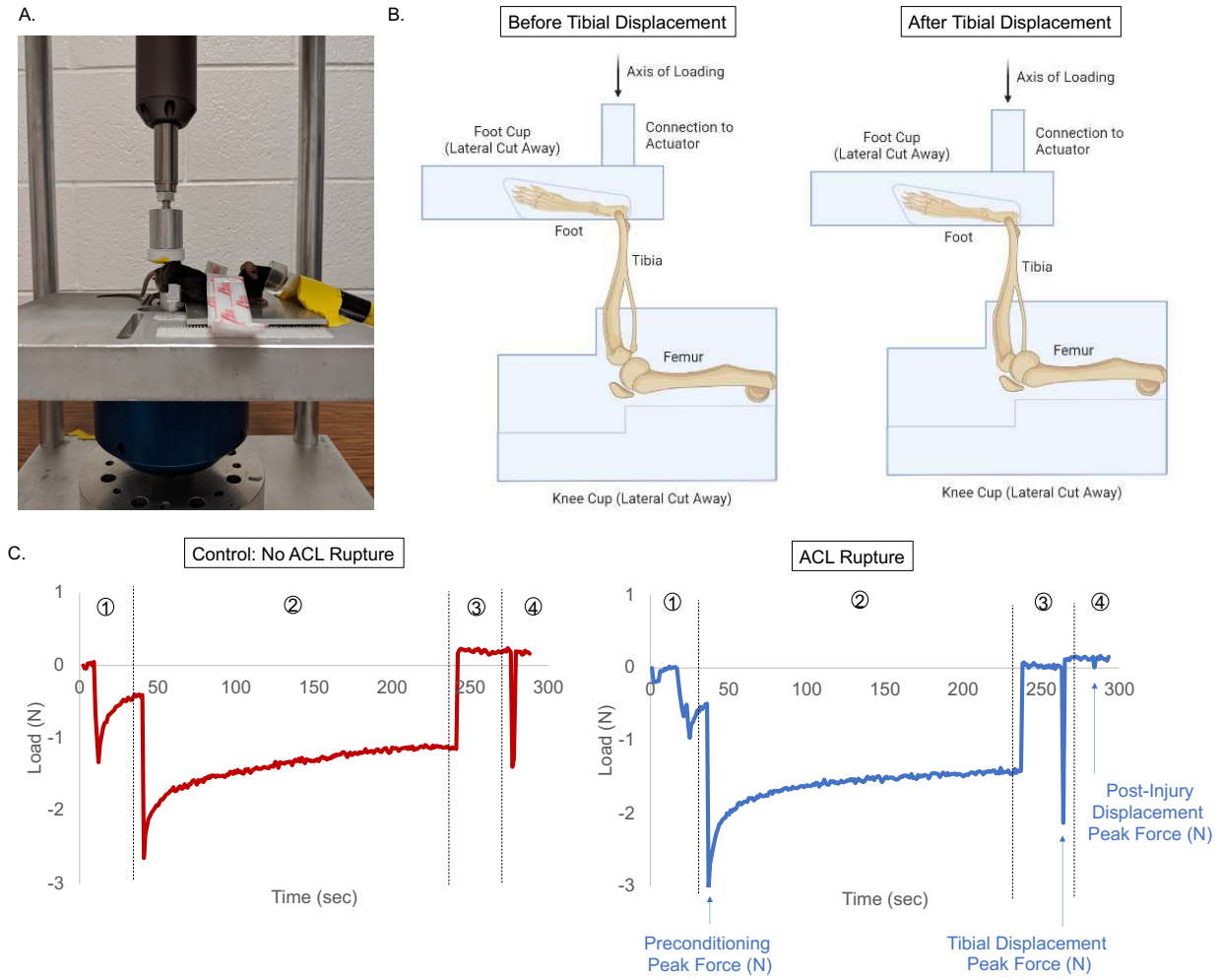

Figure 2.2 (A) Custom setup to induce ACL rupture in anesthetized rodents. **(B)** Pictorial representation for displacement of the tibia to incite an ACL rupture (2mm). **(C, left)** Output loading curve for representative control animal including 1) preload, 2) preconditioning, 3) no tibial displacement, and 4) negative (decrease in load) post-injury displacement peak force **(C, right)** Output loading curve for full rupture including 1) preload, 2) preconditioning, 3) tibial displacement, and 4) and positive (no load changes) post-injury displacement peak force For output loading curves, data was outputted at 1Hz; therefore, preconditioning, tibial displacement, and post-injury displacement test phases demonstrate peak loads.

A.

Result	Male		Female	
	No Pre-Conditioning	Pre-Conditioning	No Pre-Conditioning	Pre-Conditioning
	n=10	n=10	n=10	n=9
1.6mm Tibial Displacement				
Partial	70%	67%	50%	89%
Full	30%	33%	50%	11%
Intact	0%	10%	0%	0%
2.0mm Tibial Displacement				
Partial	30%	0%	30%	22%
Full	70%	100%	50%	78%
Intact	0%	0%	20%	0%

B.

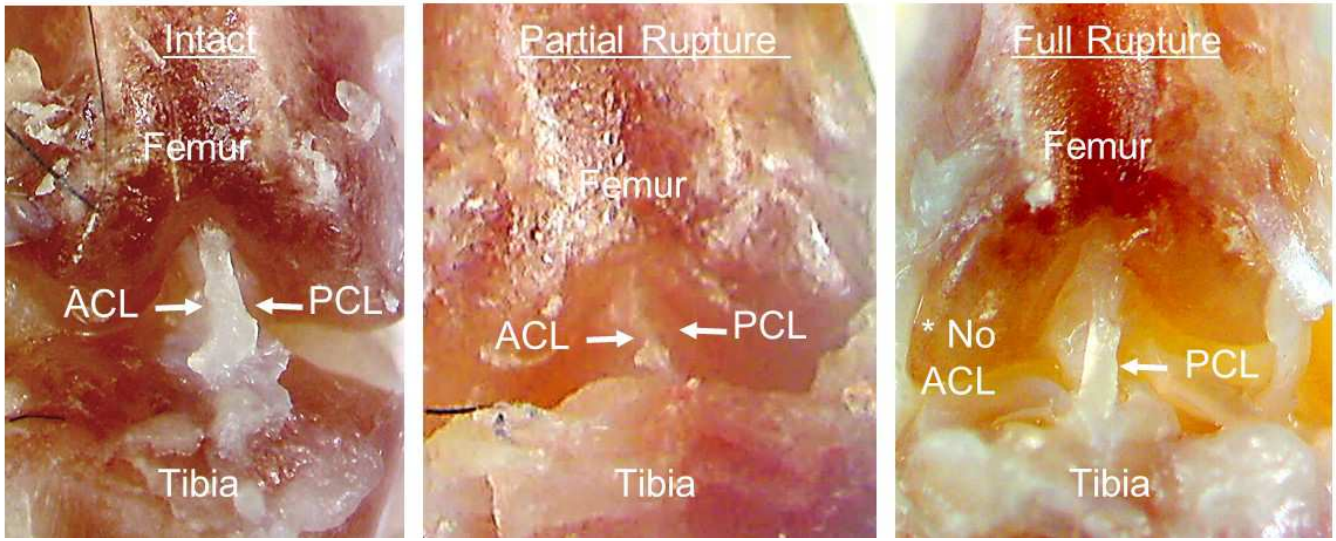

Figure 2.3 (A) Table of success rates for incidence of partial, full, and the absence of ACL rupture, with and without preconditioning as determined by macroscopic imaging. **(B)** Representative macroscopic images of intact, partial, and full ACL ruptures (all right limbs).

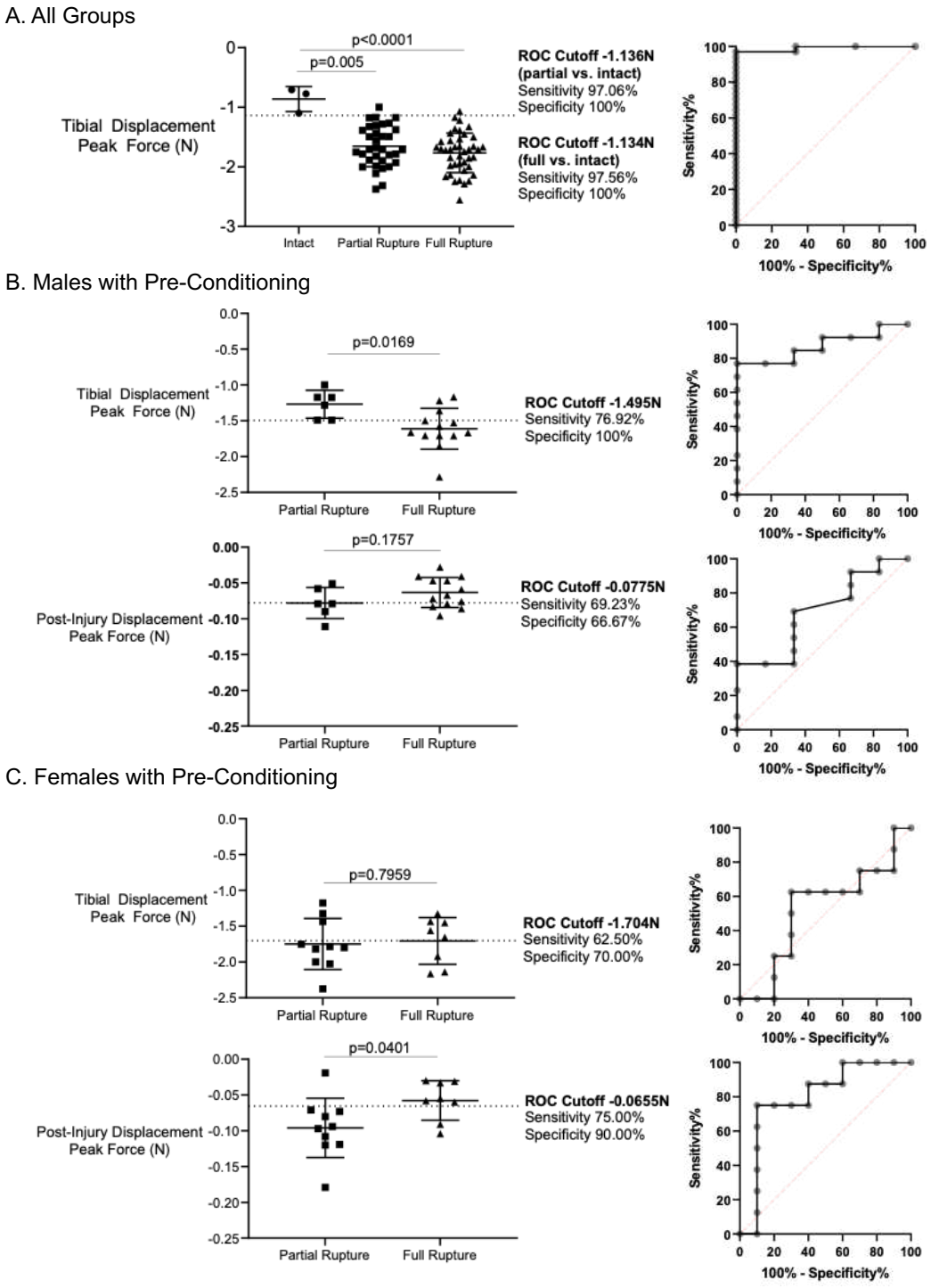

Figure 2.4 Receiver operating characteristics (ROC) were generated for each of the loading curve parameters. **(A)** Breakdown of tibial displacement peak force (N) for all groups distinguished between intact versus full or partial rupture. Tibial displacement peak force (N) and post-injury displacement peak force (N) ROC cutoff points for distinguishing between either a full and partial rupture in: **(B)** males with pre-conditioning and **(C)** females with pre-conditioning. The p-values for significant differences between groups are listed for each comparison.

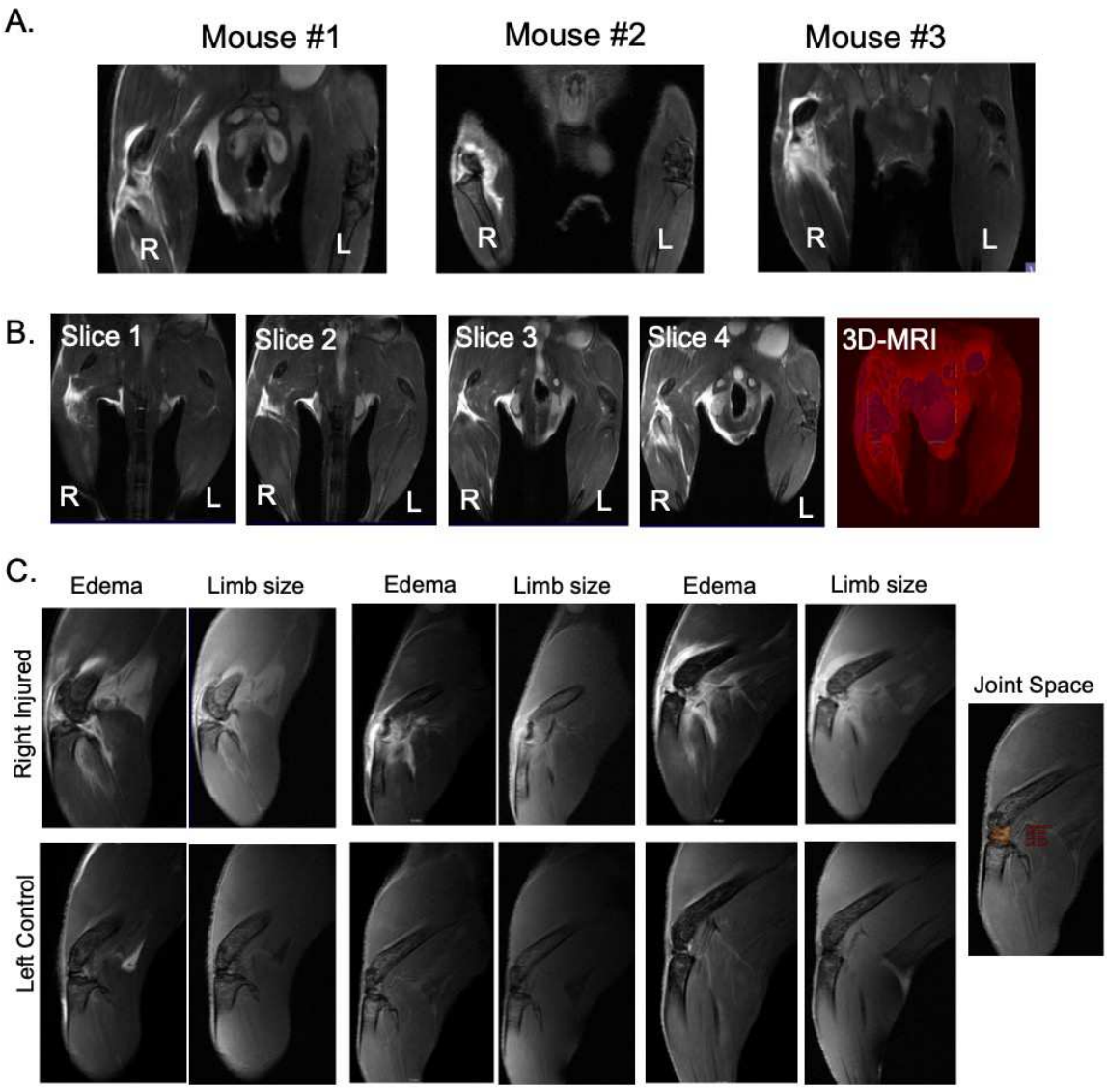

D.

	Joint Space			Edema
	Right Knee	Left Knee	Change (R vs. L)	Right Knee
Mouse #1	3.61 mm^3	3.18 mm^3	12%	127.3 mm^3
Mouse #2	3.23 mm^3	2.89 mm^3	11%	80.7 mm^3
Mouse #3	4.24 mm^3	3.52 mm^3	19%	161.2 mm^3

Figure 2.5 Representative MR images and image analysis on three animals at day 3 post-injury: **(A)** proton density (PD)-weighted coronal images on 3 male mice; **(B)** limb volume assessment from 3D-reconstructed RARE-PD coronal slices; **(C)** water-only DIXON (edema) images from the right and contralateral left limb in sagittal plane; with a representative ROI of the joint space; **(D)** quantitative MR image analysis.

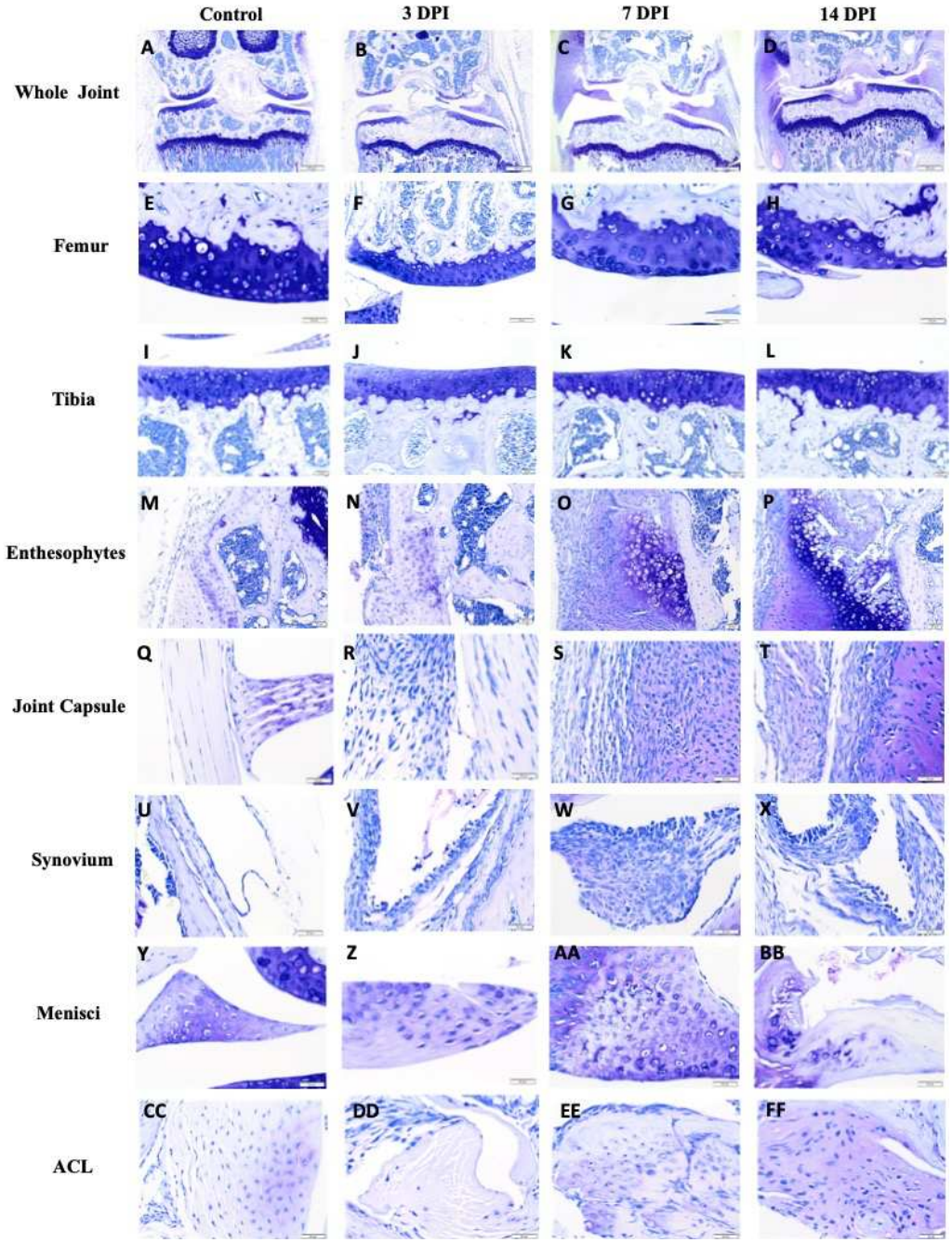

Figure 2.6 Toluidine blue photomicrographs from control (left) and injured (right) limbs 3, 7-, and 14-days post ACL rupture (3DPI, 7DPI, and 14DPI, respectively). **(A-D)** Low magnification image of whole knee joints from control **(A, left column)**, 3-days **(B, left middle column)**, 7-days **(C, right middle column)**, and 14-days **(D, right column)** post ACL rupture. Injured limbs have diminished **(A-D)** femoral condyle convexity, **(E-H)** mild femoral condyle articular cartilage degeneration, **(I-L)** mild medial tibial plateau articular cartilage degeneration, **(M-P)** enthesophytes, **(Q-T)** reactive joint capsules, **(U-X)** reactive synovial membranes, **(Y-BB)** meniscal degeneration and tears, and **(CC-FF)** anterior cruciate ligament degeneration. *A-D, 4x, bar=200um; E-H, 20x, bar=20um; I-BB, 40x, bar=20um; DPI=days post injury.*

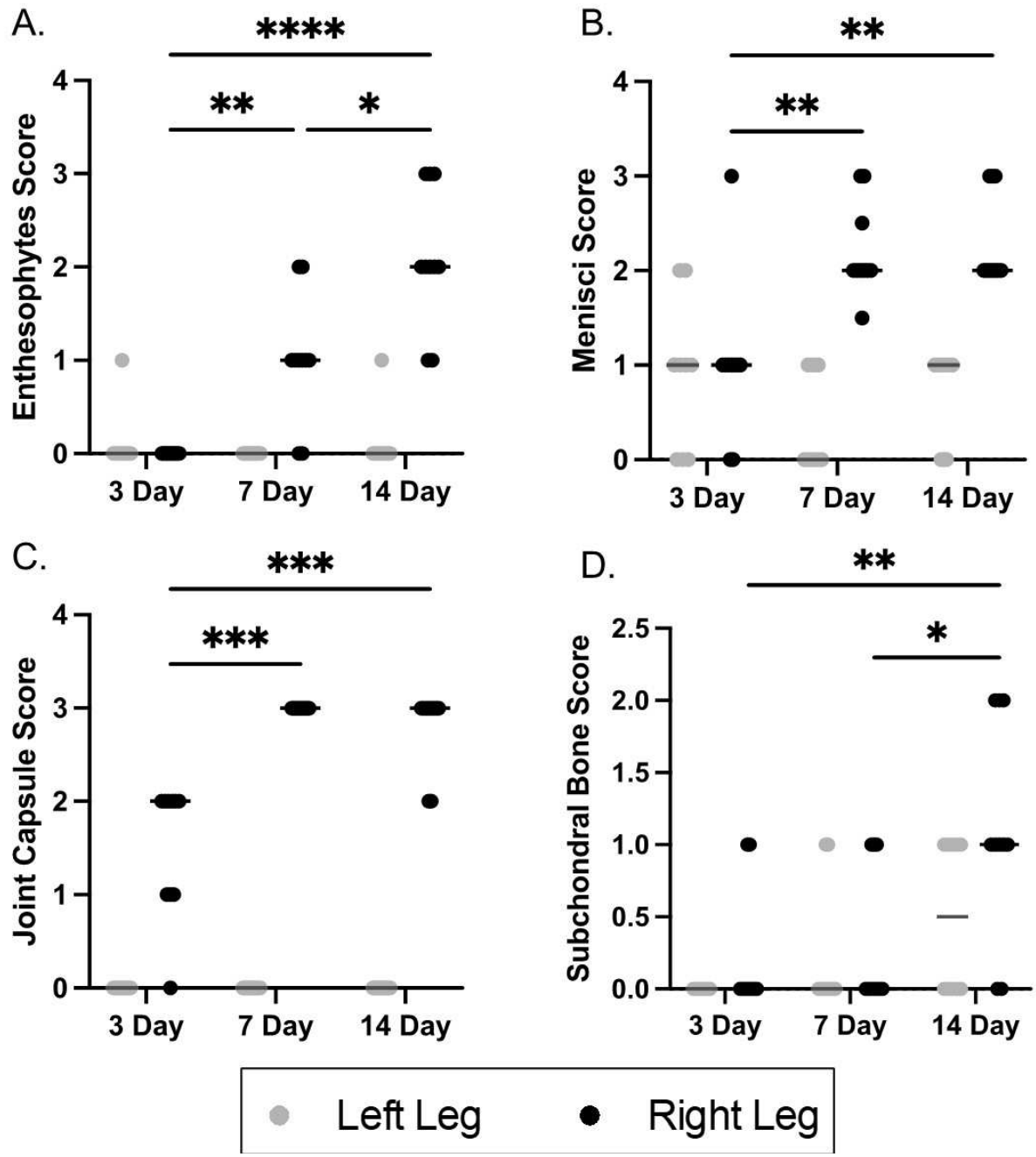

Figure 2.7 Median modified OARSI histopathology scores for OA, following full ACL rupture on the right hind limb (black) of mice. Contralateral sham left limb scores (gray) included for reference. Parameters with significant differences include: **(A)** Total Joint Score, **(B)** Enthesophytes Score, **(C)** Menisci Score, and **(D)** Joint Capsule Score. Significant differences over time labeled (*p<0.05, **p<0.005, ***p<.0005, ****p<.0001).

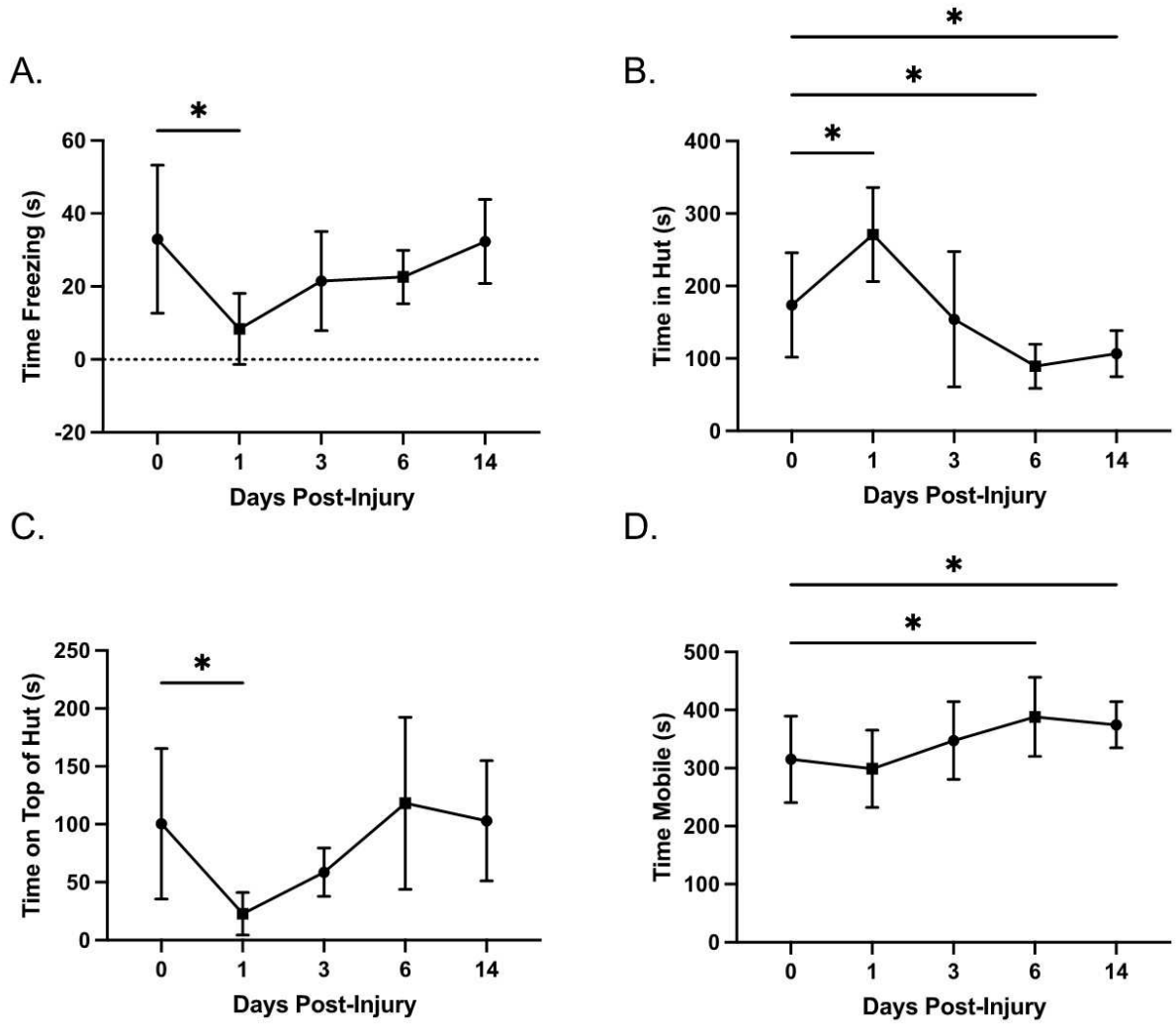

Figure 2.8 *ANY-maze*^{TM} cage monitoring parameters following full ACL rupture on the right hind limb of mice. Parameters with significant differences include: **(A)** Time Freezing (s), **(B)** Time in Hut (s), **(C)** Time on Top of Hut (s), and **(D)** Time Mobile (s). Significant differences over time labeled (*p<0.05, **p<0.005).

2.6 References

1. Lohmander LS, Ostenberg A, Englund M, Roos H. High prevalence of knee osteoarthritis, pain, and functional limitations in female soccer players twelve years after anterior cruciate ligament injury. *Arthritis Rheum*. Oct 2004;50(10):3145-52. doi:10.1002/art.20589

2. Beynnon BD, Johnson RJ, Abate JA, Fleming BC, Nichols CE. Treatment of anterior cruciate ligament injuries, part I. *Am J Sports Med*. Oct 2005;33(10):1579-602. doi:10.1177/0363546505279913

3. Carbone A, Rodeo S. Review of current understanding of post-traumatic osteoarthritis resulting from sports injuries. *J Orthop Res*. 03 2017;35(3):397-405. doi:10.1002/jor.23341

4. Owens BD, Mountcastle SB, Dunn WR, DeBerardino TM, Taylor DC. Incidence of anterior cruciate ligament injury among active duty U.S. military servicemen and servicewomen. *Mil Med*. Jan 2007;172(1):90-1. doi:10.7205/milmed.172.1.90

5. Tennent DJ, Posner MA. The Military ACL. *J Knee Surg*. Feb 2019;32(2):118-122. doi:10.1055/s-0038-1676565

6. Lohmander LS, Englund PM, Dahl LL, Roos EM. The long-term consequence of anterior cruciate ligament and meniscus injuries: osteoarthritis. *Am J Sports Med*. Oct 2007;35(10):1756-69. doi:10.1177/0363546507307396

7. Muthuri SG, McWilliams DF, Doherty M, Zhang W. History of knee injuries and knee osteoarthritis: a meta-analysis of observational studies. *Osteoarthritis Cartilage*. Nov 2011;19(11):1286-93. doi:10.1016/j.joca.2011.07.015

8. Thomas AC, Hubbard-Turner T, Wikstrom EA, Palmieri-Smith RM. Epidemiology of Posttraumatic Osteoarthritis. *J Athl Train*. Jun 2017;52(6):491-496. doi:10.4085/1062-6050-51.5.08

9. Kuyinu EL, Narayanan G, Nair LS, Laurencin CT. Animal models of osteoarthritis: classification, update, and measurement of outcomes. *J Orthop Surg Res*. Feb 2016;11:19. doi:10.1186/s13018-016-0346-5

10. Christiansen BA, Guilak F, Lockwood KA, et al. Non-invasive mouse models of post-traumatic osteoarthritis. *Osteoarthritis Cartilage*. Oct 2015;23(10):1627-38. doi:10.1016/j.joca.2015.05.009

11. Christiansen BA, Anderson MJ, Lee CA, Williams JC, Yik JH, Haudenschild DR. Musculoskeletal changes following non-invasive knee injury using a novel mouse model of post-traumatic osteoarthritis. *Osteoarthritis Cartilage*. Jul 2012;20(7):773-82. doi:10.1016/j.joca.2012.04.014

12. Poulet B, Hamilton RW, Shefelbine S, Pitsillides AA. Characterizing a novel and adjustable noninvasive murine joint loading model. *Arthritis Rheum*. Jan 2011;63(1):137-47. doi:10.1002/art.27765

13. Duan X, Rai MF, Holguin N, et al. Early changes in the knee of healer and non-healer mice following non-invasive mechanical injury. *J Orthop Res*. 03 2017;35(3):524-536. doi:10.1002/jor.23413

14. Lockwood KA, Chu BT, Anderson MJ, Haudenschild DR, Christiansen BA. Comparison of loading rate-dependent injury modes in a murine model of post-traumatic osteoarthritis. *J Orthop Res*. Jan 2014;32(1):79-88. doi:10.1002/jor.22480

15. Gilbert SJ, Bonnet CS, Stadnik P, Duance VC, Mason DJ, Blain EJ. Inflammatory and degenerative phases resulting from anterior cruciate rupture in a non-invasive murine model of post-traumatic osteoarthritis. *J Orthop Res*. Feb 2018;doi:10.1002/jor.23872

16. Chang JC, Sebastian A, Murugesh DK, et al. Global molecular changes in a tibial compression induced ACL rupture model of post-traumatic osteoarthritis. *J Orthop Res*. 03 2017;35(3):474-485. doi:10.1002/jor.23263

17. Bengtson H, Giangarra C. Osteochondral avulsion fracture of the anterior cruciate ligament femoral origin in a 10-year-old child: a case report. *J Athl Train*. 2011 Jul-Aug 2011;46(4):451-5. doi:10.4085/1062-6050-46.4.451

18. Fayard JM, Sonnery-Cottet B, Vrgoc G, et al. Incidence and Risk Factors for a Partial Anterior Cruciate Ligament Tear Progressing to a Complete Tear After Nonoperative Treatment in Patients Younger Than 30 Years. *Orthop J Sports Med*. Jul 2019;7(7):2325967119856624. doi:10.1177/2325967119856624

19. Temponi EF, de Carvalho Junior LH, Sonnery-Cottet B, Chambat P. Partial tearing of the anterior cruciate ligament: diagnosis and treatment. *Rev Bras Ortop*. Jan-Feb 2015;50(1):9-15. doi:10.1016/j.rboe.2015.02.003

20. Colombet P, Dejour D, Panisset JC, Siebold R, Society FA. Current concept of partial anterior cruciate ligament ruptures. *Orthop Traumatol Surg Res*. Dec 2010;96(8 Suppl):S109-18. doi:10.1016/j.otsr.2010.09.003

21. Bell NS, Mangione TW, Hemenway D, Amoroso PJ, Jones BH. High injury rates among female army trainees: a function of gender? *Am J Prev Med*. Apr 2000;18(3 Suppl):141-6. doi:10.1016/s0749-3797(99)00173-7

22. The female ACL: Why is it more prone to injury? *J Orthop*. Jun 2016;13(2):A1-4. doi:10.1016/S0972-978X(16)00023-4

23. Foley PL, Liang H, Crichlow AR. Evaluation of a sustained-release formulation of buprenorphine for analgesia in rats. *J Am Assoc Lab Anim Sci*. Mar 2011;50(2):198-204.

24. Blaker CL, Ashton DM, Doran N, Little CB, Clarke EC. Sex- and injury-based differences in knee biomechanics in mouse models of post-traumatic osteoarthritis. *J Biomech*. 01 04 2021;114:110152. doi:10.1016/j.jbiomech.2020.110152

25. van Osch GJ, Blankevoort L, van der Kraan PM, et al. Laxity characteristics of normal and pathological murine knee joints in vitro. *J Orthop Res*. Sep 1995;13(5):783-91. doi:10.1002/jor.1100130519

26. Wang VM, Banack TM, Tsai CW, Flatow EL, Jepsen KJ. Variability in tendon and knee joint biomechanics among inbred mouse strains. *J Orthop Res*. Jun 2006;24(6):1200-7. doi:10.1002/jor.20167

27. Ruan MZ, Dawson B, Jiang MM, Gannon F, Heggeness M, Lee BH. Quantitative imaging of murine osteoarthritic cartilage by phase-contrast micro-computed tomography. *Arthritis Rheum*. Feb 2013;65(2):388-96. doi:10.1002/art.37766

28. Xu H, Bouta EM, Wood RW, Schwarz EM, Wang Y, Xing L. Utilization of longitudinal ultrasound to quantify joint soft-tissue changes in a mouse model of posttraumatic osteoarthritis. *Bone Res*. 2017;5:17012. doi:10.1038/boneres.2017.12

29. Lim NH, Wen C, Vincent TL. Molecular and structural imaging in surgically induced murine osteoarthritis. *Osteoarthritis Cartilage*. 07 2020;28(7):874-884. doi:10.1016/j.joca.2020.03.016

30. Knipe H, Bell DJ. Osteoarthritis of the knee. Radiopaedia.org. 2022. https://radiopaedia.org/articles/37587

31. Glasson SS, Chambers MG, Van Den Berg WB, Little CB. The OARSI histopathology initiative - recommendations for histological assessments of osteoarthritis in the mouse. *Osteoarthritis Cartilage*. Oct 2010;18 Suppl 3:S17-23. doi:10.1016/j.joca.2010.05.025

32. Faul F, Erdfelder E, Lang AG, Buchner A. G*Power 3: a flexible statistical power analysis program for the social, behavioral, and biomedical sciences. *Behav Res Methods*. May 2007;39(2):175-91. doi:10.3758/bf03193146

33. Schatzmann L, Brunner P, Stäubli HU. Effect of cyclic preconditioning on the tensile properties of human quadriceps tendons and patellar ligaments. *Knee Surg Sports Traumatol Arthrosc*. 1998;6 Suppl 1:S56-61. doi:10.1007/s001670050224

34. Teramoto A, Luo ZP. Temporary tendon strengthening by preconditioning. *Clin Biomech (Bristol, Avon)*. Jun 2008;23(5):619-22. doi:10.1016/j.clinbiomech.2007.12.001

35. Khorasani MS, Diko S, Hsia AW, et al. Effect of alendronate on post-traumatic osteoarthritis induced by anterior cruciate ligament rupture in mice. *Arthritis Res Ther*. Feb 2015;17:30. doi:10.1186/s13075-015-0546-0

36. Hunter DJ, Lohmander LS, Makovey J, et al. The effect of anterior cruciate ligament injury on bone curvature: exploratory analysis in the KANON trial. *Osteoarthritis Cartilage*. Jul 2014;22(7):959-68. doi:10.1016/j.joca.2014.05.014

37. Neogi T, Bowes MA, Niu J, et al. Magnetic resonance imaging-based three-dimensional bone shape of the knee predicts onset of knee osteoarthritis: data from the osteoarthritis initiative. *Arthritis Rheum*. Aug 2013;65(8):2048-58. doi:10.1002/art.37987

38. Reichenbach S, Guermazi A, Niu J, et al. Prevalence of bone attrition on knee radiographs and MRI in a community-based cohort. *Osteoarthritis Cartilage*. Sep 2008;16(9):1005-10. doi:10.1016/j.joca.2008.02.001

39. van Meer BL, Oei EH, Meuffels DE, et al. Degenerative Changes in the Knee 2 Years After Anterior Cruciate Ligament Rupture and Related Risk Factors: A Prospective Observational Follow-up Study. *Am J Sports Med*. Jun 2016;44(6):1524-33. doi:10.1177/0363546516631936

40. Fratzl P. *Collagen structure and mechanics*. Springer,; 2008:1 online resource (xviii, 506 p.). https://go.openathens.net/redirector/unimelb.edu.au?url=http%3A%2F%2Fdx.doi.org%2F10.1007%2F978-0-387-73906-9 Connect to ebook (University of Melbourne only) SpringerLink

41. Hess T, Rupp S, Hopf T, Gleitz M, Liebler J. Lateral tibial avulsion fractures and disruptions to the anterior cruciate ligament. A clinical study of their incidence and correlation. *Clin Orthop Relat Res*. Jun 1994;(303):193-7.

42. Holguin N, Brodt MD, Sanchez ME, Kotiya AA, Silva MJ. Adaptation of tibial structure and strength to axial compression depends on loading history in both C57BL/6 and BALB/c mice. *Calcif Tissue Int*. Sep 2013;93(3):211-21. doi:10.1007/s00223-013-9744-4

43. Blaker CL, Little CB, Clarke EC. Joint loads resulting in ACL rupture: Effects of age, sex, and body mass on injury load and mode of failure in a mouse model. *J Orthop Res*. 08 2017;35(8):1754-1763. doi:10.1002/jor.23418

44. Friel NA, Chu CR. The role of ACL injury in the development of posttraumatic knee osteoarthritis. *Clin Sports Med*. Jan 2013;32(1):1-12. doi:10.1016/j.csm.2012.08.017

45. Øiestad BE, Engebretsen L, Storheim K, Risberg MA. Knee osteoarthritis after anterior cruciate ligament injury: a systematic review. *Am J Sports Med*. Jul 2009;37(7):1434-43. doi:10.1177/0363546509338827

46. Shabani B, Bytyqi D, Lustig S, Cheze L, Bytyqi C, Neyret P. Gait changes of the ACL-deficient knee 3D kinematic assessment. *Knee Surg Sports Traumatol Arthrosc*. Nov 2015;23(11):3259-65. doi:10.1007/s00167-014-3169-0

47. March L, Smith EU, Hoy DG, et al. Burden of disability due to musculoskeletal (MSK) disorders. *Best Pract Res Clin Rheumatol*. Jun 2014;28(3):353-66. doi:10.1016/j.berh.2014.08.002

48. Anderson MJ, Diko S, Baehr LM, Baar K, Bodine SC, Christiansen BA. Contribution of mechanical unloading to trabecular bone loss following non-invasive knee injury in mice. *J Orthop Res*. 10 2016;34(10):1680-1687. doi:10.1002/jor.23178

49. Jacobs BY, Kloefkorn HE, Allen KD. Gait analysis methods for rodent models of osteoarthritis. *Curr Pain Headache Rep*. Oct 2014;18(10):456. doi:10.1007/s11916-014-0456-x

50. Shultz SJ, Sander TC, Kirk SE, Perrin DH. Sex differences in knee joint laxity change across the female menstrual cycle. *J Sports Med Phys Fitness*. Dec 2005;45(4):594-603.

51. Boguszewski DV, Cheung EC, Joshi NB, Markolf KL, McAllister DR. Male-Female Differences in Knee Laxity and Stiffness: A Cadaveric Study. *Am J Sports Med*. Dec 2015;43(12):2982-7. doi:10.1177/0363546515608478

52. Temponi EF, de Carvalho Júnior LH, Sonnery-Cottet B, Chambat P. Partial tearing of the anterior cruciate ligament: diagnosis and treatment. *Rev Bras Ortop*. 2015 Jan-Feb 2015;50(1):9-15. doi:10.1016/j.rboe.2015.02.003

53. Duthon VB, Barea C, Abrassart S, Fasel JH, Fritschy D, Ménétrey J. Anatomy of the anterior cruciate ligament. *Knee Surg Sports Traumatol Arthrosc*. Mar 2006;14(3):204-13. doi:10.1007/s00167-005-0679-9

Chapter 3: TLR4 Antagonism Provides Short Term but Not Long-Term Clinical Benefit in a Full Depth Cartilage Defect Mouse Model

3.1 Overview

Post-traumatic osteoarthritis (PTOA) is a debilitating condition affecting millions of people worldwide. As there is currently no cure for this ailment, novel therapies are needed to suppress the progression of pathology after joint injury. *Our central premise is that sterile inflammation mediated via damage associated molecular patterns (DAMPs) and, subsequently, the Toll-like receptor 4 (TLR4) pathway is a principal driver in the early progression of PTOA*. We postulate that TLR4 activation is initiated/perpetuated by damage associated molecular patterns released following joint damage. Thus, antagonism of the TLR4 pathway or treatment with a TLR4 antagonist immediately after injury may suppress the development of PTOA. To test this theory, four groups were utilized: (1) 8-week-old, wild type mice treated with a known TLR4 antagonist; (2) and mice injected with a vehicle control. The right knee of each mouse was scraped with an 18g needle on the midline of the patellofemoral groove to produce a full-depth cartilage lesion. The left knee was used as a sham surgery control. Using a quantitative gait analysis system, we evaluated gait changes over time. Following study completion, animals were harvested, and knee joints were processed for Nanostring® gene expression and pathologic assessment. We found that short term treatment with a systemic antagonist of TLR4 significantly improved relevant gait parameters, and improved cartilage metrics and modified Mankin OA scores implying modification of clinical signs. Additionally, gene analyses showed reduced expression of inflammatory

genes in animals treated with the TLR4 antagonist at 2-weeks post-injury. Collectively, this work demonstrates that systemic treatment with a TLR4 antagonist mitigates osteoarthritis 14-days post-injury in a murine model of induced disease.

3.2 Introduction

Post-traumatic osteoarthritis (PTOA) is a debilitating, degenerative condition affecting more than 5.6 million people in the United States[1,2]. Following injury to the knee, a person is 4.2 times more likely to develop PTOA in that joint, compared to an uninjured joint[2,3]. PTOA is characterized by clinical symptoms such as pain, swelling, and decreased range of motion of the knee or affected joint. As a leading cause of pain and disability, PTOA is a major contributor to a decreased quality of life[4]. Notably, loss of mobility associated with PTOA can increase the risk of a multitude of other ailments including heart disease and diabetes[5]. To date, there is no cure for this disease, which highlights a critical need for novel therapies to mitigate the progression of pathology of OA after injury. Current treatments for PTOA, such as nonsteroidal anti-inflammatory drugs (NSAIDs) and corticosteroids, do not change the progression of the disease but help to alleviate symptoms. Unfortunately, long-term administration of these drugs is associated with severe adverse side effects[6].

For this study, we focused on injury-induced sterile inflammation associated with PTOA[7-9], with an emphasis on innate immune responses mediated through the toll-like receptor 4 (TLR4) pathway. Toll-like receptors are a critical aspect of the innate immune system. They belong to a class of receptors called pattern-recognition receptors and are

responsible for recognizing conserved or invariable structures known as pathogen-associated molecular patterns. Some TLRs, such as TLR4, can also detect some host-derived molecules that occur following injury called damage-associated molecular patterns (DAMPs)[10,11]. Importantly, TLR4 is highly expressed by a variety of immune cells including macrophages, monocytes, and dendritic cells[12]. Cells within the joint also express TLR4 including chondrocytes, synoviocytes and osteoblasts and it has also been shown that TLR4 is increased within the cartilage during the development of OA, indicating a probable role for TLR4 during OA progression[6]. While the role of TLR4 in recognizing bacterial pathogens through recognition of their lipopolysaccharide (LPS) membrane and the associated signaling cascade is well established[6,13-15], it is established that other molecules that may bind the TLR4 receptor, thereby initiating a negative innate immune system response.

We expect that TLR4 activation is initiated and perpetuated by the release of extracellular matrix fragments, such as low molecular weight fragments of hyaluronan and fibronectin, as well as released intracellular proteins and fractionated blood products[16]. These molecules are collectively known as damaged associated molecular patterns (DAMPs), which are released after tissue damage. TLR4 is not only found on immune cells[6,17], but this receptor is also expressed on chondrocytes[18], synoviocytes[11] and osteoblasts[19], indicating a role in joint morphology and a potential role in OA.

Importantly, a variety of TLRs, including TLR4, are upregulated in OA patient synovium[20,21], which is important as synovitis has been correlated with severity of

cartilage damage[22]. TLR4 has also been shown to be increased in the cartilage of OA patients[23,24], including damaged areas of cartilage[25]. As cartilage damage is a hallmark feature of OA progression, the mouse model used in this study utilizes a mouse full depth cartilage regeneration model[26], which creates a cartilage lesion without added joint instability. Utilization of this model allows for the assessment of TLR4 antagonism as a potential way to decrease sterile inflammation leading to decreased chondrocyte apoptosis, collagen degradation and other cartilage specific features of PTOA progression.

Prior studies have demonstrated that short term administration of a TLR4 antagonist in a sodium mono-iodacetate induced rat model of joint degeneration showed decreased movement-induced nociception; however, no effect on cartilage loss was noted at up to 2 weeks following antagonist administration[27]. Additionally, a mouse model of lower back pain and disc degeneration demonstrated that chronic TLR4 antagonism decreased behavioral signs of back pain and decreased secretion of proinflammatory cytokines[28]. To date, however, few TLR4 PTOA studies have focused on cartilage repair and defect at early time points. Current published TLR4 knockout studies show potentially conflicting and contradictory results. A TLR4 knockout study of PTOA induced by knee meniscectomy did not see a difference in cartilage lesions, synovial inflammation, and cartilage metabolism at 8-weeks post-surgery[29]. Additionally, a destabilization of the medial meniscus study concluded similar results after 16 weeks post-surgery[30]. Interestingly, studies looking at shorter timepoints in a temporal-mandibular joint (TMJ) OA model saw that inhibition of TLR4 decreased cartilage

damage in the model[31]. Therefore, for this study, we focused on TLR4 antagonism at early timepoints in a PTOA model.

Our central premise is that sterile inflammation mediated via DAMPs and, subsequently, the Toll-like receptor 4 pathway is a principal driver in the early stages of PTOA progression. We hypothesized that animals injected with a TLR4 antagonist will have decreased whole knee joint histopathology scores after post-traumatic injury compared to saline injected animals along with improved healing of the full depth cartilage lesion, with benefit primarily seen at earlier timepoints.

3.3 Materials and Methods

Animals

All procedures were conducted in accordance with the Guide for the Care and Use of Laboratory Animals and approved by the university's Institutional Animal Care and Use Committee. Thirty-two 8-week-old, male C57Bl/6J mice (Jackson Laboratories) were used in this study. All mice were group housed in solid bottom cages and allowed ad libitum water and standard rodent chow. Animals were housed at a 12-12h light-dark cycle, 20-26° C temperature, and 30-70% humidity. Mice were assessed by a veterinarian daily. Animals were euthanized via CO_2 inhalation and confirmed by cervical dislocation at designated time points.

Strategy

Mice were randomly assigned to two groups of 16 mice: (1) negative control group, receiving intraperitoneal saline, only; and (2) treatment group, receiving intraperitoneal injections of lipopolysaccharide from *Rhodobacter sphaeroides* (ultrapure LPS-RS), a well-characterized TLR4 antagonist [32,33]. Animals were evaluated at 2-weeks and 4-weeks post-surgery (n=8/group per time point).

Surgical manipulation of the knee joint

The right knee of 8-week old male mice were injured utilizing a previously published surgical injury model[26]. 8-week-old mice were used to match the aforementioned study. After medial parapatellar arthrotomy, the patella was luxated laterally, permitting access to the femoral groove. Cartilage was removed from the midline of the femoral groove via a single, controlled “scraping” motion with an 18g needle that has been modified to provide uniform defect depth. The patella was repositioned, and the incision closed. An identical sham procedure, without cartilage defect, was performed on the left knee, which served as an internal control for each animal.

Intraperitoneal injection of LPS-RS

The dose and frequency of ultrapure LPS-RS in this study has been previously shown to be effective in blocking TLR4[32,33]. Each mouse in the treatment group received 1 μg LPS-RS (Invitrogen) in 100 μL sterile saline via intraperitoneal injection every 3 days until termination starting immediately after surgery. Negative control mice received an intraperitoneal injection of an equivalent volume of sterile saline. Alternative doses and

frequency of LPS-RS administration were evaluated in a pilot study **(Supplemental Figure 3.1)**; however, increased benefit was not observed to justify modifying dosage for this study.

Gait analysis to determine functional mobility

Videographic gait analysis is an objective, sensitive, and reproducible means of monitoring joint pathology in rodent models of OA, particularly when a treadmill is utilized to normalize walking speeds[34]. This technique has been shown to be reliable for clinically relevant evaluation of movement-related nociception, the hallmark of OA-induced pain[35]. Animals were acclimated to a treadmill-based gait analysis system DigiGait™ (Mouse Specifics, Inc., Framingham, MA) over 1 week, during which baseline was collected, with data collection occurring on days 7, 14, 21, and 27 post-surgery. The order of which animals were utilized for gait analysis at each time point was randomly selected. Paw statistics, automatically calculated by associated software, were collected for all mice walking at 30 cm/s at 0 degrees incline. Prioritized gait parameters included: Stance (s), Brake (s), Propel (s) and min dA/dt (a measure of the maximal rate of change of paw area during the propulsion phase, an indication of a clinical “limp”); additional parameters provided in **Supplemental Figure 3.2.**

Macroscopic imaging of femoral joint pathology

Knee joint tissues were dissected with care to avoid damage to articular surfaces and preserve peri-articular tissues. India Ink was applied to all surfaces followed by surface photography using a VWR Trinocular inverted microscope with a Moticam X wireless

camera and the Motic Live Imaging Module (Richmond, BC). India ink was used to visualize damage to the patellofemoral groove as it adheres to damaged tissues. High-resolution photography focused on the areas of the femoral groove that were damaged during injury **(Supplemental Figure 3.3)**.

Histologic assessment of knee joints

Structural and histopathological evaluation of the articular cartilage of the surface of the patellofemoral groove was performed. Limbs were fixed in 10% neutral buffered formalin followed by decalcification in EDTA/PBS and paraffin embedding. Five μm transverse sections were cut on a microtome, deparaffinized, and stained with Safranin-O/Fast Green. A veterinary pathologist (KSS) graded sections using the modified Mankin score[36]. Abnormalities were evaluated blinded to experimental group, paying particular attention to patella groove margins and any associated cartilage surface changes (new deposition, roughening, or erosion). Additional measurements of stained histology sections were made using Olympus cellSens software (Olympus Life Science).

Gene expression of knee joints using NanoString technology

Total RNA was extracted from remaining joint structures, sans femur, using TRIzol reagent and RNeasy Mini Kit (Qiagen, Hilden, Germany). Tissue was homogenized using a Qiagen TissueLyser and spherical ball bearings kit. RNA was quantified spectrophotometrically with a NanoDrop™ 2000 (ThermoFisher Scientific, Waltham, MA). Total RNA was sent to the University of Arizona Genetics Core for analysis. The

premade mouse nCounter® Inflammation Panel by NanoString was utilized to evaluate total RNA. Data analysis was performed using nSolver™ software provided by NanoString Technologies. Results, reported as absolute transcript counts, were normalized to standard mouse housekeeping genes.

Statistical Analyses

All data was subjected to normality testing via the Shapiro-Wilk test. Gait analysis was performed by two-way ANOVA and mixed-effects analysis with Sidak correction. Histopathology scoring and measurements was assessed by two-way ANOVA with Sidak correction for multiple comparisons. For Nanostring data, a two-way ANOVA and multiple comparisons with Sidak correction was performed to view between group differences. Statistical significance was set at $P < 0.05$. All statistical analyses were performed with Prism (version 9.3.1; Graph Pad Software, La Jolla, CA). Genes with an adjusted p-value of <0.1 were aligned with KEGG pathways on string-db.org to determine pathways that included genes of interest. Formal pathway analysis and statistical analysis was not conducted on pathway hits.

3.4 Results

Evaluation of femoral joint pathology

Subjectively, histopathology demonstrated increased Patellofemoral articular cartilage proteoglycan staining in unaffected surfaces but decreased defect fibrocartilage development in mice injected with the TLR4 antagonist **(Figure 1B)** versus vehicle

control **(Figure 1A)**. at 2 weeks post-surgery **(Figure 1B)**. By 4 weeks post-surgery, cartilage healing and proteoglycan staining appeared similar between both sterile saline injected animals and LPS-RS injected animals **(Figure 1C and D)**.

Total modified Mankin OA scoring indicated decreased OA progression at 2-weeks post injury for animals treated with LPS-RS versus sterile saline **(Figure 2A)**. Components of the modified Mankin score showed significant differences between groups at 2-weeks post-injury for cellular abnormalities **(Figure 2C)** and matrix staining **(Figure 2D)**, but not structure score **(Figure 2B)**. Gross evaluation of the joint pathology two-weeks post-surgery demonstrated increased India ink staining in sterile saline treated animals compared to LPS-RS treated animals; no major visual difference between groups was seen by four-weeks post-surgery **(Supplemental Figure 3.3)**.

Features from the stained histopathology sections were measured/quantitated to compare defect and cartilage features between groups **(Figure 3A)**. Interestingly, saline injected control animals did show increased fibrocartilage formation at 2 weeks post-injury **(Figure 3B**, p=0.0190); this was not present at 4 weeks. Measurements of cartilage unaffected by the original defect indicated that average cartilage thickness in animals treated with LPS-RS trended towards thicker cartilage at 2-weeks post-surgery (p=0.0819) and demonstrated significantly increased cartilage thickness by 4 weeks post-surgery **(Figure 3C)**. To determine the proportion of the defect that was filled with fibrocartilage, the percent of the defect that was filled was calculated. At 2-weeks post-injury, sterile saline injected animals trended towards having more %filling than the

LPS-RS injected animals (p=0.0610). Interestingly, this trend reversed by 4-weeks post-injury to show that LPS-RS treated animals had a higher %filled than saline injected animals **(Figure 3D**, p=0.0647). Importantly, consistency in surgical defect creation across animals was confirmed, as: (i) defect depth did not differ between groups **(Figure 3E)** and (ii) no significant differences were noted at either timepoint for average length of remaining articular cartilage **(Figure 3F)**.

Gait analysis to determine functional mobility

Locomotion parameters were assessed using a Digigait treadmill system where mice ran at 30cm/s on a flat surface (0 degrees incline/decline). The Digigait system divides an animal's stride into two main components: swing time (the amount of time during a full stride where the limb is not in contact with the ground) and stance time (the amount of time during which the limb is in contact with the belt). A short-term decrease in stance (s) was seen in the sterile saline group at one-week post-surgery (p=0.004) but resolved at later timepoints **(Figure 4A)**. When subtracted from baseline no significant differences were seen between groups for either swing (s) **(Supplemental Figure 3.2)** or stance (s) **(Figure 4B)**.

The stance stage of an animal's stride can be further broken down into brake and propel. Brake is the portion of the stride when the foot initially touches the belt until the foot is fully flat; the propel portion of the stride starts once the foot is fully flat on the belt until the foot fully comes off the belt. Compared to baseline data (Day 0, immediately prior to surgery), gait analysis revealed increased brake (s) starting at 2 weeks-post

injury for sterile saline injected animals; this persisted through the duration of the study **(Figure 4C)**. LPS-RS treated animals did not show a difference in brake (s) until 3 weeks post injury **(Figure 4C)**. Additionally, after correcting for differences in each animal's individual baseline, brake (s) was different ($p=0.0665$) between LPS-RS treated group compared to control at 2 weeks post-injury **(Figure 4D)**. Complementary results were seen when looking at propel (s). Sterile saline treated animals demonstrated a significantly decreased propel (s) from baseline starting at 1-week post-surgery and persisting through the duration of the study, while LPS-RS treated animals did not differ from baseline until 3 weeks post injury **(Figure 4E)**. Similarly, at 2 weeks post-injury propel (s) was significantly different ($p=0.0169$) between the LPS-RS treated group compared to the sterile saline control group at 2 weeks post-injury **(Figure 4F)**.

Another Digigait parameter of interest is min dA/dt, which indicates how rapidly the animal propels itself onto the next step. A decreased min dA/dt value is indicative of a limp. Sterile saline animals demonstrated a significantly decreased min DA/dt from baseline starting at 1-week post-surgery, which lasted the duration of the study **(Figure 4G)**. In contrast, LPS-RS treated animals-maintained baseline min dA/dt levels until 3 weeks post-surgery **(Figure 4G)**. Importantly, at 2 weeks post-surgery, min dA/dt in LPS-RS treated animals was significantly increased ($p <0.0001$) from sterile saline control animals **(Figure 4H)**.

Gene expression of knee joints

Nanostring gene expression was conducted on remaining knee joint structures, sans femur, using a mouse inflammation panel. A total of 16 genes were different at 2 weeks between saline control animals and LPS-RS treated animals **(Figure 5 and Table 1)**. Genes with an adjusted p-value of <0.1 were aligned with KEGG pathways on string-db.org, and many genes at 2 weeks post-surgery were contained in pathway hits within cytokine-cytokine receptor interaction, IL-17 signaling pathway, complement and coagulation cascades, TNF signaling pathways, and NOD-like receptor signaling pathways **(Table 2)**. By 4 weeks post-surgery, only 2 genes demonstrated significantly different RNA transcript counts between saline control animals and LPS-RS treated animals **(Table 1)**.

3.5 Discussion

This study demonstrated that, at 2 weeks post-surgery, mice injected with the TLR4 antagonist demonstrated decreased OA progression and increased cartilage thickness around the surgical defect. A difference between OA scores between saline control animals and TLR4 antagonist treated animals was no longer visible by 4 weeks post-surgery, although animals treated with LPS-RS persisted in having an increased cartilage thickness. Importantly, the chosen PTOA model provided a full depth cartilage lesion without joint biomechanical instability. This allows us to view TLR4 antagonist effects following cartilage injury, without the added repeated damage that occurs after joint stability is lost.

Prior TLR4 antagonism studies have demonstrated variable and conflicting results. One study saw that TLR4 antagonism 14 to 28 days following OA induction by sodium mono-iodoacetate injection, decreased movement induced nociception but saw no effect on cartilage loss[27]. Similarly, TLR4 knockout mice that had PTOA induction by knee meniscectomy saw no difference in cartilage lesions, synovial inflammation and cartilage metabolism when compared to age-matched menisectomized wild-type mice 8-weeks post-surgery[29]. Another TLR4 knockout study saw similar results following PTOA induction by the destabilization of the medial meniscus (DMM) surgery. After 16 weeks that study concluded that mice were not protected from either mechanical allodynia or DMM associated joint damage[30]. Conversely, a study looking at shorter endpoints with a TMJOA mouse model, saw that injections with a TLR4 inhibitor ameliorated the reduction of cartilage proteoglycans at 2-, 4- and 6- weeks post-OA induction[31]. In the aforementioned study, the most drastically significant results were seen at both 2- and 4- weeks post-OA induction, with results at 6-weeks post-OA induction still being significant. Importantly, in our study, we saw a trend for increased average cartilage thickness around the defect in mice treated with a TLR4 antagonist compared to saline injected control mice at 2-weeks post-surgery. Interestingly, this increase in cartilage thickness persisted to 4-weeks post-surgery. Additionally, mice treated with a TLR4 antagonist showed decreased total modified Mankin score at 2-weeks post-surgery, but not 4-weeks, specifically in the subcategories of cellular abnormalities and matrix staining. We hypothesize, based on our results and historical TLR4 knockout/antagonism findings, that TLR4 plays an early role in PTOA

development. Early intervention with a TLR4 antagonist may be beneficial, with benefits waning further into the course of PTOA progression.

Loss of mobility and painful locomotion are primary complaints from patients suffering from PTOA[4]. As such, tracking mobility and gait related changes is an important complementary assessment of treatment benefit along with histological changes. Videographic gait analysis is an objective, sensitive, and reproducible means of monitoring joint pathology in rodent models of OA, particularly when a treadmill is utilized to normalize walking speeds[34]. This is especially important as histological and radiographical changes and severity of joint changes do not always correlate to the intensity of the clinical symptoms reported by the patient[37]. Importantly, the TLR4 pathway has some nociception association and treatment with a different TLR4 antagonist has been shown to reduce movement-induced nociception in a rat injection-based OA model[27]. Rodents, and other quadrupeds, tend to move with a balanced and symmetrical gait and as such gait analysis systems can be used to access mobility and function[38]. Loss of symmetrical gait and alterations in gait can be an indicator of pain and/or compensation to protect an injured limb[39,40]. Notably, animals treated with LPS-RS maintained gait parameters similar to baseline through 2-weeks post injury. Additionally, saline injected control animals demonstrated a difference in brake (s), propel (s) and Min dA/dt compared to LPS-RS treated animals at 2-weeks post injury, though this difference was mitigated by 4-weeks post injury. As such, it appears that LPS-RS treatments allows for short term, up to 2 weeks, pain modulation, that returns to control levels by 4 weeks post injury.

Nanostring gene expression using the mouse inflammation panel demonstrated decreased RNA counts in inflammatory genes within animals treated with a TLR4 antagonist, primarily at 2 weeks post-injury. Interestingly, KEGG pathway analysis of modulated genes demonstrated that six genes at two-weeks post-injury were direct members of the complement pathways. This is important as the toll like receptor pathways and complement pathways have previously been demonstrated to interact and cross-talk between each other[41]. Interestingly, TLR4 specifically has been shown to regulate extrahepatic complement production[42]. Additionally, a variety of complement factors have been implicated in the joint inflammation seen with OA[43]. As such, treatment with a TLR4 antagonist, decreased inflammatory gene transcripts within the joint.

Other pathways of interest that were decreased at two weeks post-injury with LPS-RS treatment were genes involved in cytokine-cytokine receptor interaction and the IL-17 signaling pathway. We saw a significant decrease in C-C Motif Chemokine Ligand 2 (CCL2, also known as MCP-1), a gene present in both aforementioned pathways, following treatment with LPS-RS compared to saline treated animals at 2 weeks post-surgery. Importantly, TLR4 activation has been directly linked to increased CCL2 production[44]. Other members of these pathways, including C-C Motif Chemokine Ligand 7 (CCL7), have also been implicated in PTOA progression along with CCL2[45,46]. Interestingly, CCL2 has been shown to play a role in post-traumatic osteoarthritis pain in

a destabilization of the medial meniscus mouse model as CCL2 knockout mice demonstrated delayed onset of pain-related behavior[47].

Previous work has suggested that TLR4 signaling in the spine contributes to neuropathic sensitivity in male, but not female mice[48]. In contrast, when LPS-RS was injected into the hind paw, equivalent allodynia results were viewed in both sexes[48]. As this study focused exclusively on male mice, future work will be required to determine if similar results are found with systemic injection of LPS-RS, a TLR4 antagonist, in female mice. Additionally, this study utilized systemic intraperitoneal injections of the TLR4 antagonist. There is the possibility that intraarticular injections may give more robust and longer lasting therapeutic effects, as it may allow for the TLR4 antagonist to affect the tissue and location of interest more specifically and directly. The authors would also like to reiterate that the model used for this study was intended to examine proof of principle from a cartilage perspective. A full defect cartilage model does not provide any clinical model relevance but allowed us to examine TLR4 antagonism on cartilage response in the absence of joint instability.

Collectively, this work demonstrates that systemic treatment with a TLR4 antagonist mitigates osteoarthritis 14-days post-injury in a murine model of induced disease. Therefore, we support our hypothesis that TLR4 activation contributes to the pathogenesis of PTOA. Importantly, TLR4 antagonism provides short, but not long-term clinical benefit in a full depth cartilage lesion model of post-traumatic osteoarthritis. Gene expression profiling showed a decrease in inflammatory genes, including several

within the toll-like receptor pathway in mice injected with a TLR4 antagonist. Given this, we conclude that post-injury interruption of the TLR-DAMP interaction may serve as a novel therapy for preventing the onset and progression of secondary osteoarthritis. Additionally, future work should look at producing a ‘cocktail’ or sequentially timed administration of antagonists and drugs for extended clinical improvement.

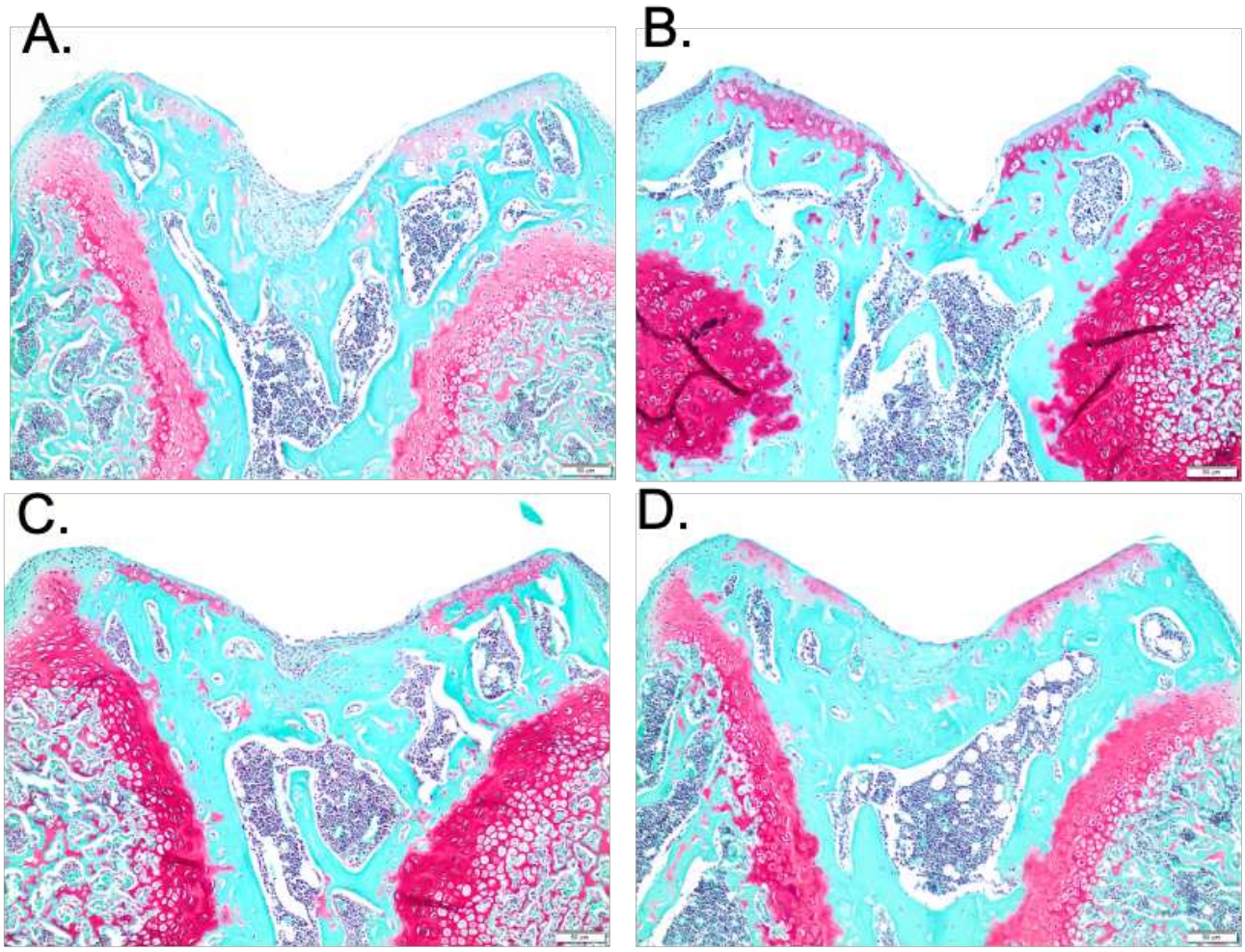

Figure 3.1: Safranin O/Fast green stained photomicrographs from sterile saline injected animals (left) and TLR4 antagonist injected animals (right). Images of femoral condyles for evaluation of cartilage and defect surfaces. Representative image of animals two-weeks post-injury (top) treated with sterile saline **(A)** or LPS-RS **(B)**. Animals four-weeks post-injury (bottom) treated with sterile saline **(C)** or LPS-RS **(D)**. *10X, bar = 50um.*

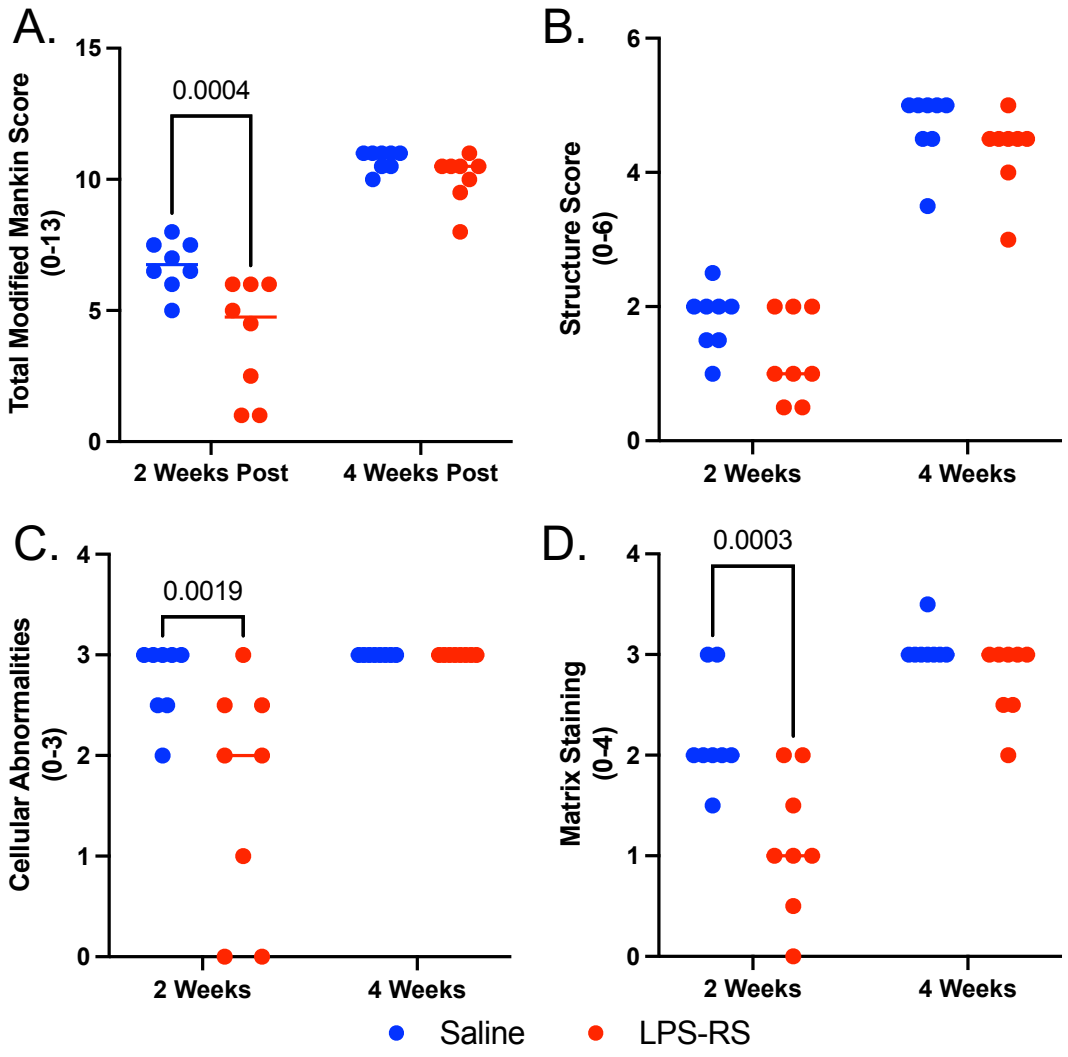

Figure 3.2: Modified Mankin histopathology scores following a full cartilage defect and treatment with sterile saline (blue) or LPS-RS (red). Parameters listed include total modified Mankin score **(A)**, structure score **(B)**, cellular abnormalities score **(C)**, and matrix staining score **(D)**. Significant differences are labeled with p-values <0.05.

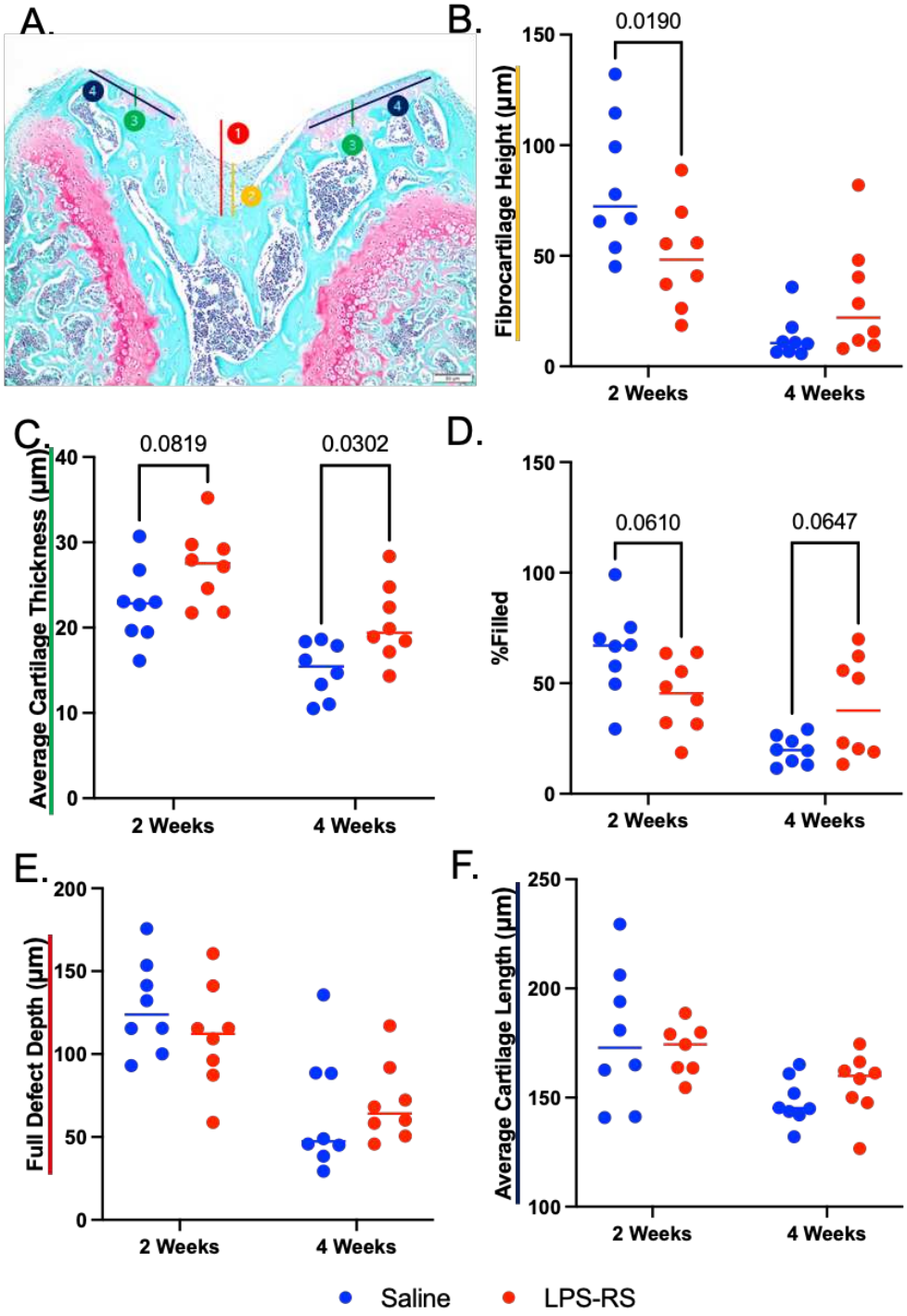

Figure 3.3: Measurements of histopathology images. Representative image with measurement locations noted **(A)**, measurement legend as follows (1) full defect depth, (2) fibrocartilage height, (3) cartilage height, and (4) cartilage length. Measured parameters listed following treatment with sterile saline (blue) or LPS-RS (red) include fibrocartilage height **(B)**, average cartilage thickness **(C)**, %filled (calculated as fibrocartilage height, divided by full defect depth, times 100) **(D)**, full defect depth **(E)**, and average cartilage length **(F)**. P-values <0.1 are notated on figures B-F.

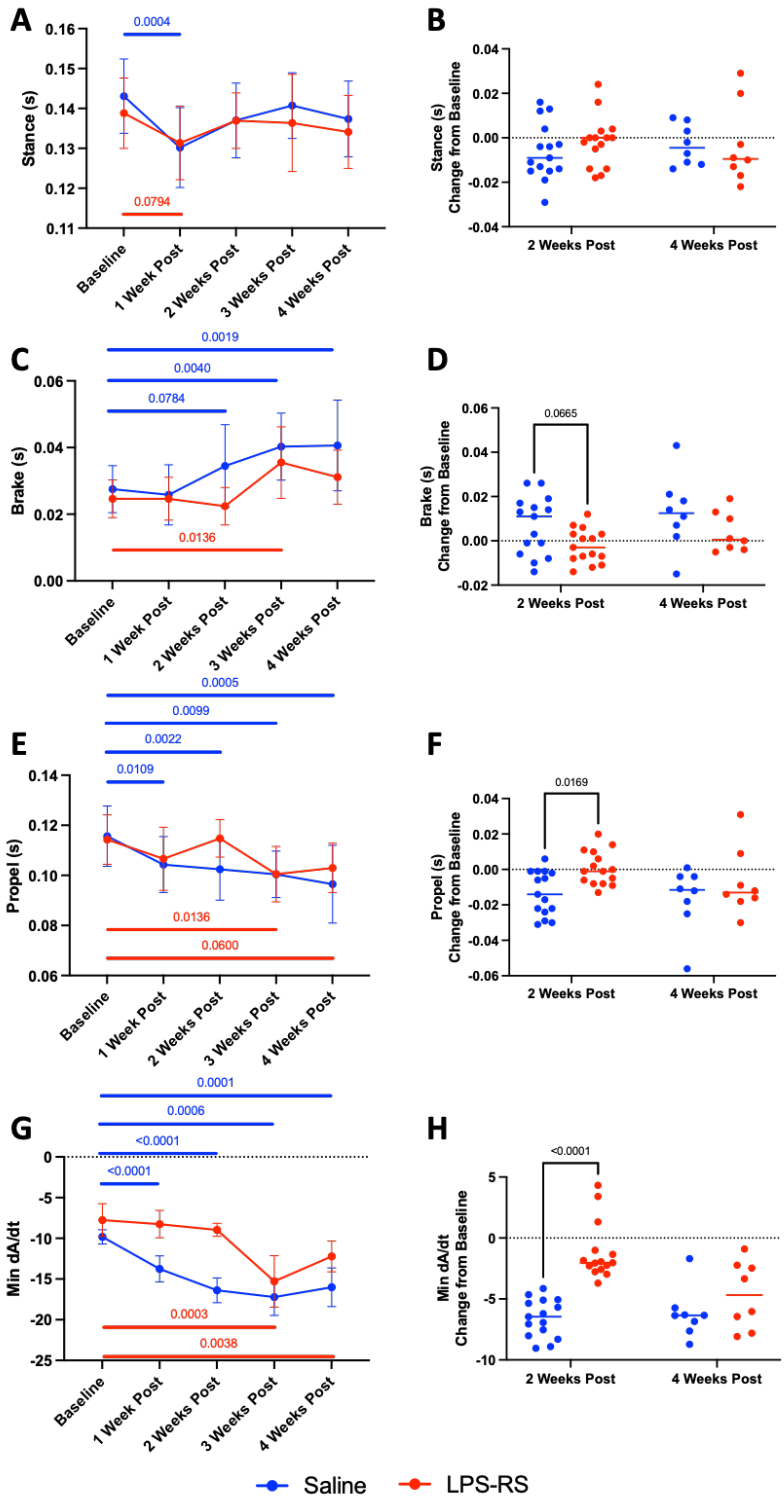

Figure 3.4: Digigait controlled treadmill walking at 30cm/s at a 0-degree inclined/declined (flat). Parameters of interest are shown both overtime and between groups for stance (s) **(A, B)**, brake (s) **(C, D)**, propel (s) **(E, F)**, and Min dA/dt **(G, H)**. Sterile Saline treated animals are labeled in blue with LPS-RS treated animals labeled in red. Significant differences noted, with p-values shown <0.1.

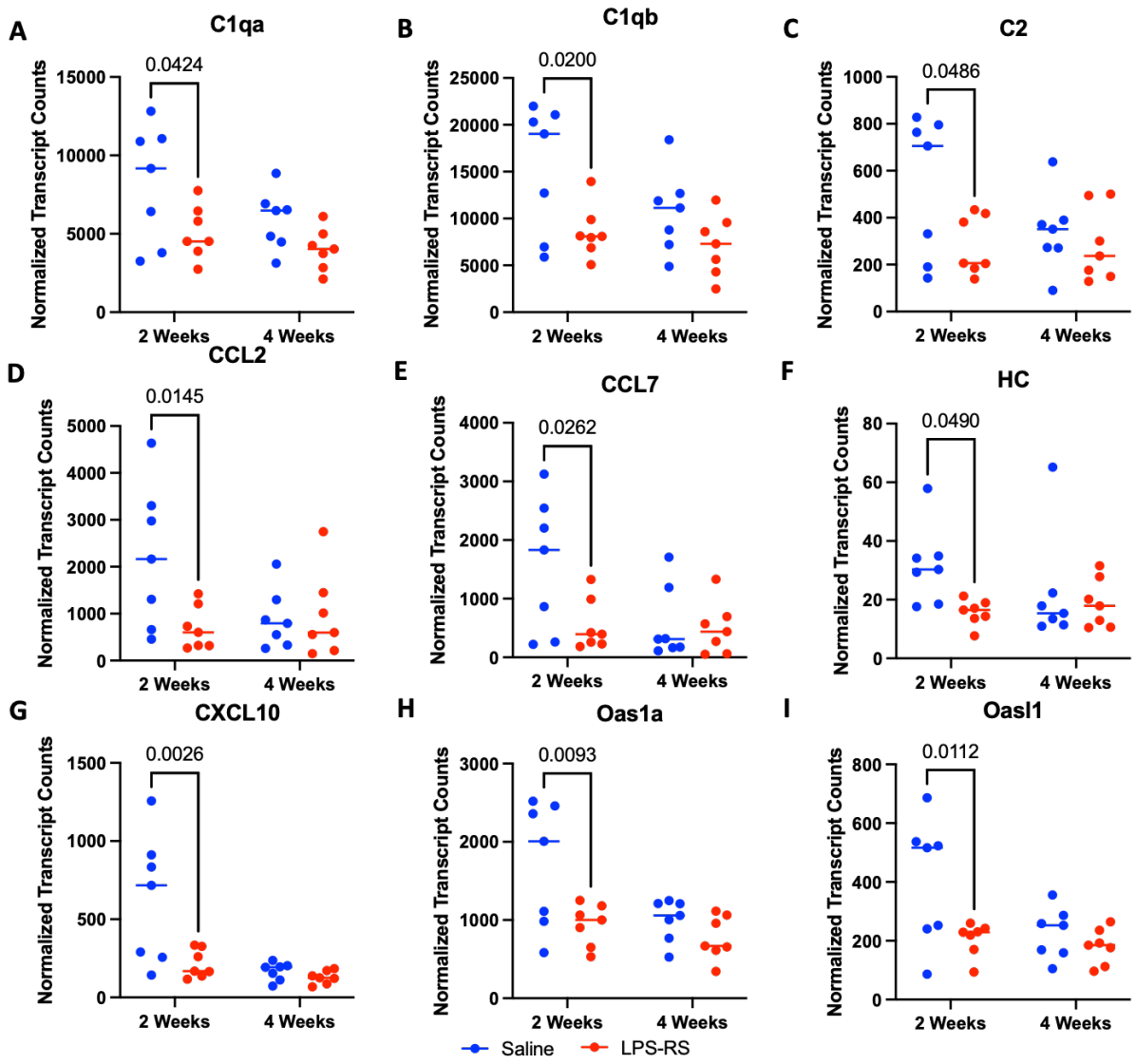

Figure 3.5: NanoString gene analysis of specific inflammatory genes following treatment with either sterile saline (blue) or LPS-RS (red). Gene expression levels are expressed as normalized transcript counts. Some genes of interest are presented including Complement C1q A Chain (C1qa) **(A)**, Complement C1q B Chain (C1qb) **(B)**, Complement C2 (C2) **(C)**, C-C Motif Chemokine Ligand 2 (CCL2) **(D)**, C-C Motif Chemokine Ligand 7 (CCL7) **(E)**, Hemolytic Complement (HC) **(F)**, C-X-C motif chemokine ligand 10 (CXCL10) **(G)**, 2'-5' oligoadenylate synthetase 1A (Oas1a) **(H)**, and 2'-5' oligoadenylate synthetase-like 1 (Oasl1) **(I)**. Significant differences noted, with p-values shown <0.1.

Table 3.1: Table of NanoString genes with an adjusted p-value of <0.05 at either 2- or 4-weeks post-injury

Gene Name	Gene Symbol	Timepoint Significant	Adjusted p-value	Decreased in LPS-RS treated group
C-X-C motif chemokine ligand 10	CXCL10	2 Weeks	0.0026	YES
2'-5' oligoadenylate synthetase 1A	Oas1a	2 Weeks	0.0093	YES
2'-5' oligoadenylate synthetase-like 1	Oasl1	2 Weeks	0.0112	YES
Interferon-induced protein 44	IFI44	2 Weeks	0.0113	YES
C-C Motif Chemokine Ligand 2	Ccl2	2 Weeks	0.0145	YES
Complement C1q B Chain	C1qb	2 Weeks	0.02	YES
C-C Motif Chemokine Ligand 8	Ccl8	2 Weeks	0.0219	YES
Interferon-Inducible GTPase 1	IIGP1	2 Weeks	0.0242	YES
C-C Motif Chemokine Ligand 7	Ccl7	2 Weeks	0.0262	YES
Nitric Oxide Synthase 2	Nos2	2 Weeks	0.0389	YES
Complement C1q A Chain	C1qa	2 Weeks	0.0424	YES
Interferon induced protein with tetratricopeptide repeats 3	Ifit3	2 Weeks	0.0438	YES
Complement C3a Receptor 1	C3AR1	2 Weeks	0.0446	YES
Interferon-induced protein with tetratricopeptide repeats 1	Ifit1	2 Weeks	0.0457	YES
Complement C2	C2	2 Weeks	0.0486	YES
Hemolytic Complement	HC	2 Weeks	0.049	YES
Heat shock protein beta-1	HSPB1	4 Weeks	0.0223	YES
CCAAT Enhancer Binding Protein Beta	CEBPB	4 Weeks	0.0313	YES

Table 3.2: Table of KEGG Pathway hits on genes with an adjusted p-value of <0.1 at 2 weeks post-injury

KEGG Pathway	Number of Genes with adjusted p-value <0.1 in pathway	Genes
Cytokine-cytokine receptor interaction	7	Ccl2, Ccl7, Ccl8, Ccl11, Ccl20, Cxcl10, Ilr1
IL-17 signaling pathway	6	Ccl2, Ccl7, Ccl11, Ccl20, Cxcl10, Mmp3
Complement and coagulation cascades	6	C1qa, C1qb, C2, C3ar1, Cfb, HC
TNF signaling pathway	4	Ccl2, Ccl20, Cxcl10, Mmp3
NOD-like receptor signaling pathway	4	Ccl2, Irf7, Oas1a, Oas2

3.6 References

1. Brown TD, Johnston RC, Saltzman CL, Marsh JL, Buckwalter JA. Posttraumatic osteoarthritis: a first estimate of incidence, prevalence, and burden of disease. *J Orthop Trauma*. 2006 Nov-Dec 2006;20(10):739-44. doi:10.1097/01.bot.0000246468.80635.ef

2. Thomas AC, Hubbard-Turner T, Wikstrom EA, Palmieri-Smith RM. Epidemiology of Posttraumatic Osteoarthritis. *J Athl Train*. Jun 2017;52(6):491-496. doi:10.4085/1062-6050-51.5.08

3. Muthuri SG, McWilliams DF, Doherty M, Zhang W. History of knee injuries and knee osteoarthritis: a meta-analysis of observational studies. *Osteoarthritis Cartilage*. Nov 2011;19(11):1286-93. doi:10.1016/j.joca.2011.07.015

4. March L, Smith EU, Hoy DG, et al. Burden of disability due to musculoskeletal (MSK) disorders. *Best Pract Res Clin Rheumatol*. Jun 2014;28(3):353-66. doi:10.1016/j.berh.2014.08.002

5. Turkiewicz A, Kiadaliri AA, Englund M. Cause-specific mortality in osteoarthritis of peripheral joints. *Osteoarthritis Cartilage*. 06 2019;27(6):848-854. doi:10.1016/j.joca.2019.02.793

6. Gómez R, Villalvilla A, Largo R, Gualillo O, Herrero-Beaumont G. TLR4 signalling in osteoarthritis--finding targets for candidate DMOADs. *Nat Rev Rheumatol*. Mar 2015;11(3):159-70. doi:10.1038/nrrheum.2014.209

7. Stolberg-Stolberg J, Boettcher A, Sambale M, et al. Toll-like receptor 3 activation promotes joint degeneration in osteoarthritis. *Cell Death Dis*. 03 11 2022;13(3):224. doi:10.1038/s41419-022-04680-5

8. Barreto G, Manninen M, K Eklund K. Osteoarthritis and Toll-Like Receptors: When Innate Immunity Meets Chondrocyte Apoptosis. *Biology (Basel)*. Mar 30 2020;9(4)doi:10.3390/biology9040065

9. Chen GY, Nuñez G. Sterile inflammation: sensing and reacting to damage. *Nat Rev Immunol*. Dec 2010;10(12):826-37. doi:10.1038/nri2873

10. Juarranz Y, Gutiérrez-Cañas I, Arranz A, et al. VIP decreases TLR4 expression induced by LPS and TNF-alpha treatment in human synovial fibroblasts. *Ann N Y Acad Sci*. Jul 2006;1070:359-64. doi:10.1196/annals.1317.045

11. Midwood K, Sacre S, Piccinini AM, et al. Tenascin-C is an endogenous activator of Toll-like receptor 4 that is essential for maintaining inflammation in arthritic joint disease. *Nat Med*. Jul 2009;15(7):774-80. doi:10.1038/nm.1987

12. Chang EJ, Kim HJ, Ha J, et al. Hyaluronan inhibits osteoclast differentiation via Toll-like receptor 4. *J Cell Sci*. Jan 01 2007;120(Pt 1):166-76. doi:10.1242/jcs.03310

13. Gangloff M. Different dimerisation mode for TLR4 upon endosomal acidification? *Trends Biochem Sci*. Mar 2012;37(3):92-8. doi:10.1016/j.tibs.2011.11.003

14. Akira S, Takeda K. Toll-like receptor signalling. *Nat Rev Immunol*. Jul 2004;4(7):499-511. doi:10.1038/nri1391

15. Takeda K, Akira S. TLR signaling pathways. *Semin Immunol*. Feb 2004;16(1):3-9. doi:10.1016/j.smim.2003.10.003

16. Nair A, Kanda V, Bush-Joseph C, et al. Synovial fluid from patients with early osteoarthritis modulates fibroblast-like synoviocyte responses to toll-like receptor 4 and toll-like receptor 2 ligands via soluble CD14. *Arthritis Rheum*. Jul 2012;64(7):2268-77. doi:10.1002/art.34495

17. Medzhitov R, Preston-Hurlburt P, Janeway CA. A human homologue of the Drosophila Toll protein signals activation of adaptive immunity. *Nature*. Jul 24 1997;388(6640):394-7. doi:10.1038/41131

18. Wang P, Zhu F, Tong Z, Konstantopoulos K. Response of chondrocytes to shear stress: antagonistic effects of the binding partners Toll-like receptor 4 and caveolin-1. *FASEB J*. Oct 2011;25(10):3401-15. doi:10.1096/fj.11-184861

19. Kikuchi T, Matsuguchi T, Tsuboi N, et al. Gene expression of osteoclast differentiation factor is induced by lipopolysaccharide in mouse osteoblasts via Toll-like receptors. *J Immunol*. Mar 01 2001;166(5):3574-9. doi:10.4049/jimmunol.166.5.3574

20. Tamaki Y, Takakubo Y, Hirayama T, et al. Expression of Toll-like receptors and their signaling pathways in rheumatoid synovitis. *J Rheumatol*. May 2011;38(5):810-20. doi:10.3899/jrheum.100732

21. Ospelt C, Brentano F, Rengel Y, et al. Overexpression of toll-like receptors 3 and 4 in synovial tissue from patients with early rheumatoid arthritis: toll-like receptor expression in early and longstanding arthritis. *Arthritis Rheum*. Dec 2008;58(12):3684-92. doi:10.1002/art.24140

22. Ayral X, Pickering EH, Woodworth TG, Mackillop N, Dougados M. Synovitis: a potential predictive factor of structural progression of medial tibiofemoral knee osteoarthritis -- results of a 1 year longitudinal arthroscopic study in 422 patients. *Osteoarthritis Cartilage*. May 2005;13(5):361-7. doi:10.1016/j.joca.2005.01.005

23. Schelbergen RF, Blom AB, van den Bosch MH, et al. Alarmins S100A8 and S100A9 elicit a catabolic effect in human osteoarthritic chondrocytes that is dependent on Toll-like receptor 4. *Arthritis Rheum*. May 2012;64(5):1477-87. doi:10.1002/art.33495

24. Karlsson C, Dehne T, Lindahl A, et al. Genome-wide expression profiling reveals new candidate genes associated with osteoarthritis. *Osteoarthritis Cartilage*. Apr 2010;18(4):581-92. doi:10.1016/j.joca.2009.12.002

25. Kim HA, Cho ML, Choi HY, et al. The catabolic pathway mediated by Toll-like receptors in human osteoarthritic chondrocytes. *Arthritis Rheum*. Jul 2006;54(7):2152-63. doi:10.1002/art.21951

26. Eltawil NM, De Bari C, Achan P, Pitzalis C, Dell'accio F. A novel in vivo murine model of cartilage regeneration. Age and strain-dependent outcome after joint surface injury. *Osteoarthritis Cartilage*. Jun 2009;17(6):695-704. doi:10.1016/j.joca.2008.11.003

27. Ferreira-Gomes J, Garcia MM, Nascimento D, et al. TLR4 Antagonism Reduces Movement-Induced Nociception and ATF-3 Expression in Experimental Osteoarthritis. *J Pain Res*. 2021;14:2615-2627. doi:10.2147/JPR.S317877

28. Krock E, Millecamps M, Currie JB, Stone LS, Haglund L. Low back pain and disc degeneration are decreased following chronic toll-like receptor 4 inhibition in a mouse model. *Osteoarthritis Cartilage*. 09 2018;26(9):1236-1246. doi:10.1016/j.joca.2018.06.002

29. Nasi S, Ea HK, Chobaz V, et al. Dispensable role of myeloid differentiation primary response gene 88 (MyD88) and MyD88-dependent toll-like receptors (TLRs) in a murine model of osteoarthritis. *Joint Bone Spine*. Jul 2014;81(4):320-4. doi:10.1016/j.jbspin.2014.01.018

30. Miller RE, Belmadani A, Ishihara S, et al. Damage-associated molecular patterns generated in osteoarthritis directly excite murine nociceptive neurons through Toll-like receptor 4. *Arthritis Rheumatol*. Nov 2015;67(11):2933-43. doi:10.1002/art.39291

31. Liu X, Cai HX, Cao PY, et al. TLR4 contributes to the damage of cartilage and subchondral bone in discectomy-induced TMJOA mice. *J Cell Mol Med*. 10 2020;24(19):11489-11499. doi:10.1111/jcmm.15763

32. Baker PJ, Taylor CE, Stashak PW, et al. Inactivation of suppressor T cell activity by the nontoxic lipopolysaccharide of Rhodopseudomonas sphaeroides. *Infect Immun*. Sep 1990;58(9):2862-8.

33. Lu Z, Zhang X, Li Y, Lopes-Virella MF, Huang Y. TLR4 antagonist attenuates atherogenesis in LDL receptor-deficient mice with diet-induced type 2 diabetes. *Immunobiology*. Nov 2015;220(11):1246-54. doi:10.1016/j.imbio.2015.06.016

34. Plaas A, Li J, Riesco J, Das R, Sandy JD, Harrison A. Intraarticular injection of hyaluronan prevents cartilage erosion, periarticular fibrosis and mechanical allodynia and normalizes stance time in murine knee osteoarthritis. *Arthritis Res Ther*. Mar 2011;13(2):R46. doi:10.1186/ar3286

35. Ferreira-Gomes J, Adães S, Mendonça M, Castro-Lopes JM. Analgesic effects of lidocaine, morphine and diclofenac on movement-induced nociception, as assessed by the Knee-Bend and CatWalk tests in a rat model of osteoarthritis. *Pharmacol Biochem Behav*. Jun 2012;101(4):617-24. doi:10.1016/j.pbb.2012.03.003

36. van der Sluijs JA, Geesink RG, van der Linden AJ, Bulstra SK, Kuyer R, Drukker J. The reliability of the Mankin score for osteoarthritis. *J Orthop Res*. Jan 1992;10(1):58-61. doi:10.1002/jor.1100100107

37. Murphy SL, Lyden AK, Phillips K, Clauw DJ, Williams DA. Association between pain, radiographic severity, and centrally-mediated symptoms in women with knee osteoarthritis. *Arthritis Care Res (Hoboken)*. Nov 2011;63(11):1543-9. doi:10.1002/acr.20583

38. Lakes EH, Allen KD. Gait analysis methods for rodent models of arthritic disorders: reviews and recommendations. *Osteoarthritis Cartilage*. 11 2016;24(11):1837-1849. doi:10.1016/j.joca.2016.03.008

39. Allen KD, Adams SB, Setton LA. Evaluating intra-articular drug delivery for the treatment of osteoarthritis in a rat model. *Tissue Eng Part B Rev*. Feb 2010;16(1):81-92. doi:10.1089/ten.teb.2009.0447

40. Jacobs BY, Kloefkorn HE, Allen KD. Gait analysis methods for rodent models of osteoarthritis. *Curr Pain Headache Rep*. Oct 2014;18(10):456. doi:10.1007/s11916-014-0456-x

41. Hajishengallis G, Lambris JD. Crosstalk pathways between Toll-like receptors and the complement system. *Trends Immunol*. Apr 2010;31(4):154-63. doi:10.1016/j.it.2010.01.002

42. Pope MR, Hoffman SM, Tomlinson S, Fleming SD. Complement regulates TLR4-mediated inflammatory responses during intestinal ischemia reperfusion. *Mol Immunol*. 2010 Nov-Dec 2010;48(1-3):356-64. doi:10.1016/j.molimm.2010.07.004

43. Assirelli E, Pulsatelli L, Dolzani P, et al. Complement Expression and Activation in Osteoarthritis Joint Compartments. *Front Immunol*. 2020;11:535010. doi:10.3389/fimmu.2020.535010

44. Akhter N, Hasan A, Shenouda S, et al. TLR4/MyD88 -mediated CCL2 production by lipopolysaccharide (endotoxin): Implications for metabolic inflammation. *J Diabetes Metab Disord*. Jun 2018;17(1):77-84. doi:10.1007/s40200-018-0341-y

45. Grandi FC, Baskar R, Smeriglio P, et al. Single-cell mass cytometry reveals cross-talk between inflammation-dampening and inflammation-amplifying cells in osteoarthritic cartilage. *Sci Adv*. 03 2020;6(11):eaay5352. doi:10.1126/sciadv.aay5352

46. Sebastian A, Chang JC, Mendez ME, et al. Comparative Transcriptomics Identifies Novel Genes and Pathways Involved in Post-Traumatic Osteoarthritis Development and Progression. *Int J Mol Sci*. Sep 07 2018;19(9)doi:10.3390/ijms19092657

47. Miotla Zarebska J, Chanalaris A, Driscoll C, et al. CCL2 and CCR2 regulate pain-related behaviour and early gene expression in post-traumatic murine osteoarthritis but

contribute little to chondropathy. *Osteoarthritis Cartilage*. 03 2017;25(3):406-412. doi:10.1016/j.joca.2016.10.008

48. Sorge RE, LaCroix-Fralish ML, Tuttle AH, et al. Spinal cord Toll-like receptor 4 mediates inflammatory and neuropathic hypersensitivity in male but not female mice. *J Neurosci*. Oct 26 2011;31(43):15450-4. doi:10.1523/JNEUROSCI.3859-11.2011

Chapter 4: Erythrocyte Removal from Bone Marrow Aspirate Concentrate Improves Efficacy as Intra-Articular Cellular Therapy in Rodent Osteoarthritis Model

4.1 Overview

Despite the high prevalence of osteoarthritis (OA), there remains a need for additional therapeutic options. Cellular therapies with minimally manipulated cells such as bone marrow aspirate concentrate (BMAC) are increasingly popular in the U.S. but clear-cut evidence of efficacy has not been established. In theory BMAC injections provide a source of stem cells to stimulate healing in OA and ligamentous injuries but BMAC injections are also often associated with inflammation and short-term pain and mobility impairment. Given that blood is known to trigger inflammation in joints, we hypothesized that removing erythrocytes (RBC) from BMAC preparations prior to intra-articular injection would improve the efficacy for OA treatment. To test this hypothesis, BMAC was collected from the bone marrow of mice, and either depleted of RBC by ACK lysis, or untreated, and then injected into the femorotibial joint of mice where OA had been induced by destabilization of the medial meniscus (DMM). To assess the impact of BMAC treatment on joint function, individual cage monitoring (ANY-maze) and Digigait gait analyses were performed over four weeks. At study completion joint histology was assessed. Significant improvements in activity and gait parameters and histology scores were seen in animals receiving RBC-depleted compared to untreated mice, whereas animals treated with non-depleted BMAC did not experience significant improvement. These findings indicate that RBC depletion in BMAC prior to intra-articular

injection improves treatment efficacy in an animal model of OA and may have translational therapeutic potential for humans suffering from similar disease processes.

4.2 Introduction

Osteoarthritis (OA) is a multifaceted disease process impacting more than 10% of the US adult population and is highly associated with pain, disability, and economic burden[1,2]. Current options to treat OA include nonsteroidal anti-inflammatories, intra-articular injections of corticosteroids or biological therapies, and arthroscopic debridement with chondral resurfacing techniques[3]. Despite the high prevalence of OA, there remains a lack of effective treatment options that offer pain relief and improve quality of life without the risk of significant adverse effects (e.g., gastrointestinal side effects associated with nonsteroidal anti-inflammatory use). Cellular therapies, in many cases touted as “stem cell therapy”, for treatment of OA and other chronic orthopedic conditions have emerged as an attractive new option in both human and veterinary surgery[4-9]. While cellular therapy is increasingly popular, efficacy remains unclear due to variability in composition of cellular products and lack of consistency in terms of study design supporting different therapies.

Increased FDA regulation of cellular therapies has prompted evaluation of minimally manipulated treatments. Currently, biological therapies employed for human OA include autologous bone marrow aspirate concentrate (BMAC) and enriched autologous platelet products[4-6,9-11]. Bone marrow aspirate concentrate has demonstrated benefit in healing

full thickness cartilage defects in both animal models with full-thickness cartilage defects[12,13] and human clinical patients with naturally occurring disease[14-20]. In equine models of induced full-thickness chondral defects, BMAC treatment resulted in improved macroscopic and histologic scoring of cartilage tissue quality with greater type-II collagen content and improved orientation of the collagen as compared to microfracture alone[12] and reduced surgical trauma to subchondral bone[13]. It was further suggested by the authors of the paper that 'given the few mesenchymal stem cells in minimally manipulated BMAC, other mechanisms such as paracrine, anti- inflammatory, or immunomodulatory effects may have been responsible for the tissue regeneration observed[13].' In clinical patients, BMAC has demonstrated therapeutic potential in several orthopedic conditions following intra-articular injection, including knee and spinal OA[21-25], in uncontrolled, open-label trials[24].

The cellular product BMAC consists of a mixture of multiple different cell types, including red blood cells (RBC), stromal cells, immune cells (macrophages, neutrophils, B and T lymphocytes), and true hematopoietic stem cells, all of which are concentrated by the centrifugation and washing steps required to prepare BMAC[9]. Although BMAC is used as a cellular therapy, along with PRP therapy, in the management of acute and chronic OA in humans, the individual contribution of the diverse cell populations in BMAC in suppressing inflammation and stimulating cartilage repair has not been established[4,26,27]. Of note, BMAC injections are reportedly highly inflammatory and anecdotally result in significant morbidity following injection in many recipients[25]. Indeed, numerous previous studies have highlighted the role that hemarthrosis plays in joint

degeneration, demonstrating blood-induced joint damage with increased levels of pro-inflammatory cytokines and eventual cartilage degradation[28-45]. Thus, we hypothesized that the RBC component within BMAC might interfere with the potential benefits of the overall cellular therapeutic effects of BMAC. If it was shown the RBC elimination improved the efficacy of BMAC in a rodent model, it might be possible to remove RBCs from BMAC clinically to improve activity in patients.

Therefore, the overall objectives of this work were: (i) to compare the relative anti-inflammatory properties of RBC-lysed and non-lysed BMAC *in vitro* assays; and (ii) to determine whether RBC-removal improved the efficacy of BMAC in a rodent DMM model of OA. The results of these studies could improve cellular therapies for OA by providing mechanistic understanding of optimal BMAC cellular therapies.

4.3 Materials and Methods

All procedures were approved by the Colorado State University Institutional Animal Care and Use Committee (protocol #1017) and were performed in accordance with the NIH Guide for the Care and Use of Laboratory Animals.

<u>In vitro assays for BMAC-induced inflammatory responses.</u>

In vitro assays using macrophages as the indicator cells were used to assess the relative immunogenicity (cytokine release) of BMAC and RBC-depleted BMAC. BMAC was prepared from mouse bone marrow from two 12-week-old (skeletally mature) male C57BL/6Nci mice (Charles River Laboratories, Wilmington, MA), as described for

preparation of human BMAC[4,9]. BMAC and RBC-depleted BMAC preparations were added at 1:3 ratio to mouse AMJ murine alveolar macrophages (ATCC) cultured in RPMI media (10% fetal bovine serum (FBS) + glutamine)[46,47] and plated at a density of $2x10^5$ macrophage cells per triplicate wells of 96-well plates in complete DMEM culture medium, as described recently[48-51]. Controls included macrophages cultured in complete DMEM media alone and RBC-depleted BMAC. After 48h in culture, macrophage supernatants were assayed for TNF-α concentrations by ELISA, according to manufacturer's instructions.

Animals

Studies were done using 12-week-old male and female C57BL/6Nci mice (Charles River Laboratories, Wilmington, MA). Thus, this study considered sex as a biological variable, as male mice develop PTOA more severely in the DMM model than female mice[52]. Animals were housed together by sex in groups of five in solid bottom cages with corncob bedding and allowed *ad libitum* water and standard rodent chow. Mice were assessed by a veterinarian daily with body weights monitored weekly. At the conclusion of the study, mice were euthanized via CO2 inhalation with confirmation by cervical dislocation.

Bone marrow collection and preparation of BMAC

Bone marrow was collected from the tibia and femur of 12 healthy mice (two mice per treatment group and per sex) by extrusion with a #27 needle. The cell suspension was processed to produce BMAC using two centrifugation steps, as described previously[9].

Destabilization of the medial meniscus model of OA

Osteoarthritis was created in mice using a well-established method by destabilization of the medial meniscus (DMM)[53]. To perform DMM, the right stifle (knee) of all mice was injured as previously described[53]. After medial parapatellar arthrotomy, the infrapatellar fat pad was temporarily repositioned laterally, allowing access to the anterior medial meniscotibial ligament. This ligament was severed using a #11 scalpel blade. The IFP was repositioned, and the incision closed using 6-0 monofilament absorbable suture in simple interrupted pattern. Opposite limbs served as naïve controls.

Intra-articular cell injections

Purified cell populations from BMAC were counted and 250,000 cells of each population (complete versus RBC-depleted BMAC) were suspended in 10ul PBS for each intra-articular injection (one joint per mouse injected). Mice were anesthetized with isoflurane and injections were done using a 30# needle and a Hamilton syringe. Control mice were anesthetized but not injected.

Gait and activity monitoring to assess OA severity

Mice were monitored for three weeks following intra- articular injection by two methods: individual cage monitoring and Digigait gait analysis. To determine general animal behavior and mobility, each mouse underwent individual cage monitoring for 10 minutes weekly during the experimental time-course. In all cases, animals were placed in their resident cage with their environmental enrichment hut for the duration of the

assessment. Animals were acclimated to the system over one week, after which one baseline measurement was collected immediately before the start of the study. Animals received testing on days 14, 21, and 27 post DMM surgery. Training and data collection occurred randomly among animals during the same time of day (8am – 12pm) and involved the same handlers. The video analysis software (ANY- maze, Wood Dale, IL) automatically collected mobility parameters including, total distance traveled, mean speed, time in hut, and entries to the top of hut.

Animals were monitored for gait abnormalities using the Digigait analysis system (Mouse Specifics, Inc., Framingham, MA) [26]. Briefly, animals were placed on a treadmill at 35cm/s (flat or 10° inclined; three runs per time point for each grade) and video recorded for analysis. Animals were acclimated to the system over 1 week, during which baseline was collected in triplicate at one timepoint immediately prior to starting the study. Subsequent DigiGait data collection occurred on days 14, 21, and 27 post-surgery. Animal testing order was randomly selected at each timepoint for data acquisition and testing occurred during the same time of day (1pm – 4pm) and involved the same handlers. Data processing was performed using Digigait software. Parameters evaluated included % swing stride, % stance stride, % brake stride, and % propel stride.

Joint histology and immunohistochemistry

Knee/stifle joints were fixed in 10% neutral buffered formalin for 24 hours, followed by decalcification in EDTA and paraffin embedding. Sections (5μm) were taken from the center of the medial tibial plateau and stained with toluidine blue. Histological grading of

joint tissues was conducted using established criteria for OA and were completed by two blinded, independent individuals trained in using this scoring method[54].

Data analysis

Data for three or more sample comparisons were analyzed using a one-way non-parametric ANOVA (Kruskal-Wallis. Test) with Dunn's multiple comparisons test. The experimental sample size for the in vivo study was calculated using GPower Version 3.1.1[55]. An *a-priori* power analysis was conducted from pilot gait data (stride length) obtained using this injury model in mice. This power analysis resulted in a power of 80%, using a 95% confidence interval and typical standard deviation of 1.00 within groups. To account for biological variability related to sex, both male and female mice were analyzed. Longitudinal data was compared using repeated-measures ANOVA with Dunnett's correction; each timepoint was compared to baseline values. Cross-sectional data was normalized to baseline values and were compared using repeated-measures ANOVA with Tukey's correction. Histological scoring at end-term was evaluated using a one-way non-parametric ANOVA (Kruskal-Wallis Test) with Dunn's multiple comparisons test. Statistical analysis was performed using GraphPad Prism v9.3.1 (GraphPad Software Inc., La Jolla, CA). For all comparisons, significance was assessed at $p<0.05$ or $p<0.1$.

4.4 Results

Macrophage responses to BMAC and impact of RBC depletion on inflammatory cytokine production

Initial studies were done using *in vitro* assays to assess the relative inflammation inducing properties of BMAC, and to determine whether RBC depletion modulated any inflammatory effects of BMAC. These studies were conducted using AMJ macrophages as the readout for inflammatory responses, as we have previously used this cell line as a sensitive indicator of immune responses *in vitro*[56]. To assess inflammatory responses, macrophages were incubated with BMAC cells or RBC-depleted BMAC cells (adjusted to add equivalent numbers of nucleated cells for each cell population) and incubated for 48 hours. At this time, the release of pro-inflammatory cytokine TNF-α was assessed by ELISA, using cell culture supernatants. We observed that BMAC stimulated significant production of TNF- α compared to resting AMJ macrophages ($p=0.0001$), and that RBC-depleted BMAC stimulated significantly less TNF-α than non-depleted BMAC ($p<0.0001$) (**Figure 4.1**). These results indicated that RBC depletion had the potential to reduce the inherent inflammatory properties of BMAC *in vitro*, and removal of RBCs may improve overall treatment outcomes for BMAC treatment.

Comparison of functional impact of treatment with BMAC or RBC-depleted BMAC in mice with induced OA.

The *in vitro* findings (above) indicated that RBC depletion might reduce BMAC inflammation, but the critical question was whether this effect would also translate to

greater improvement in overall joint function in the case of established OA. To assess functional improvement, both activity monitoring and gait analysis were employed.

Overhead cage activity monitoring

Activity was monitored in three groups of animals with DMM-induced OA (sham treated, BMAC-treated, and RBC-depleted BMAC treated) using the *ANY-maze*^{TM} overhead cage monitoring system. *ANY-maze*^{TM} overhead cage monitoring was utilized as a behavior/mobility assessment. Parameters of interest were accessed both (i) longitudinally overtime and (ii) cross-sectionally among groups normalized to pre-DMM surgery baseline. No longitudinal overtime differences in any group persisted out to day 27 (**Figure 4.2A, C, E, G)**. When cross-sectional data was assessed, mice treated with RBC-depleted BMAC exhibited increased distance traveled (**Figure 4.2B,** p=0.0551) and mean speed **(Figure 4.2D**, p=0.0398) compared to no treatment control animals at day 27 post-DMM surgery. Additionally, RBC-depleted BMAC animals spent less time in their security huts at day 27 post-surgery relative to no injection controls **(Figure 4.2F**, p=0.098). Both BMAC (**Figure 4.2H,** p=0.0271) and RBC-depleted BMAC animals (**Figure 4.2H,** p=0.0545) showed an increase in their top of hut entries at day 27 compared to no injection control animals, indicating greater willingness to propel off their operated hindlimbs. These findings are important because they indicate that compared to BMAC treated animals, animals treated with RBC-depleted BMAC regained significantly more activity, compared to non-treated animals. This effect could

reflect several processes, including reduction of intra-articular inflammation and/or improved cartilage integrity.

Digigait Treadmill walking

We next assessed the impact of BMAC treatment and RBC depletion on gait in animals with OA. Digigait controlled treadmill walking was performed to view gait changes at 35cm/s at both a 10-degree incline (**Figure 4.3**) and on a flat surface (**Supplemental Figure 4.1**). Results are depicted from animals evaluated at a 10-degree incline both (i) longitudinally overtime (**Figures 4.3A, C, E, G**) and (ii) cross-sectionally among groups (**Figures 4.3B, D, F, H**) when normalized to pre-DMM surgery baseline Digigait values. The first parameter evaluated was %swing stride. By day 27 post-injury, no injection control animals showed an increased %swing stride longitudinally from baseline **(Figure 4.3A**, p=0.0347**)**. In addition, cross-sectional analyses demonstrated a trend towards no injection animals having a higher %swing stride than either BMAC or RBC-lysed BMAC animals **(Figure 4.3B**; p=0.0703 and p=0.0895, respectively). Similarly, longitudinal data revealed that no injection control animals showed a decreased %stance stride compared to baseline by day 27 **(Figure 4.3C**; p=0.0346**)**. No injection animals also trended towards a cross-sectional decrease at day 27 compared to BMAC treated animals **(Figure 4.3D**; p=0.0703**)**.

The %stance stride was further broken down into %brake stride and %propel stride. %Brake stride refers to the portion of the step from initial touchdown onto the belt until the maximum amount of the paws area is touching the belt. %Propel stride starts as

soon as the maximum amount of the paw is touching the belt until the paw is lifted off the belt. With %brake stride, no longitudinal differences were noted in any group at day 27 **(Figure 4.3E)** or cross-sectionally among groups at day 27 **(Figure 4.3F)**.

In contrast, no injection animals showed a longitudinal decrease in %propel stride at day 27 post-injury **(Figure 4.3G**; p=0.0087**)**; this group also trended toward decreased %propel stride from both BMAC and RBC-lysed BMAC animals at day 27 **(Figure 4.3H**; p=0.0507 and p=0.0775, respectively**)**.

Impact of BMAC treatment on cartilage integrity

We next evaluated the impact of BMAC treatment on joint pathology, with a particular focus on articular cartilage integrity. Joint tissues were collected from the three treatment groups at d27 after OA was induced in the DMM model. Tissues were processed for histological analysis, which was conducted by a pathologist (KS) blinded as to treatment group assignment. Images from these studies are depicted in **Figure 4.4**. In untreated animals with DMM-induced OA there was: (i) loss of proteoglycan, synovitis, and fibrillations and/or clefts on the cartilage surface in the medial compartments **(4.4D, left column)**; and (ii) small fibrillations and loss of proteoglycan on the lateral surfaces **(4.4G, left column)**. By contrast, BMAC treated animals showed smaller fibrillations and reduced loss of proteoglycan within both the medial and lateral compartments **(4.4E and H, middle column)**. In animals treated with RBC-depleted BMAC, there was improved proteoglycan content and decreased OA progression in both the medial and lateral compartments compared to the other groups **(4.4F, and I, right column)**.

To support the subjective descriptions, these histologic changes were quantified using the Osteoarthritis Research Society International (OARSI) scoring system. In animals treated with RBC-depleted BMAC, there was a reduction in overall OARSI score compared to untreated animals (p=0.0115) or animals treated with BMAC (p=0.0693) **(Figure 4.5A)**. Additionally, significantly decreased synovitis was seen in the RBC-depleted BMAC animals compared to untreated animals or animals treated with BMAC treatment **(Figure 4.5B**; p=0.0007 and p=0.0336, respectively**)**. As expected with the DMM mouse OA model, the majority of OA changes were noted within the medial compartment of the joint rather than in the untreated lateral compartment of the stifle joint. As such, the OARSI scores for the medial compartment were significantly improved for mice treated with RBC-depleted BMAC, compared to untreated animals or animals treated with BMAC **(Figure 4.5C**; p=0.0003 and p=0.0086, respectively**)**, with similar changes noted in the medial compartment proteoglycan scores **(Figure 4.5D**; p=0.0003 and p=0.0185, respectively**)**. OARSI scores for the lateral compartment were not different for any of the 3 treatment groups **(Figure 4.5F)**. Additional scored and individual OARSI parameters are listed in **Supplemental Figure 4.2.**

4.5 Discussion

Bone marrow aspirate concentrate products have demonstrated therapeutic potential in preclinical models of osteoarthritis and clinically in various musculoskeletal disorders[20,24]. The most notable findings from the present work were that RBC depletion from BMAC reduced BMAC-induced inflammation and improved multiple functional

parameters associated with disease stabilization from OA, as assessed in a rodent model. Key observations included. significant improvement and/or maintenance of lameness in cage monitoring parameters (distance traveled, mean speed, time in hut, entries to top of hut zone). Similarly, gait parameters (lower %swing stride, higher %propel stride) at day 27 also improved in mice treated with RBC-depleted BMAC compared to control mice. In contrast, treatment with BMAC failed to improve either activity or gait parameters compared to control animals in this study. Importantly, treatment with RBC-depleted BMAC also significantly improved cartilage integrity and OARSI scores compared to control animals, which BMAC failed to do. Thus, our study findings indicate that the overall effectiveness of BMAC therapy for OA can be significantly improved by RBC depletion prior to intra-articular injection.

While it has been previously noted that BMAC preparations can induce inflammatory responses in patients[4]. This is the first study to our knowledge to demonstrate that the presence of RBC in BMAC can interfere with joint healing and functional improvement. Given that it is nearly impossible to avoid blood contamination of BMAC using conventional aspiration techniques, our findings indicate that direct RBC elimination (by lysing) is necessary to fully remove RBC. It is also possible to remove RBC from bone marrow aspirates by Ficoll density separation, but this technique requires biosafety cabinets, considerable manual dexterity, and laboratory centrifuges to perform. Thus, a closed system using RBC lysis with agents such as ACK would be preferable for the direct to bedside use of autologous BMAC for treatment of orthopedic injuries and OA.

Mobility and pain were assessed via cage monitoring and gait analysis in this study, as these represent primary reasons people seek treatment for OA[57]. Open-field testing, or cage monitoring can be an effective method to obtain objective research data on behavior and mobility measures[58]. Cage monitoring systems, such as AnyMaze, can track rodents within a designated area to view post-injury behavior and mobility differences compared to baseline. Notably in this study, mice injected with RBC-depleted BMAC demonstrated increased activity, as seen by a greater distance traveled and overall mean speed and spent less time in their security huts compared to noninjected mice. Furthermore, both RBC-depleted BMAC and complete BMAC treated animals entered the top of their hut more frequently compared to control mice, indicating a maintained ability to utilize their hind limbs despite injury and OA progression. Climbing requires use of the hind limbs, and as such, a willingness to enter the top of hut, indicating a maintained ability to utilize the hind limb despite injury. Importantly, similar to our results, intra-articular autologous BMAC injections have been shown clinically in humans to decrease pain, increase functionality and knee related quality of life, along with increasing patient physical function[59]. These improvements have been seen in multiple studies out to 12 months post injection[59,60].

Gait analysis systems can be an effective way to assess mobility and function[61]. As rodents tend to walk with balanced symmetrical gait, alterations in gait can be indicative of pain and/or an attempt to protect the injured limb[62]. As such, these deviations from a symmetrical gait can be used as an indicator of pain[63]. To the authors' knowledge, there have been no other studies that have utilized treadmill walking in the evaluation of

BMAC injections in rodents. Inclined treadmill running was prioritized over flat running to pose a greater challenge to the mice at this relatively early timepoint. Animals running on an inclined surface are required to work against gravity, increase muscle work and combat a “toppling moment” or the forces that may cause an animal to fall down the surface[64]. Notably, both the BMAC and RBC-depleted BMAC animals-maintained gait parameters similar to baseline by d27 post-DMM surgery while untreated animals demonstrated progressive gait abnormalities. Specifically, control animals were less inclined to put their foot down on the belt and were less likely to propel off of that foot into their next step. Overall, untreated animals demonstrated a modulated gait during controlled treadmill movement by day 27 post-DMM surgery compared to pre-surgery baseline levels.

Histopathology findings further demonstrated significant improvement in mice treated with RBC-depleted BMAC compared to animals treated with BMAC. Untreated animals demonstrated expected PTOA progression at end-term d27 postoperatively based on previously published work [53], with increased OA progression on the medial aspect of the joint compared to the lateral portion of both the tibia and femur[53]. Importantly, RBC-depleted BMAC demonstrated decreased whole joint OARSI scores compared to both the untreated control and complete BMAC treated animals. Similar to reported DMM models, osteophytes and patellar dislocation were not present in any of our mice[53]. Proteoglycan is one of the major components of the extracellular cartilage matrix. It is important for binding water to increase compressive load, but also to store a variety of factors including chemokines, cytokines and growth factors[65]. Furthermore, the RBC-

depleted BMAC treated animals demonstrated decreased synovitis and proteoglycan scores, implying improved proteoglycan health and integrity, compared to either the complete BMAC treated animals or untreated controls. Of note, in humans treated with bone marrow mononuclear cells, MRI revealed 63% of patients had improvements in synovitis and 57% showed improvements in bone marrow edema[66]. Importantly, future use of RBC depleted BMAC, rather than complete BMAC, may improve prognosis and therapeutic potential in both human and animal clinical OA patients.

There were several limitations to this study, including the use of only one BMAC cell concentration for injection, and the relatively short 28-day study duration. While significant differences in gait parameters were seen between treatment groups by day 27, additional information may have been gained by allowing osteoarthritis to progress for a more prolonged period of time, as moderate-to-severe OA is expected to progress by 8-weeks post-DMM surgery[53].. In. addition, both male and female animals were pooled for analysis in this study. However, previous studies have shown that sex can be an important influencer of disease progression in rodent models of OA[52]. The study also employed a single BMAC injection whereas repeated injections may have demonstrated greater improvement (83,84). Examination of the major cell fractions present in BMAC may also yield further insights into the mechanism(s) of action and lead to further optimization of the BMAC approach.

In summary, findings of this study demonstrated that removal of erythrocytes from BMAC improved outcomes in a mouse model of OA, as reflected by improvements in in

both gait analysis and histologic parameters compared to treatment with BMAC or to no treatment. Indeed, these studies failed to demonstrate a consistent treatment benefit from BMAC alone in this animal model, raising questions regarding the true clinical efficacy of BMAC treatment in general, given the lack of rigorous clinical evaluation. Mechanistic studies suggested that RBC-depleted BMAC may have exhibited greater disease modification through reduced induction of pro-inflammatory cytokine expression from synovial macrophages. Consideration therefore should be given to routine RBC removal when using BMAC, to improve efficacy and reduce inflammation and adverse events associated with injection. Further investigation of fractionated BMAC for improved treatment of osteoarthritis is warranted.

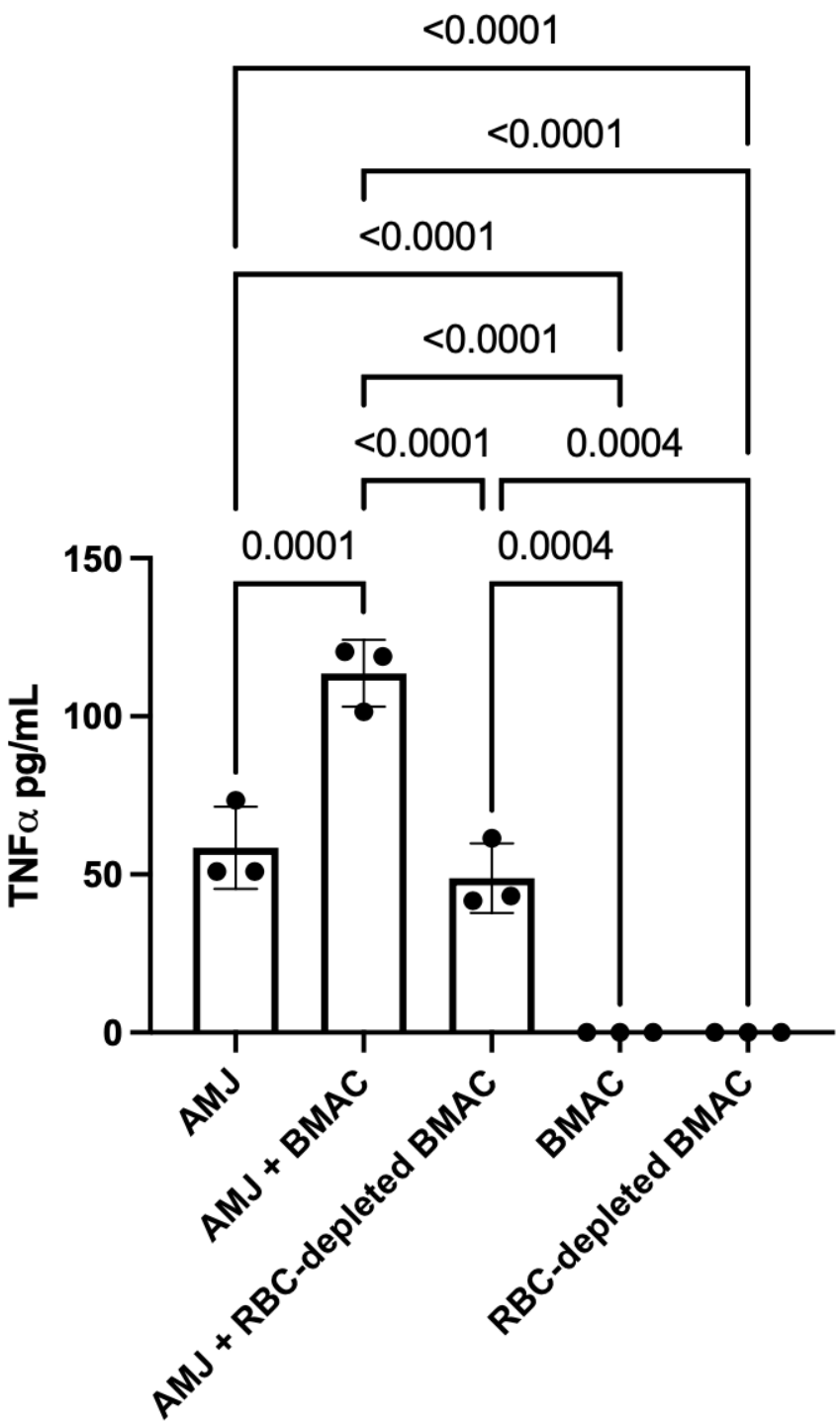

Figure 4.1: Suppression of macrophage cytokine release by BMAC cells. Purified BMAC cell subpopulations (ACK-lysed or non-lysed) were co-cultured 48h at 1:3 ratio to differentiated mouse AMJ macrophages. Controls included AMJ murine macrophages cultured in complete DMEM media alone, and BMAC and RBC-depleted BMAC. After 48h in culture, macrophage supernatants were assayed for TNF-α concentrations by ELISA. Significant differences noted with p values <0.05

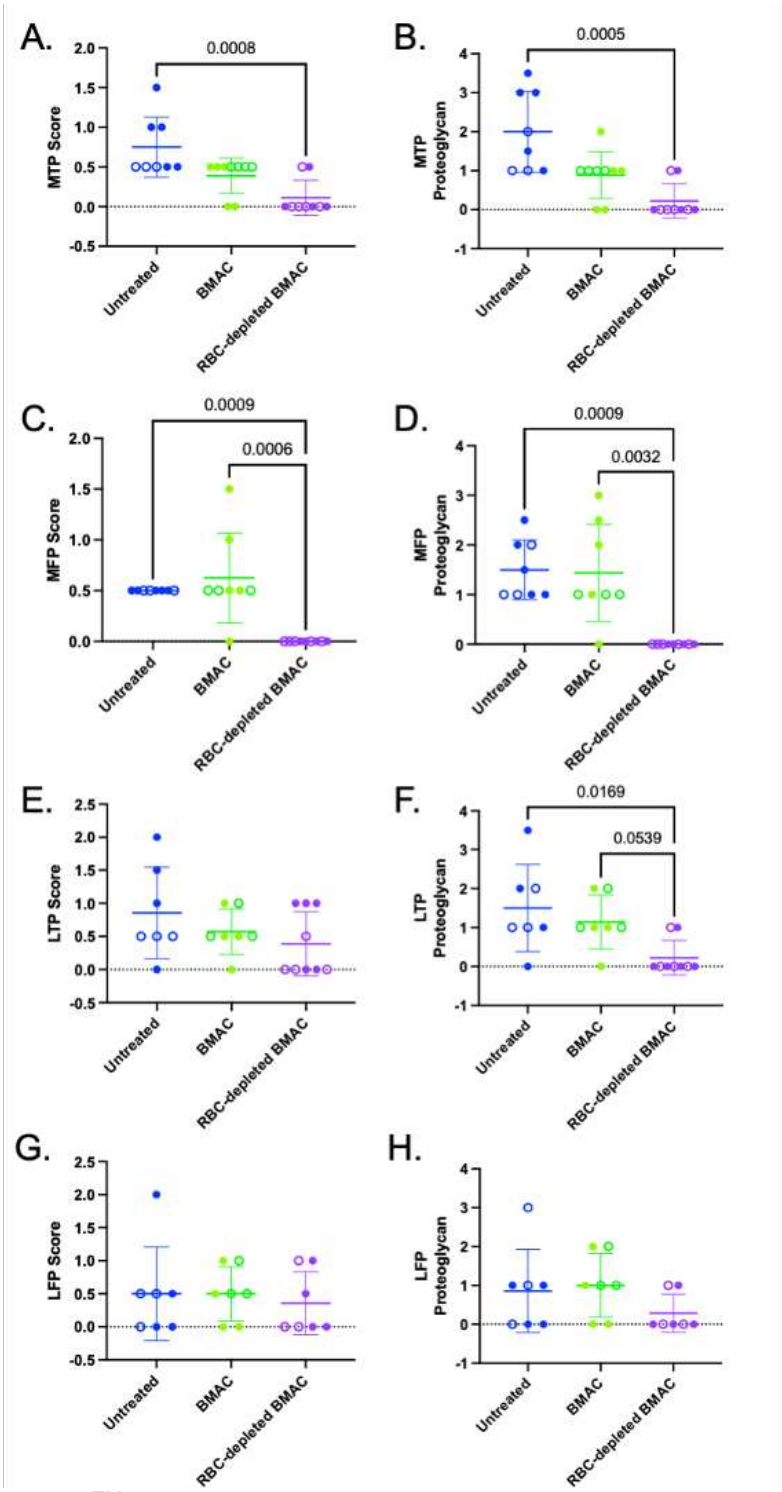

Figure 4.2: ANY-maze^{TM} cage monitoring parameters following DMM on the right hind limb of mice and treatment dependent on group. Parameters of interest statistical significance is shown overtime and between groups for distance traveled **(A, B)**, mean speed **(C, D)**, time in hut **(E, F)**, and entries to the top of hut zone **(G, H)**. Filled in symbols indicate male animals and open symbols indicate female animals. Significant differences noted, with p value noted <0.1.

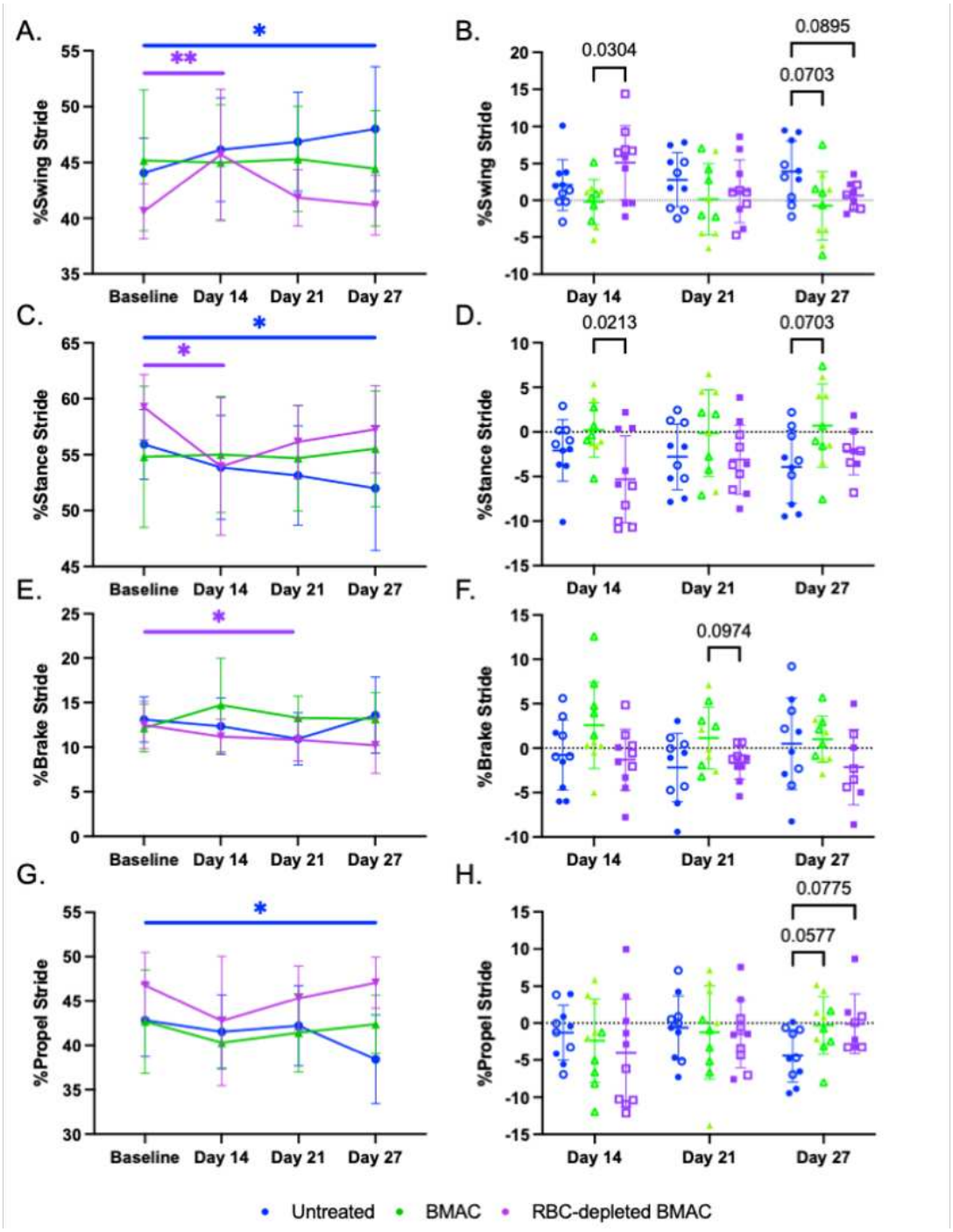

Figure 4.3: Digigait controlled treadmill walking at 35cm/s at a 10-degree incline. Parameters of interest are shown both overtime and between groups for %swing stride **(A, B)**, %stance stride **(C, D)**, %brake stride **(E, F)**, and %propel stride **(G, H)**. Filled in symbols indicate male animals and open symbols indicate female animals. Significant differences noted, with p value noted <0.1 and significant differences over time labeled (*p<0.05, **p<0.005).

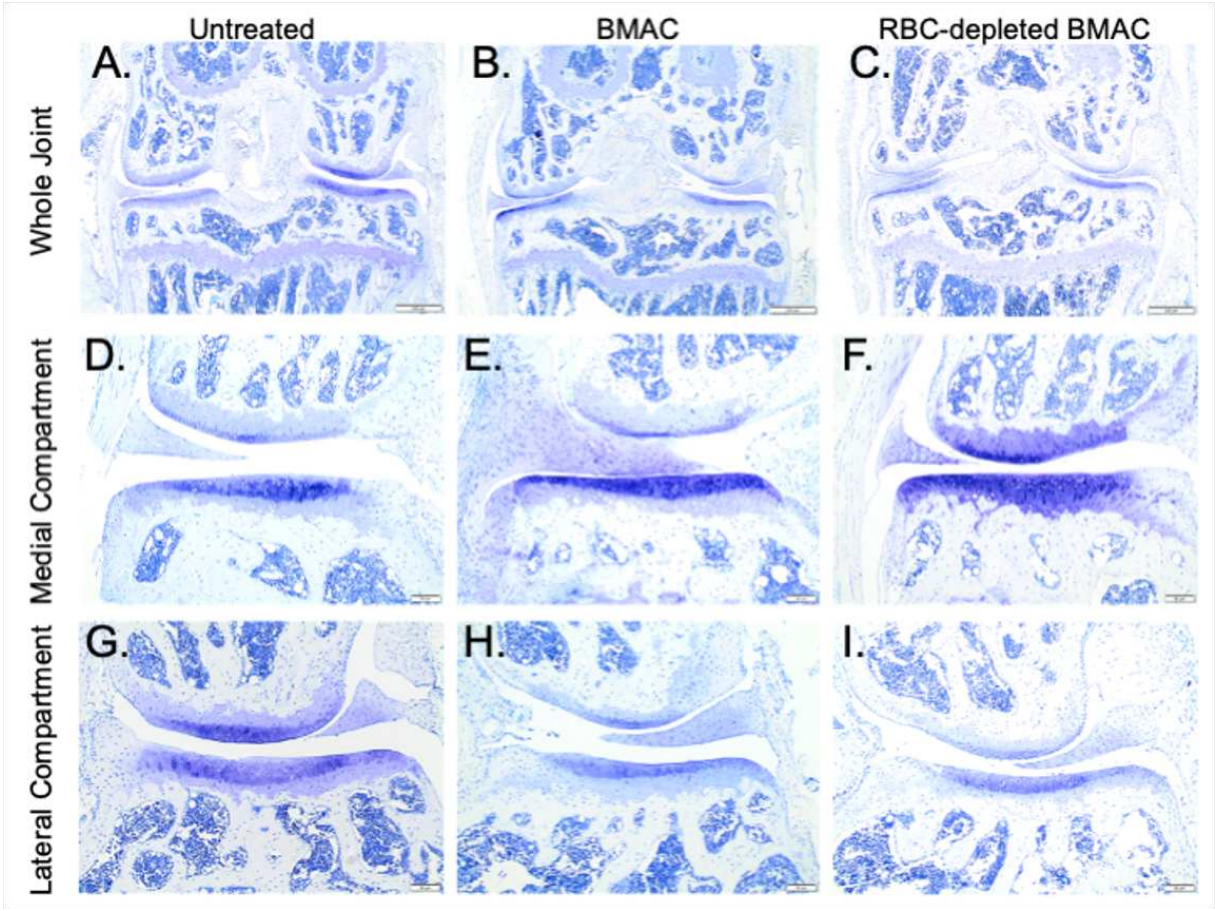

Figure 4.4: Toluidine blue photomicrographs from untreated control (left), BMAC (middle), and RBC-depleted BMAC (right) limbs. Low magnification image of whole knee joints from untreated control **(A, left column)**, BMAC **(B, middle column)**, and RBC-depleted BMAC **(C, right column)**, post DMM and applicable treatment. Higher magnification image for evaluation of the medial compartment untreated control **(A, left column)**, BMAC **(B, middle column)**, and RBC-depleted BMAC **(C, right column)**. Additional higher magnification image for evaluation of the lateral compartment for untreated control **(G, left column)**, BMAC **(H, middle column)**, and RBC-depleted BMAC **(I, right column)**. *A-C, 4x, bar=200um; D-I, 20x, bar=20um.*

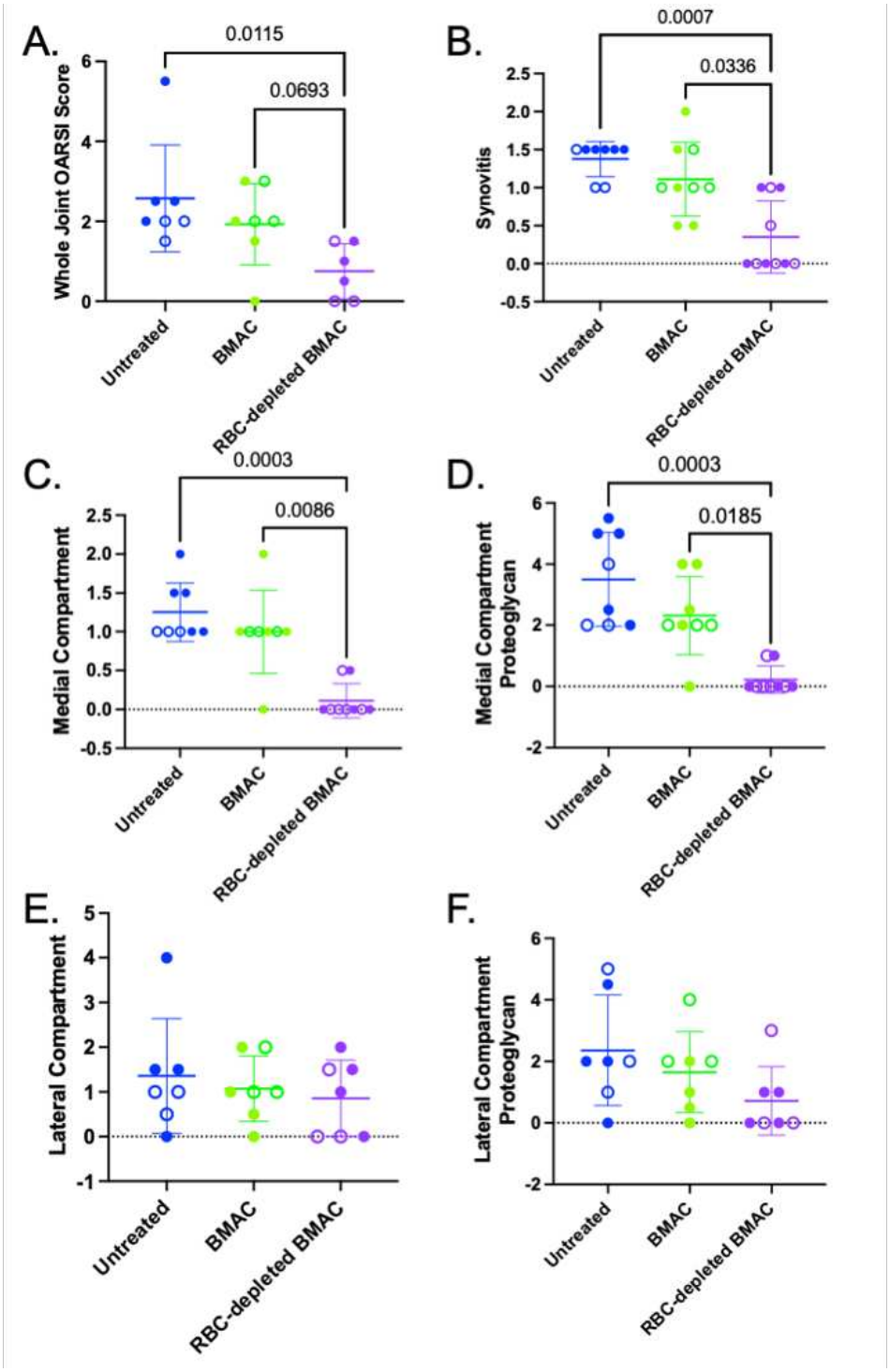

Figure 4.5: OARSI histopathology scores following DMM surgery and treatment with untreated control (blue), BMAC (green), or RBC-depleted BMAC (purple). Parameters listed include whole joint OARSI score **(A)**, synovitis score **(B)**, medial compartment OARSI score **(C)**, medial compartment proteoglycan score **(D)**, lateral compartment OARSI score **(E)**, and lateral compartment proteoglycan score **(F)**. Filled in symbols indicate male animals and open symbols indicate female animals. Significant differences noted with p values noted <0.1.

4.6 References

1. Liu Y, Ding W, Wang HL, et al. Gut microbiota and obesity-associated osteoarthritis. *Osteoarthritis Cartilage*. 09 2019;27(9):1257-1265. doi:10.1016/j.joca.2019.05.009

2. Zhao X, Shah D, Gandhi K, et al. Clinical, humanistic, and economic burden of osteoarthritis among noninstitutionalized adults in the United States. *Osteoarthritis Cartilage*. 11 2019;27(11):1618-1626. doi:10.1016/j.joca.2019.07.002

3. Zhang W, Ouyang H, Dass CR, Xu J. Current research on pharmacologic and regenerative therapies for osteoarthritis. *Bone Res*. 2016;4:15040. doi:10.1038/boneres.2015.40

4. Chahla J, Dean CS, Moatshe G, Pascual-Garrido C, Serra Cruz R, LaPrade RF. Concentrated Bone Marrow Aspirate for the Treatment of Chondral Injuries and Osteoarthritis of the Knee: A Systematic Review of Outcomes. *Orthop J Sports Med*. Jan 2016;4(1):2325967115625481. doi:10.1177/2325967115625481

5. Kraeutler MJ, Chahla J, LaPrade RF, Pascual-Garrido C. Biologic Options for Articular Cartilage Wear (Platelet-Rich Plasma, Stem Cells, Bone Marrow Aspirate Concentrate). *Clin Sports Med*. Jul 2017;36(3):457-468. doi:10.1016/j.csm.2017.02.004

6. Borakati A, Mafi R, Mafi P, Khan WS. A Systematic Review And Meta-Analysis of Clinical Trials of Mesenchymal Stem Cell Therapy for Cartilage Repair. *Curr Stem Cell Res Ther*. Feb 23 2018;13(3):215-225. doi:10.2174/1574888X12666170915120620

7. Andia I, Maffulli N. New biotechnologies for musculoskeletal injuries. *Surgeon*. Aug 2019;17(4):244-255. doi:10.1016/j.surge.2018.08.004

8. Iturriaga L, Hernáez-Moya R, Erezuma I, Dolatshahi-Pirouz A, Orive G. Advances in stem cell therapy for cartilage regeneration in osteoarthritis. *Expert Opin Biol Ther*. 08 2018;18(8):883-896. doi:10.1080/14712598.2018.1502266

9. Chahla J, Alland JA, Verma NN. Bone Marrow Aspirate Concentrate for Orthopaedic Use. *Orthop Nurs*. 2018 Nov/Dec 2018;37(6):379-381. doi:10.1097/NOR.0000000000000502

10. Gaul F, Bugbee WD, Hoenecke HR, D'Lima DD. A Review of Commercially Available Point-of-Care Devices to Concentrate Bone Marrow for the Treatment of Osteoarthritis and Focal Cartilage Lesions. *Cartilage*. 10 2019;10(4):387-394. doi:10.1177/1947603518768080

11. Fotouhi A, Maleki A, Dolati S, Aghebati-Maleki A, Aghebati-Maleki L. Platelet rich plasma, stromal vascular fraction and autologous conditioned serum in treatment of knee osteoarthritis. *Biomed Pharmacother*. Aug 2018;104:652-660. doi:10.1016/j.biopha.2018.05.019

12. Fortier LA, Potter HG, Rickey EJ, et al. Concentrated bone marrow aspirate improves full-thickness cartilage repair compared with microfracture in the equine model. *J Bone Joint Surg Am*. Aug 18 2010;92(10):1927-37. doi:10.2106/JBJS.I.01284

13. Chu CR, Fortier LA, Williams A, et al. Minimally Manipulated Bone Marrow Concentrate Compared with Microfracture Treatment of Full-Thickness Chondral Defects: A One-Year Study in an Equine Model. *J Bone Joint Surg Am*. Jan 17 2018;100(2):138-146. doi:10.2106/JBJS.17.00132

14. Gobbi A, Karnatzikos G, Scotti C, Mahajan V, Mazzucco L, Grigolo B. One-Step Cartilage Repair with Bone Marrow Aspirate Concentrated Cells and Collagen Matrix in Full-Thickness Knee Cartilage Lesions: Results at 2-Year Follow-up. *Cartilage*. Jul 2011;2(3):286-99. doi:10.1177/1947603510392023

15. Gobbi A, Karnatzikos G, Sankineani SR. One-step surgery with multipotent stem cells for the treatment of large full-thickness chondral defects of the knee. *Am J Sports Med*. Mar 2014;42(3):648-57. doi:10.1177/0363546513518007

16. Gobbi A, Scotti C, Karnatzikos G, Mudhigere A, Castro M, Peretti GM. One-step surgery with multipotent stem cells and Hyaluronan-based scaffold for the treatment of full-thickness chondral defects of the knee in patients older than 45 years. *Knee Surg Sports Traumatol Arthrosc*. Aug 2017;25(8):2494-2501. doi:10.1007/s00167-016-3984-6

17. Enea D, Cecconi S, Calcagno S, Busilacchi A, Manzotti S, Gigante A. One-step cartilage repair in the knee: collagen-covered microfracture and autologous bone marrow concentrate. A pilot study. *Knee*. Jan 2015;22(1):30-5. doi:10.1016/j.knee.2014.10.003

18. Gobbi A, Whyte GP. One-Stage Cartilage Repair Using a Hyaluronic Acid-Based Scaffold With Activated Bone Marrow-Derived Mesenchymal Stem Cells Compared

With Microfracture: Five-Year Follow-up. *Am J Sports Med*. Nov 2016;44(11):2846-2854. doi:10.1177/0363546516656179

19. Krych AJ, Nawabi DH, Farshad-Amacker NA, et al. Bone Marrow Concentrate Improves Early Cartilage Phase Maturation of a Scaffold Plug in the Knee: A Comparative Magnetic Resonance Imaging Analysis to Platelet-Rich Plasma and Control. *Am J Sports Med*. Jan 2016;44(1):91-8. doi:10.1177/0363546515609597

20. Cavallo C, Boffa A, Andriolo L, et al. Bone marrow concentrate injections for the treatment of osteoarthritis: evidence from preclinical findings to the clinical application. *Int Orthop*. 02 2021;45(2):525-538. doi:10.1007/s00264-020-04703-w

21. Jo CH, Lee YG, Shin WH, et al. Intra-articular injection of mesenchymal stem cells for the treatment of osteoarthritis of the knee: a proof-of-concept clinical trial. *Stem Cells*. May 2014;32(5):1254-66. doi:10.1002/stem.1634

22. Kouroupis D, Ahari AF, Correa D, Shammaa R. Intralesional Injection of Bone Marrow Aspirate Concentrate for the Treatment of Osteonecrosis of the Knee Secondary to Systemic Lupus Erythematosus: A Case Report. *Front Bioeng Biotechnol*. 2020;8:202. doi:10.3389/fbioe.2020.00202

23. Eder C, Schmidt-Bleek K, Geissler S, et al. Mesenchymal stromal cell and bone marrow concentrate therapies for musculoskeletal indications: a concise review of current literature. *Mol Biol Rep*. Jun 2020;47(6):4789-4814. doi:10.1007/s11033-020-05428-0

24. El-Kadiry AE, Lumbao C, Rafei M, Shammaa R. Autologous BMAC Therapy Improves Spinal Degenerative Joint Disease in Lower Back Pain Patients. *Front Med (Lausanne)*. 2021;8:622573. doi:10.3389/fmed.2021.622573

25. Kim JD, Lee GW, Jung GH, et al. Clinical outcome of autologous bone marrow aspirates concentrate (BMAC) injection in degenerative arthritis of the knee. *Eur J Orthop Surg Traumatol*. Dec 2014;24(8):1505-11. doi:10.1007/s00590-013-1393-9

26. Schäfer R, DeBaun MR, Fleck E, et al. Quantitation of progenitor cell populations and growth factors after bone marrow aspirate concentration. *J Transl Med*. 04 08 2019;17(1):115. doi:10.1186/s12967-019-1866-7

27. Sugaya H, Yoshioka T, Kato T, et al. Comparative Analysis of Cellular and Growth Factor Composition in Bone Marrow Aspirate Concentrate and Platelet-Rich Plasma. *Bone Marrow Res*. 2018;2018:1549826. doi:10.1155/2018/1549826

28. Lyons LP, Weinberg JB, Wittstein JR, McNulty AL. Blood in the joint: effects of hemarthrosis on meniscus health and repair techniques. *Osteoarthritis Cartilage*. 04 2021;29(4):471-479. doi:10.1016/j.joca.2020.11.008

29. SWANTON MC. Hemophilic arthropathy in dogs. *Lab Invest*. 1959 Nov-Dec 1959;8:1269-77.

30. Madhok R, York J, Sturrock RD. Haemophilic arthritis. *Ann Rheum Dis*. Aug 1991;50(8):588-91. doi:10.1136/ard.50.8.588

31. Valentino LA, Hakobyan N, Enockson C. Blood-induced joint disease: the confluence of dysregulated oncogenes, inflammatory signals, and angiogenic cues. *Semin Hematol*. Apr 2008;45(2 Suppl 1):S50-7. doi:10.1053/j.seminhematol.2008.03.017

32. Melchiorre D, Manetti M, Matucci-Cerinic M. Pathophysiology of Hemophilic Arthropathy. *J Clin Med*. Jun 25 2017;6(7)doi:10.3390/jcm6070063

33. Roosendaal G, Lafeber FP. Pathogenesis of haemophilic arthropathy. *Haemophilia*. Jul 2006;12 Suppl 3:117-21. doi:10.1111/j.1365-2516.2006.01268.x

34. van Meegeren ME, Roosendaal G, Jansen NW, Lafeber FP, Mastbergen SC. Blood-Induced Joint Damage: The Devastating Effects of Acute Joint Bleeds versus Micro-Bleeds. *Cartilage*. Oct 2013;4(4):313-20. doi:10.1177/1947603513497569

35. Roosendaal G, Vianen ME, van den Berg HM, Lafeber FP, Bijlsma JW. Cartilage damage as a result of hemarthrosis in a human in vitro model. *J Rheumatol*. Jul 1997;24(7):1350-4.

36. Hooiveld MJ, Roosendaal G, van den Berg HM, Bijlsma JW, Lafeber FP. Haemoglobin-derived iron-dependent hydroxyl radical formation in blood-induced joint damage: an in vitro study. *Rheumatology (Oxford)*. Jun 2003;42(6):784-90. doi:10.1093/rheumatology/keg220

37. Roosendaal G, Vianen ME, Marx JJ, van den Berg HM, Lafeber FP, Bijlsma JW. Blood-induced joint damage: a human in vitro study. *Arthritis Rheum*. May 1999;42(5):1025-32. doi:10.1002/1529-0131(199905)42:5<1025::AID-ANR23>3.0.CO;2-3

38. Hooiveld M, Roosendaal G, Wenting M, van den Berg M, Bijlsma J, Lafeber F. Short-term exposure of cartilage to blood results in chondrocyte apoptosis. *Am J Pathol*. Mar 2003;162(3):943-51. doi:10.1016/S0002-9440(10)63889-8

39. Jansen NW, Roosendaal G, Bijlsma JW, Degroot J, Lafeber FP. Exposure of human cartilage tissue to low concentrations of blood for a short period of time leads to prolonged cartilage damage: an in vitro study. *Arthritis Rheum*. Jan 2007;56(1):199-207. doi:10.1002/art.22304

40. Roosendaal G, Vianen ME, Wenting MJ, et al. Iron deposits and catabolic properties of synovial tissue from patients with haemophilia. *J Bone Joint Surg Br*. May 1998;80(3):540-5. doi:10.1302/0301-620x.80b3.7807

41. Morris CJ, Wainwright AC, Steven MM, Blake DR. The nature of iron deposits in haemophilic synovitis. An immunohistochemical, ultrastructural and X-ray microanalytical study. *Virchows Arch A Pathol Anat Histopathol*. 1984;404(1):75-85. doi:10.1007/BF00704252

42. Hakobyan N, Kazarian T, Jabbar AA, Jabbar KJ, Valentino LA. Pathobiology of hemophilic synovitis I: overexpression of mdm2 oncogene. *Blood*. Oct 01 2004;104(7):2060-4. doi:10.1182/blood-2003-12-4231

43. Øvlisen K, Kristensen AT, Jensen AL, Tranholm M. IL-1 beta, IL-6, KC and MCP-1 are elevated in synovial fluid from haemophilic mice with experimentally induced haemarthrosis. *Haemophilia*. May 2009;15(3):802-10. doi:10.1111/j.1365-2516.2008.01973.x

44. Acharya SS, Kaplan RN, Macdonald D, Fabiyi OT, DiMichele D, Lyden D. Neoangiogenesis contributes to the development of hemophilic synovitis. *Blood*. Feb 24 2011;117(8):2484-93. doi:10.1182/blood-2010-05-284653

45. Tajima T, Sekimoto T, Yamaguchi N, et al. Hemoglobin stimulates the expression of ADAMTS-5 and ADAMTS-9 by synovial cells: a possible cause of articular cartilage damage after intra-articular hemorrhage. *BMC Musculoskelet Disord*. Nov 14 2017;18(1):449. doi:10.1186/s12891-017-1815-7

46. Soontararak S, Chow L, Johnson V, et al. Mesenchymal Stem Cells (MSC) Derived from Induced Pluripotent Stem Cells (iPSC) Equivalent to Adipose-Derived MSC in Promoting Intestinal Healing and Microbiome Normalization in Mouse Inflammatory Bowel Disease Model. *Stem Cells Transl Med*. 06 2018;7(6):456-467. doi:10.1002/sctm.17-0305

47. Soontararak S, Chow L, Johnson V, et al. Humoral immune responses against gut bacteria in dogs with inflammatory bowel disease. *PLoS One*. 2019;14(8):e0220522. doi:10.1371/journal.pone.0220522

48. Chow L, Johnson V, Coy J, Regan D, Dow S. Mechanisms of Immune Suppression Utilized by Canine Adipose and Bone Marrow-Derived Mesenchymal Stem Cells. *Stem Cells Dev*. 03 01 2017;26(5):374-389. doi:10.1089/scd.2016.0207

49. Chow L, Johnson V, Regan D, et al. Safety and immune regulatory properties of canine induced pluripotent stem cell-derived mesenchymal stem cells. *Stem Cell Res*. 12 2017;25:221-232. doi:10.1016/j.scr.2017.11.010

50. Colbath AC, Dow SW, Phillips JN, McIlwraith CW, Goodrich LR. Autologous and Allogeneic Equine Mesenchymal Stem Cells Exhibit Equivalent Immunomodulatory Properties In Vitro. *Stem Cells Dev*. 04 01 2017;26(7):503-511. doi:10.1089/scd.2016.0266

51. Colbath AC, Dow SW, Hopkins LS, Phillips JN, McIlwraith CW, Goodrich LR. Allogeneic vs. autologous intra-articular mesenchymal stem cell injection within normal horses: Clinical and cytological comparisons suggest safety. *Equine Vet J*. Jan 2020;52(1):144-151. doi:10.1111/evj.13136

52. Ma HL, Blanchet TJ, Peluso D, Hopkins B, Morris EA, Glasson SS. Osteoarthritis severity is sex dependent in a surgical mouse model. *Osteoarthritis Cartilage*. Jun 2007;15(6):695-700. doi:10.1016/j.joca.2006.11.005

53. Glasson SS, Blanchet TJ, Morris EA. The surgical destabilization of the medial meniscus (DMM) model of osteoarthritis in the 129/SvEv mouse. *Osteoarthritis Cartilage*. Sep 2007;15(9):1061-9. doi:10.1016/j.joca.2007.03.006

54. Glasson SS, Chambers MG, Van Den Berg WB, Little CB. The OARSI histopathology initiative - recommendations for histological assessments of osteoarthritis in the mouse. *Osteoarthritis Cartilage*. Oct 2010;18 Suppl 3:S17-23. doi:10.1016/j.joca.2010.05.025

55. Faul F, Erdfelder E, Lang AG, Buchner A. G*Power 3: a flexible statistical power analysis program for the social, behavioral, and biomedical sciences. *Behav Res Methods*. May 2007;39(2):175-91. doi:10.3758/bf03193146

56. Bosio CM, Dow SW. Francisella tularensis induces aberrant activation of pulmonary dendritic cells. *J Immunol*. Nov 15 2005;175(10):6792-801. doi:10.4049/jimmunol.175.10.6792

57. Creamer P. Osteoarthritis pain and its treatment. *Curr Opin Rheumatol*. Sep 2000;12(5):450-5. doi:10.1097/00002281-200009000-00019

58. Molstad DHH, Bradley EW. Pain and Activity Measurements. *Methods Mol Biol*. 2021;2221:291-299. doi:10.1007/978-1-0716-0989-7_17

59. El-Kadiry AE, Lumbao C, Salame N, Rafei M, Shammaa R. Bone marrow aspirate concentrate versus platelet-rich plasma for treating knee osteoarthritis: a one-year non-randomized retrospective comparative study. *BMC Musculoskelet Disord*. Jan 03 2022;23(1):23. doi:10.1186/s12891-021-04910-5

60. Anz AW, Hubbard R, Rendos NK, Everts PA, Andrews JR, Hackel JG. Bone Marrow Aspirate Concentrate Is Equivalent to Platelet-Rich Plasma for the Treatment of Knee Osteoarthritis at 1 Year: A Prospective, Randomized Trial. *Orthop J Sports Med*. Feb 2020;8(2):2325967119900958. doi:10.1177/2325967119900958

61. Lakes EH, Allen KD. Gait analysis methods for rodent models of arthritic disorders: reviews and recommendations. *Osteoarthritis Cartilage*. 11 2016;24(11):1837-1849. doi:10.1016/j.joca.2016.03.008

62. Jacobs BY, Kloefkorn HE, Allen KD. Gait analysis methods for rodent models of osteoarthritis. *Curr Pain Headache Rep*. Oct 2014;18(10):456. doi:10.1007/s11916-014-0456-x

63. Allen KD, Adams SB, Setton LA. Evaluating intra-articular drug delivery for the treatment of osteoarthritis in a rat model. *Tissue Eng Part B Rev*. Feb 2010;16(1):81-92. doi:10.1089/ten.teb.2009.0447

64. Birn-Jeffery AV, Higham TE. The scaling of uphill and downhill locomotion in legged animals. *Integr Comp Biol*. Dec 2014;54(6):1159-72. doi:10.1093/icb/icu015

65. Bertrand J, Held A. *Role of Proteoglycans in Osteoarthritis*. Springer; 2017.

66. Goncars V, Kalnberzs K, Jakobsons E, et al. Treatment of Knee Osteoarthritis with Bone Marrow-Derived Mononuclear Cell Injection: 12-Month Follow-up. *Cartilage*. 01 2019;10(1):26-35. doi:10.1177/1947603517746721

Chapter 5: Differential Transcript Expression in Compensatory Limbs Following Destabilization of the Medial Meniscus or Sham Surgery in Male and Female Mice

5.1 Overview

Post-traumatic osteoarthritis (PTOA) is a debilitating and degenerative condition. Clinical considerations and treatment primarily – and understandably – focus on the injured limb, with relatively little attention on the compensatory leg. Interestingly, mouse models of PTOA have utilized the contralateral limb in a variety of ways, including naïve internal controls, sham surgery internal controls, or bilateral surgery. Importantly, systemic inflammatory and bone turnover exists following injury, and may ultimately confound results when the contralateral limb is used as the control. To date, comprehensive evaluations of contralateral limb changes following knee injury have been minimally investigated in animal models of PTOA. To explore this topic, we aimed to determine if there were significant transcript expression changes in key inflammatory genes in contralateral hindlimbs following the destabilization of the medial meniscus (DMM) surgery. The goals of this study were two-fold: (1) Identify transcriptional sex differences in naïve animals; and (2) Identify compensatory gene expression changes in sex that are specific to animals receiving DMM surgery as compared to a naïve animal when taking into account surgery changes (i.e., sham surgery). The results from this work demonstrate the effect of surgery on inflammatory transcript expression of contralateral knees in a widely used preclinical model of PTOA. The overall take-home message from this work is that preclinical mouse models utilizing surgical methods for PTOA induction may benefit from parallel consideration of contralateral limb changes.

This might be particularly pertinent when considering use of the opposite hindlimb as an internal control, as transcript expression in these compensatory knees may be altered relative to naive baselines.

5.2 Introduction

Post-traumatic osteoarthritis (PTOA) is a debilitating and degenerative condition that results in fibrillation and loss of articular cartilage[1]. Following joint trauma, 23% to 50% of people will eventually develop PTOA[2-4]. PTOA can lead to a decreased quality of life due to pain, swelling and decreased range of motion of the knee or the affected joint[5]. As such, clinical considerations, and treatment primarily – and understandably – focus on the injured limb, with relatively little attention given to the compensatory leg. Interestingly, mouse models of PTOA have utilized the contralateral limb in a variety of ways, including as naïve internal controls, sham surgery internal controls, or bilateral surgery. To date, comprehensive evaluations of contralateral limb changes following knee injury have been minimally investigated in animal models of PTOA. Importantly, systemic inflammatory and bone turnover exists following injury[6,7], and may ultimately confound results when the contralateral limb is used as the control. Additionally, following total joint replacement, a marker of end stage OA, the contralateral lower extremity is at an elevated risk of joint degeneration and subsequent total joint replacement[8-10]. This increased risk may be due to nonstandard joint loading, a known cause of OA initiation, which may promote quicker joint degradation[11-13]. Importantly, it has been shown that excessive loads on cartilage can cause structural deterioration[14], though biomechanical changes alone may not be the driving cause of contralateral OA

progression[15]. Additionally, PTOA is a multifaceted disease, with inflammation believed to play a central role in the pathogenesis of PTOA[16]. For this reason, we sought to describe inflammatory gene expression changes within the contralateral limb of mice following destabilization of the medial meniscus (DMM) surgery.

Most studies that utilize the DMM mouse models only study male animals and have not considered sex as a biological variable. This is in stark contrast to human clinical study data which shows that women compared to men show a higher prevalence of OA[17-20]. Additionally, studies of human cohorts assessing inflammatory markers following knee injury tend to contain a higher percentage of males[2] and either compare injured samples to an uninjured contralateral control leg[21-23] or to a healthy uninjured control[24-28]. This defines a need to understand PTOA effects on a naïve contralateral limb to further elaborate on genes and inflammatory markers we may be accidently excluding, depending on the study's choice of control.

The destabilization of the medial meniscus (DMM) mouse model is a widely used and published PTOA inducing surgery model where OA is induced by transecting the medial meniscotibial ligament. Subsequent PTOA development is believed to be due to altered joint biomechanics; of note, the histologic lesions produced in the injured joint are similar to those seen in human PTOA progression[1,29]. A variety of gene expression studies have been conducted using the DMM model, with analysis typically conducted against an associated sham surgery limb[29].

For this study, we aimed to determine if there were significant transcript expression changes in key inflammatory genes in contralateral hindlimbs following either destabilization of the medial meniscus (DMM) surgery or sham surgery in both male and female animals. Fully naïve animals were also included with sex also being considered.

The goals of this study were two-fold: (1) Identify transcriptional sex differences in naïve animals; and (2) Identify compensatory gene expression changes in sex that are specific to animals receiving DMM surgery as compared to a naïve animal when taking into account surgery changes (i.e., sham surgery).

5.3 Materials and Methods

Animals

Procedures were approved by the University's Institutional Animal Care and Use Committee and were performed in accordance with the NIH Guide for the Care and Use of Laboratory Animals. C57Bl/6J mice male and female mice were purchased from Jackson Laboratories; surgery was performed when they were 12-weeks of age. Animals were housed together in groups of 5 by sex in solid bottom cages with corncob bedding. Animals were allowed *ad libitum* water and standard rodent chow and were maintained at 22–24°C on a 12-h light/dark cycle and were assessed daily by a veterinarian.

Experimental Design

Ninety-two mice were used for this study and were split into 3 experimental surgical groups: sham surgery, DMM surgery or left truly naïve **(Figure 5.1)**. Thirty-six male and female mice (n=18 per sex) received destabilization of the medial meniscus (DMM) surgery on their right knees to initiate OA progression. DMM surgery was performed by a board certified veterinarian as previously described[1]. Another thirty-six male and female mice (n=18 per sex) received a sham surgery following the same surgical procedures as the DMM surgery, but without severing the medial meniscus. Finally, twenty mice (n=10 per sex) were left as truly naïve controls and received no surgery or manipulations to either limb. In all groups, the right leg was utilized as the 'surgery' limb, while the left limb was left naïve, as a naïve-compensatory limb, and is the contralateral limb of focus for the entirety of this study. Mice were euthanized via CO2 inhalation with confirmation by cervical dislocation at either 4- or 8-weeks post-surgery (or at matching age, 16- and 20-weeks, for non-surgery animals).

Nanostring gene expression of knee joints

Total RNA was extracted from knee joints using TRIzol reagent and RNeasy Mini Kit (Qiagen, Hilden, Germany) using manufacturer's instructions. Tissue was homogenized using a Qiagen TissueLyser and spherical ball bearings kit and RNA was quantified spectrophotometrically with a NanoDrop™ 2000 (ThermoFisher Scientific, Waltham, MA). Total RNA was sent to the University of Arizona Genetics Core for analysis and quality control testing. The premade mouse inflammation panel by NanoString was utilized to evaluate total RNA along with a mouse spike in panel consisting of OA and

iron specific genes. Data analysis was performed using nSolver™ software provided by NanoString Technologies. Results, reported as absolute transcript counts, were normalized to standard mouse housekeeping genes.

Data Analysis

Gene expression count data was normalized to standard mouse housekeeping genes using nSolver software, without background thresholding or subtraction. Normalized absolute transcript counts were evaluated with an ordinary two-way ANOVA stratified by sex and group for each timepoint, either 4- or 8-weeks. Sidak multiple comparison testing, with a single pooled variance, was used to compare male/female sex differences between each group. For all comparisons, significance was assessed at $p<0.05$ with statistical analysis performed using GraphPad Prism v9.4.1 (GraphPad Software Inc., La Jolla, CA). Significant genes were aligned to gene ontology (GO) pathways using https://string-db.org/ to determine pathways of interest. No formal pathway analysis or statistical analysis was performed.

5.4 Results

Sex differences in naïve animals

Normalized RNA transcript counts were utilized to determine sex differences in 278 inflammatory related genes in naïve mice. Our goal was to find transcripts that showed sex differences in naïve animals that are common to both timepoints. To do this, total RNA transcript counts were evaluated at both 4- and 8- weeks post-surgery when

animals were 16- and 20- weeks of age, respectively. 2-way ANOVAs of each gene stratified by sex for each treatment group at each timepoint identified 16 genes different between sexes in fully naïve animals at 16-weeks of age and 16 genes different at 20-weeks of age. Of these genes, 9 genes were different between sexes of fully naïve animals at both timepoint studied **(Figure 5.2A)**. Of these 9 genes, four showed increased total normalized RNA transcript counts in naïve female mice compared to naïve male mice. Male animals are utilized as the reference as compared to females based on the historical data utilizing primarily male animals in DMM surgery. These genes include Ccl22 **(Figure 5.2B)**, IL7 **(Figure 5.2C)**, Tgfb3 **(Figure 5.2D)**, and slc2a4 **(Figure 5.2E)**. Additionally, the remaining 5 overlapping sex difference naïve genes demonstrated a decreased total normalized RNA transcript count in naïve female mice compared to naïve male mice. The genes showing a decrease in female RNA transcripts compared to males include Cebpb **(Figure 5.2F)**, Il1rap **(Figure 5.2G)**, Tlr2 **(Figure 5.2H)**, Trem2 **(Figure 5.2I)**, and slc11a2 **(Figure 5.2J)**. Other groups, naïve-compensatory sham surgery and naïve-compensatory DMM surgery, were provided for reference, but are not the current focus of these differences.

4-weeks (early) post-surgery sex differences in naïve-compensatory legs

Next, we sought to identify compensatory gene expression changes in sex that were specific to animals receiving DMM surgery as compared to a naïve animal when taking into account surgery changes (i.e., sham surgery). To do this, we compiled genes at 4-weeks post-surgery that demonstrated significant sex differences for each group. 4-weeks post-surgery was chosen as lesions within the DMM mouse OA model progress

from mild-to-moderate OA at 4 weeks post-surgery in male mice[1]. These genes are laid out visually in a Venn diagram **(Figure 5.3)** or textually in a table **(Table 5.1)**, for ease of viewing. Of these genes, we focused specifically on genes that were unique sex differences to the naïve-compensatory limb on the DMM surgery animals. Therefore, we could view sex changes specific to DMM surgery as they are not general surgery changes that showed up in our sham surgery naïve compensatory limbs or naïve sex differences that were present regardless of surgery type. We found there were 9 genes significant and specific to the naïve-compensatory DMM leg when compared by sex **(Figure 5.4)**. Of these 9 genes, five showed increased expression in the naïve-compensatory DMM surgery limbs of females compared to males and included Ccr7 **(Figure 5.4A)**, Il18 **(Figure 5.4B)**, Pla2g4a **(Figure 5.4C)**, Il10rb **(Figure 5.4D)**, and Tlr1 **(Figure 5.4E)**. Additionally, the remaining four genes showed decreased expression in the naive-compensatory DMM surgery limbs of females compared to males and these genes were Mef2d **(Figure 5.4F)**, Hdac4 **(Figure 5.4G)**, Map2k6 **(Figure 5.4H)**, and Ppp1r12b **(Figure 5.4I)**. These genes were aligned with gene ontology (GO) biological processes and many genes significant by sex in the naïve-compensatory DMM limb were contained in pathway hits within positive regulation of cellular process, positive regulation of cellular process, cellular response to stimulus, positive regulation of cellular metabolic process, positive regulation of response to stimulus and regulation of apoptotic process **(Table 5.2)**.

8-weeks (late) post-surgery sex differences in naïve-compensatory legs

Finally, we sought to identify compensatory limb gene transcript changes specific to DMM surgery at 8-weeks post-surgery. This timepoint has been previously been defined to show moderate-to-severe OA changes within the DMM model in male mice[1]. Naïve-compensatory limbs on DMM surgery mice showed 67 genes that were significantly different between the sexes. Forty-six of these genes were also significant in either the naïve compensatory limb of fully naïve mice or of sham-surgery mice. This left 21 significant gene transcripts that are specific to the naïve-compensatory limb of mice receiving DMM surgery when stratified by sex which can be seen visually in a Venn diagram **(Figure 5.5)** or laid out textually **(Table 5.3)**. A subset of naïve-compensatory DMM surgery genes are included in **Figure 5.6** and include Ccl2 **(Figure 5.6A)**, Ccl8 **(Figure 5.6B)**, Prkcb **(Figure 5.6C)**, Il5 **(Figure 5.6D)**, Irf3 **(Figure 5.6E)**, TIMP3 **(Figure 5.6F)**, Hdac4 **(Figure 5.6G)**, Nod1 **(Figure 5.6H)**, and Nlrp3 **(Figure 5.6I)**. Of note, the only gene demonstrating only significance in the naïve-compensatory DMM surgery limbs at both 4- and 8-weeks post-surgery is Hdac4. The 21 significant gene transcripts specific to the naïve-compensatory limb of mice receiving DMM surgery were aligned with gene ontology pathways and many of the significant genes were contained within a variety of pathways **(Table 5.4)**.

Interestingly, histone deacetylase 4 (HDAC4) is the only gene defined as having a significant sex difference within the naïve-compensatory DMM surgery limb, after accounting for naïve-compensatory and naïve-compensatory sham surgery changes, at

both 4- and 8-weeks post-surgery **(Figure 5.4G and Figure 5.6G, respectively)**. Importantly, additional two-way ANOVAs stratified by timepoint and group for each sex demonstrates that male animals had a significantly decreased expression of HDAC4 at 8-weeks compared to 4-weeks (p=0.0133, **Supplementary Figure 5.1A**) for the naive-compensatory DMM limb. In contrast, female animals showed a significantly increased expression of HDAC4 at 8-weeks compared to 4-weeks (p=0.0447, **Supplementary Figure 5.1B**) in the naïve-compensatory DMM limb.

5.5 Discussion

This study provided an in-depth look at naïve-compensatory limbs following sham surgery and DMM surgery as compared to a fully naïve mouse as well as comparing gene expression sex differences in naïve animals.

Sex differences in naïve animals

Interestingly, inflammatory gene expression data of naïve mice demonstrated that 41 genes showed a sex difference over both timepoints studied. Of these genes, we saw that 9 genes were significantly different between male and female naïve mice at both 16- and 20- weeks of age. This inherent inflammatory sex difference in naïve mice may be a reason why in some PTOA mouse models, for example DMM, male mice develop worse and more consistent OA[30]. Importantly, this contrasts with historical clinical data where studies have consistently reported a higher prevalence of OA in women rather than men[17-20]. Additionally, human women tend to develop end-stage OA more often

than their male counterparts[31] and report worse OA-related pain and an overall lower quality of life and lack of function[32].

One of the inflammatory genes demonstrating differential expression levels between male and female animals in fully naïve animals is C-C motif chemokine 22 (CCL22). Interestingly, CCL22 is a chemokine that drives trafficking of a variety of T-lymphocytes[33] and is both constitutively expressed during homeostatic conditions, and also can be induced beyond constitutive levels during inflammation[34]. Additionally, it has been shown that PTOA joint tissue with visual damage demonstrated increased CCL22 expression in the cartilage and/or synovium of mice and CCL22 is associated with chondrocyte apoptosis within human cartilage[33]. Therefore, the inherent biological difference within naïve mice related to their CCL22 gene expression levels may play a role in the severity or ability of these mice to develop PTOA following DMM surgery. Additionally, CCL22 has been previously implicated in a variety of other chronic inflammatory diseases including atopic dermatitis[35] and multiple sclerosis[36], which are both diseases with higher prevalence in female human populations than males[37,38], similar to OA. Understanding these inherent inflammatory gene sex differences, may help us to further our understanding of not only PTOA, but a multitude of other chronic inflammatory diseases.

Interestingly, other genes seen to demonstrate inherent sex different expression levels in naïve mice have previously been implicated in OA progression. Of these, interleukin-7 (IL-7) has a role in T- and B-cell homeostasis in mice and has been implicated as

having a role in joint diseases[39]. Specifically, IL-7 has been shown to be expressed at significant levels within synovial tissues of patients with OA[40]. Both toll-like receptor 2 (TLR2) and triggering receptor expressed on myeloid cells 2 (Trem2) showed up as having sex differences in gene expression within the naïve mice. Importantly, both TLR2 and Trem2 have been implicated in joint inflammation, particularly related to rheumatoid arthritis[41,42]. The inflammatory gene sex differences seen within naïve animals provides an interesting insight into biological differences and potential differences in how the sexes will respond to chronic inflammatory diseases. Additionally, these inherent sex differences reiterate a need to include both male and female animals in future studies and to consider sex as a biological variable.

Post-surgery sex differences in naïve-compensatory legs

The second goal of this study was to identify compensatory gene expression changes in sex that are specific to animals receiving DMM surgery as compared to a naïve animal when taking into account surgery changes (i.e., sham surgery). These sex differences in the naïve-compensatory limb were assessed at two different timepoints post-surgery, 4- and 8-weeks, when mild-to-moderate or moderate-to-severe PTOA has progressed, respectively[1]. At 4-weeks post-surgery, 9 genes were defined as showing significant sex differences within only the naïve-compensatory DMM surgery limbs. These 9 genes can therefore be described as sex differences that occur in the naïve-compensatory limb following DMM surgery on the contralateral limb. Of these 9 genes, some of them have been previously implicated or proposed to have a role in OA progression including, Ccr7[43], IL18[44], Pla2g4a[45], Map2k6[46] and ppp1r12b[47] . It is important to note that some

of the aforementioned studies defining a role for these inflammatory genes, may have only been conducted in one sex based on historical context. Aligning genes that demonstrated a significant difference between sex at 4-weeks post-DMM surgery indicated that these genes have been implicated in a variety of regulatory pathways. These regulatory pathways included a variety of cellular processes including response to stimuli, cellular metabolic processes and most interestingly, regulation of apoptotic process. Further research will need to be conducted to determine if sex changes in the naïve-compensatory limbs caused any dysregulation of these pathways and what detrimental effects that may have within the naïve-compensatory limbs.

Importantly, only one gene was defined as having a significant sex difference within the naïve-compensatory DMM surgery limb, after accounting for naïve-compensatory and naïve-compensatory sham surgery changes, at both 4- and 8-weeks post-surgery. Histone deacetylase 4, also known as HDAC4, has been previously identified as a regulator of chondrocyte hypertrophy during skeletogenesis[48]. Interestingly, HDAC4 has been shown to be significantly higher in cartilage from people with OA than healthy cartilage and has been negatively correlated with OA severity[49]. It has also been proposed that HDAC4 may contribute to early stages of OA and associated cartilage catabolism rather than the end stages of OA[49]. Of note, at 4-weeks post-DMM surgery male animals showed significantly increased RNA transcript counts of HDAC4 compared to female animals within the naïve-compensatory DMM leg. Conversely, at 8-weeks post-surgery male animals showed a significantly decreased expression of HDAC4. Importantly, additional two-way ANOVAs stratified by timepoint and group for

each sex demonstrates that male animals had a significantly decreased expression of HDAC4 at 8-weeks compared to 4-weeks ($p=0.0133$, **Supplementary Figure 5.1A**) for the naive-compensatory DMM limb. In contrast, female animals showed a significantly increased expression of HDAC4 at 8-weeks compared to 4-weeks ($p=0.0447$, **Supplementary Figure 5.1B**) in the naïve-compensatory DMM limb. This difference in gene expression between male and female mice brings up interesting sex differences that need to be explored further to understand how sex differences may affect not only the naïve-compensatory limbs but also the OA surgery limbs.

Interestingly, at 8-weeks post-DMM surgery, there were 21 significant gene transcripts that were specific to the naïve-compensatory limb of mice receiving DMM surgery when stratified by sex. This timepoint has been previously been defined to show moderate-to-severe OA changes within the DMM model in male mice[1]. As such, the increase in significant gene transcripts at 8-weeks post-surgery compared to 4-weeks post-surgery was less surprising. Additionally, in human patients following total joint replacement, a marker of end stage OA, the contralateral lower extremity is at an elevated risk of joint degeneration and subsequent total joint replacement[8-10]. This increased risk may be due to nonstandard joint loading, a known cause of OA initiation, which may promote quicker joint degradation[11-13]. As OA progresses in our mice, it is possible there may be improper loading of the contralateral naïve limb, which could account for the increase in gene transcripts seen in this study. Further work would need to be conducted to determine if these gene expression changes are leading to joint degradation within the compensatory naïve limb, as seen in human patients.

Importantly, a variety of genes seen to be significantly different by sex within the naïve compensatory limb of mice receiving DMM surgery have been previously implicated or proposed to have a role in OA progression. Some of these include C-C motif chemokine ligand 2 (CCL2, also known as MCP-1) and C-C motif chemokine ligand 8 (CCL8, also known as MCP-2). Of note, the sequence homology between CCL2 and CCL8 is high[50], and they share the receptor, C-C chemokine receptor type 2 (CCR2)[51]. Interestingly, CCL2 has been shown to play a role in post-traumatic osteoarthritis pain in a destabilization of the medial meniscus mouse model as CCL2 knockout mice demonstrated delayed onset of pain-related behavior[52]. Additionally, both CCL2 and CCL8 have previously been seen to be upregulated in symptomatic patients with OA[53].

Aligning genes that demonstrated a significant difference between sex at 8-weeks post-DMM surgery indicated that these genes are included in a variety of regulatory pathways, with all 21-genes appearing in the regulation of cellular process pathway. Other regulation pathways seen following gene alignment, are regulation of molecular function and positive regulation of macromolecule metabolic process. Further study would be necessary to determine if the aforementioned sex changes in the naïve-compensatory limbs at 8-weeks post-DMM surgery have any detrimental effects within the naïve-compensatory limbs, such as increased pain or cause any dysregulation of the aligned pathways.

Study Limitations and Potential Caveats

Of note, we did not conduct gene expression testing on any indicators of systemic animal health. Therefore, it is not known if these gene expression changes are specific to the tested knee joint or may be systemic changes throughout the entire animal. Additionally, protein expression testing was not performed. As such, it is important to remember that RNA expression may not match protein expression and further testing would need to be conducted to confirm complementary protein levels. Future work will also need to be performed to see if there are any PTOA changes in the naïve-compensatory limb.

Conclusion

This study characterized inflammatory gene sex differences within both fully naïve mice at 16- and 20-weeks of age, and gene changes specific to the naïve-compensatory limb of mice who received DMM surgery at both 4- and 8-weeks post-surgery. Future studies should be conscious of inherent sex difference and biological differences between male and female animals and should design their studies to reflect that. Additionally, when selecting/designating use of contralateral controls for mouse PTOA studies, the potential for compensatory limb changes should be carefully considered during conceptualization of the experimental design.

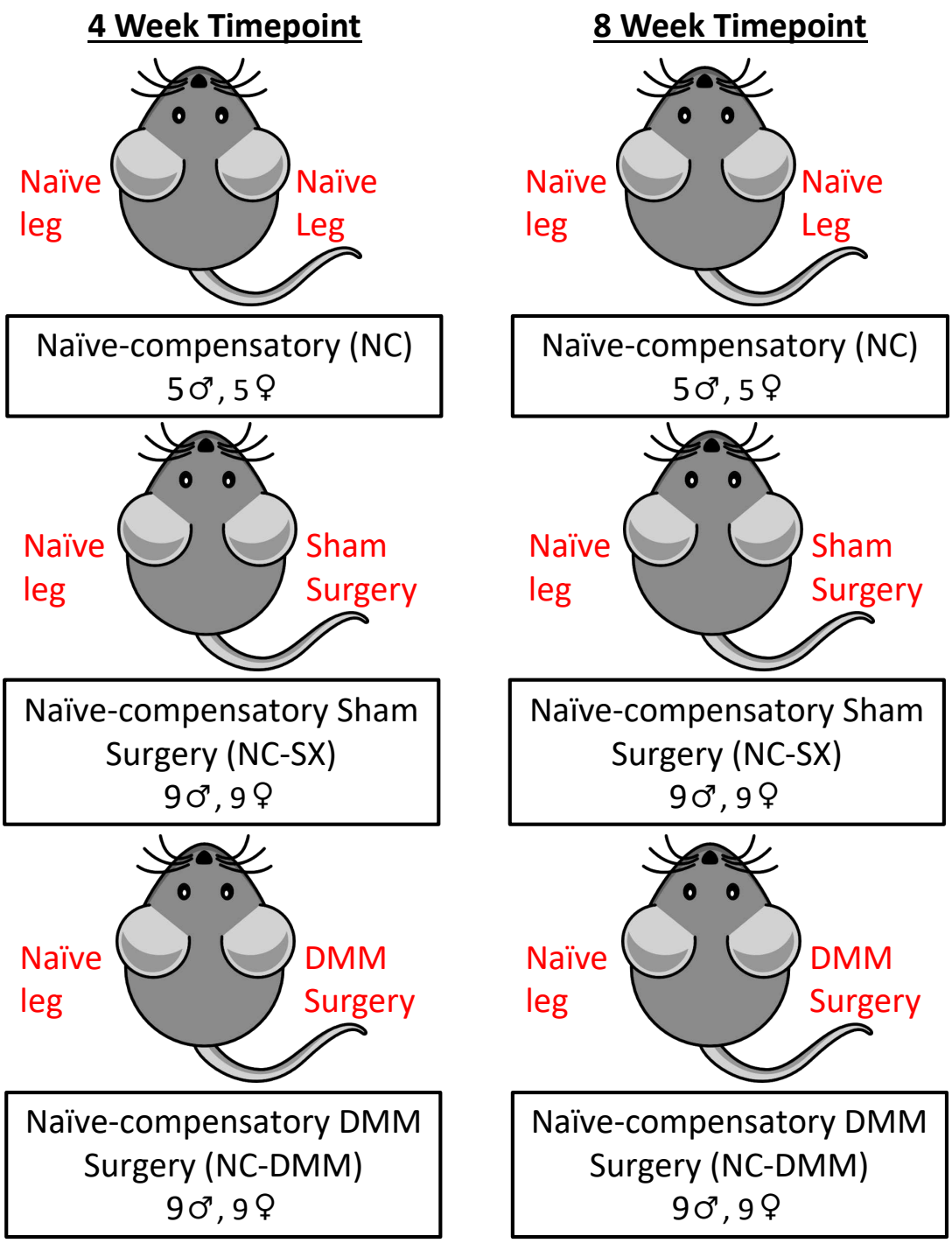

Figure 5.1: Schematic showing overall study design, with timepoints, animal counts and surgical groups.

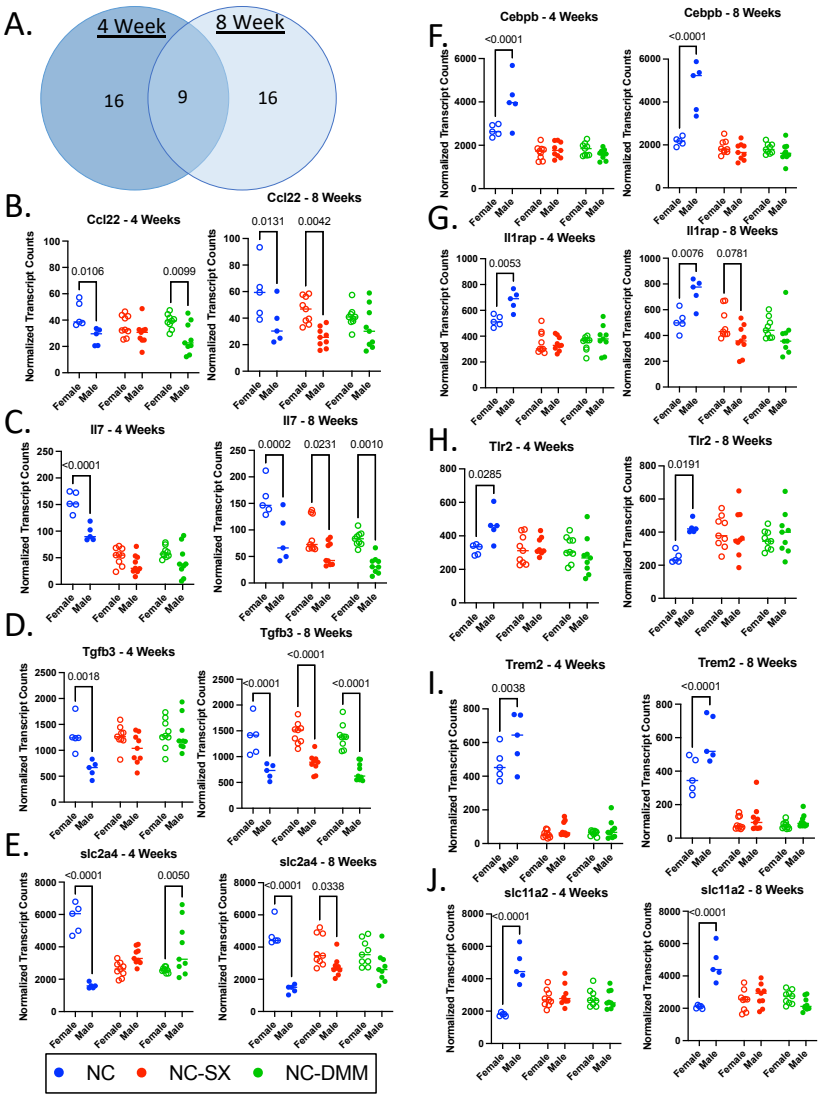

Figure 5.2: Nanostring gene expression transcripts demonstrating significant sex differences in naïve animals. Venn diagram showing sex differences in naïve animals at each of the studied timepoints **(A)**. Genes that demonstrated an overlap in naïve sex differences are included with genes with increased expression in females is on the left **(B-E)** and genes with decreased expression in females compared to males is on the right **(F-J)**. Naïve sex differences in genes at both four and eight weeks are C-C motif chemokine 22 (Ccl22) **(B)**, interleukin 7 (Il7) **(C)**, transforming growth factor beta-3 (Tgfb3) **(D)**, solute carrier family 2 member 4 (slc2a4) **(E)**, CCAAT enhancer binding protein beta (Cebpb) **(F)**, interleukin 1 receptor accessory protein (Il1rap) **(G)**, toll-like receptor 2 (Tlr2) **(H)**, triggering receptor expressed on myeloid cells 2 (Trem2) **(I)**, and solute carrier family 11 member 2 (slc11a2) **(J)**. Differences in naïve compensatory sham surgery limbs and naïve compensatory DMM surgery limbs for ease of reference. Significance differences noted, with p values shown <0.1. NC - Naïve-compensatory (Blue); NC-SX - Naïve-compensatory Sham Surgery (Red); NC-DMM - Naïve-compensatory DMM Surgery (Green).

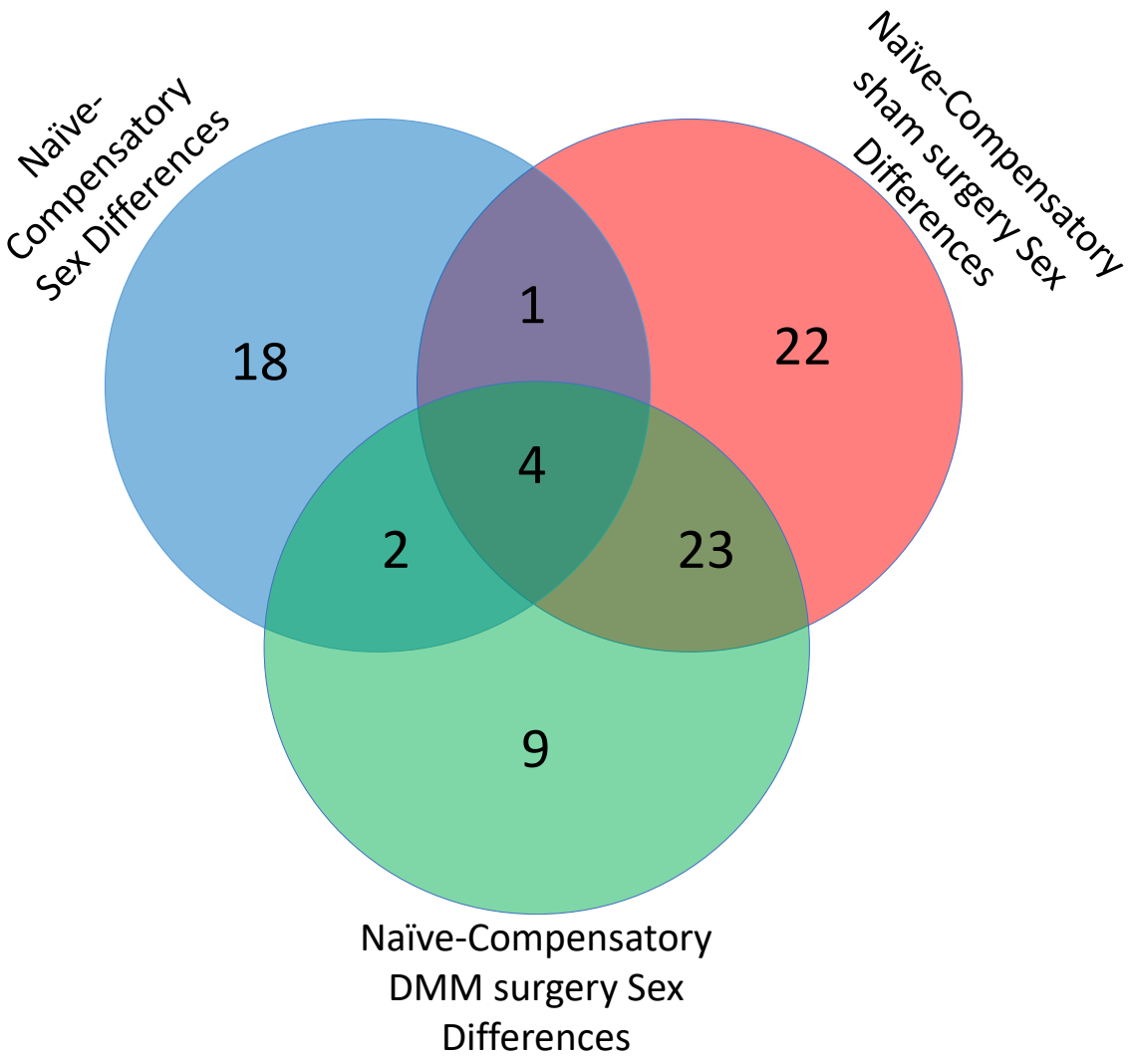

Figure 5.3: Venn diagram of genes demonstrating naïve-compensatory limb sex differences and showing overlap between groups at 4-weeks post-surgery.

Table 5.1: Gene transcripts from the naïve-compensatory limb demonstrating significant differences when evaluated by sex at 4-weeks post-surgery. Red box denotes genes that only appear in the Naïve-Compensatory DMM (NC-DMM) limb. Genes are listed and grouped by their overlap between treatment groups. NC - Naïve-compensatory; NC-SX - Naïve-compensatory Sham Surgery; NC-DMM - Naïve-compensatory DMM Surgery.

NC Only Genes	NC-SX Only Genes	NC-DMM Only Genes	NC/NC-SX ONLY overlap	NC/NC-DMM ONLY overlap	NC-SX/NC-DMM ONLY overlap	NC/NC-SX/NC-DMM Overlap
Bcl2l1	Arg1	Ccr7	adamst4	Ccl22	AdipoQ	Ccl5
Cebpb	C1ra	Hdac4		slc2a4	C7	Flt1
Csf1	C1s	Il10rb			Cd86	Irf7
Fos	C4a	Il18			Cysltr1	Kng1
Il1b	Ccl17	Map2k6			Hif1a	
Il1rap	Ccl20	Mef2d			Hmgb1	
Il7	Ccl24	Pla2g4a			Ifi44	
Ltb	Cdc42	Ppp1r12b			Ifit1	
Mafk	Cfd	Tlr1			Il22	
Nlrp3	Chi3l3				Ly96	
Rela	Gnas				Mrc1	
Tgfb3	Il1a				Oas1a	
Tlr2	Masp1				Oas2	
Trem2	Mef2a				Oasl1	
osm	Nfatc3				Pparg	
slc11a2	Nod2				Ptgfr	
sod1	Ptger4				Ripk2	
tfr2	Ptk2				Tlr4	
	Retnla				Tlr7	
	Tlr3				Tlr9	
	nr4a1				col10A1	
	osmr				col2a1	
					mmp13	
18	**22**	**9**	**1**	**2**	**23**	**4**

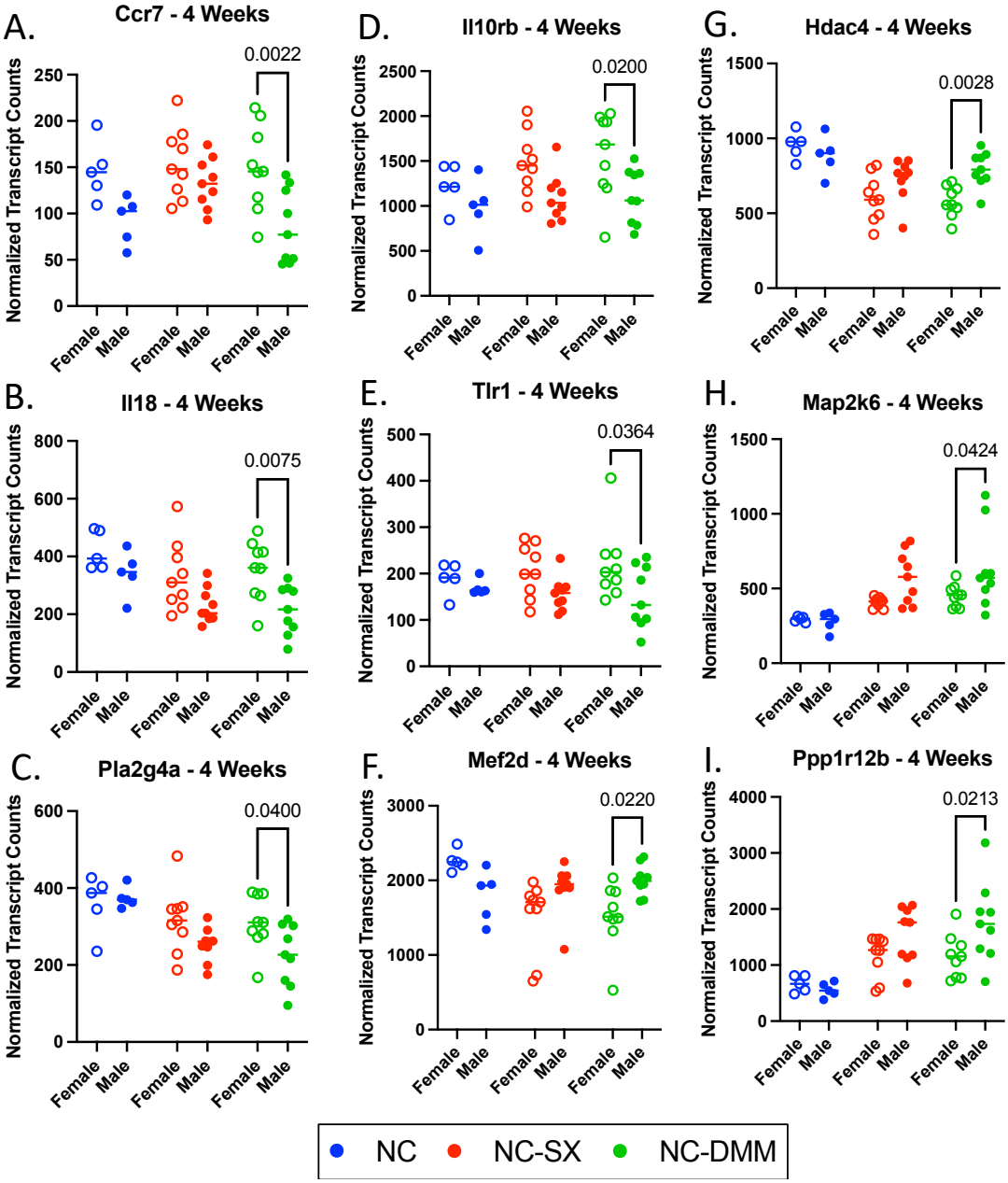

Figure 5.4: Normalized gene expression data showing significant sex differences at 4-weeks post-surgery in the naïve-compensatory DMM limb. Differences in naïve compensatory sham surgery limbs and naïve compensatory DMM surgery limbs for ease of reference. Genes shown include C-C Motif Chemokine Receptor 7 (Ccr7) **(A)**, Interleukin 18 (Il18) **(B)**, Cytosolic phospholipase A2 (Pla2g4a) **(C)**, Interleukin 10 Receptor Subunit Beta (Il10rb) **(D)**, Toll-like receptor 1 (Tlr1) **(E)**, Myocyte Enhancer Factor 2D (Mef2d) **(F)**, Histone deacetylase 4 (Hdac4) **(G)**, Mitogen-Activated Protein Kinase Kinase 6 (Map2k6) **(H)**, and Protein Phosphatase 1 Regulatory Subunit 12B (Ppp1r12b) **(I)**. Significance differences noted, with p values shown <0.1. NC - Naïve-compensatory (Blue); NC-SX - Naïve-compensatory Sham Surgery (Red); NC-DMM - Naïve-compensatory DMM Surgery (Green).

Table 5.2: Genes showing significant sex differences at 4-weeks post-surgery in the naïve-compensatory DMM limb aligned to Gene Ontology (GO) pathways.

GO-term	Description	Count in Network	Genes
GO:0048522	Positive regulation of cellular process	8 of 5407	Ccr7, Hdac4, Il10rb, Il18, Map2k6, Mef2d, Pla2g4a, Tlr1
GO:0051716	Cellular response to stimulus	8 of 5497	Ccr7, Hdac4, Il10rb, Il18, Map2k6, Pla2g4a, Ppp1r12b, Tlr1
GO:0031325	Positive regulation of cellular metabolic process	7 of 3320	Ccr7, Hdac4, Il18, Map2k6, Mef2d, Pla2g4a, Tlr1
GO:0048584	Positive regulation of response to stimulus	6 of 2080	Ccr7, Il10rb, Il18, Map2k6, Pla2g4a, Tlr1
GO:0042981	Regulation of apoptotic process	5 of 1486	Ccr7, Hdac4, Il18, Map2k6, Pla2g4a

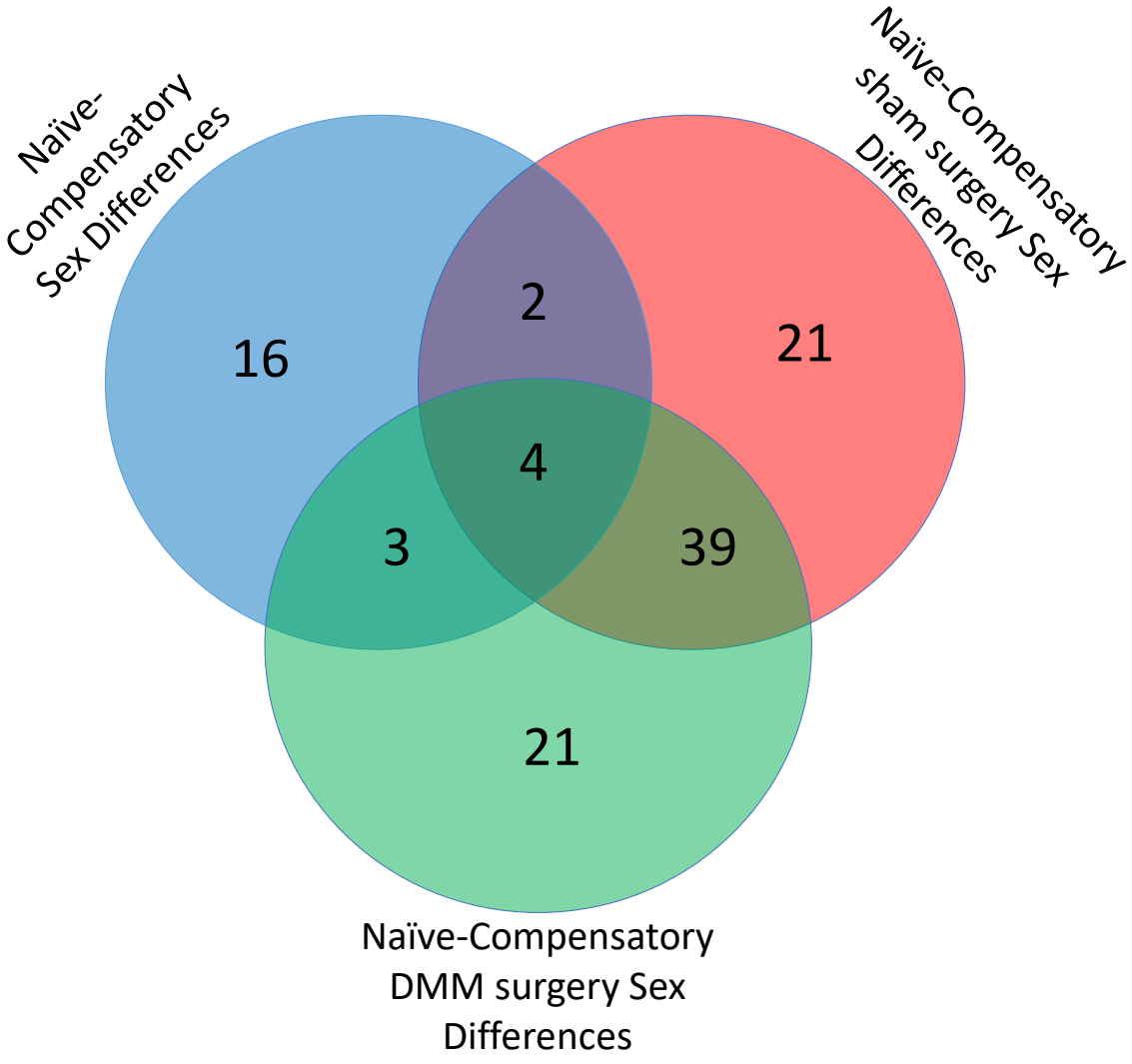

Figure 5.5: Venn diagram of genes demonstrating naïve-compensatory limb sex differences and showing overlap between groups at 8-weeks post-surgery.

Table 5.3: Gene transcripts from the naïve-compensatory limb demonstrating significant differences when evaluated by sex at 8-weeks post-surgery. Red box denotes genes that only appear in the Naïve-Compensatory DMM (NC-DMM) limb. Genes are listed and grouped by their overlap between treatment groups. NC - Naïve-compensatory; NC-SX - Naïve-compensatory Sham Surgery; NC-DMM - Naïve-compensatory DMM Surgery.

NC Only Genes	NC-SX Only Genes	NC-DMM Only Genes	NC/NC-SX ONLY overlap	NC/NC-DMM ONLY overlap	NC-SX/NC-DMM ONLY overlap	NC/NC-SX/NC-DMM Overlap
Alox5	Alox15	Bcl6	Ccl22	AdipoQ	Bcl2l1	Ifit3
Cebpb	C1qb	Ccl2	slc2a4	Ccr1	C7	Il7
Chi3l3	C2	Ccl8		Map3k9	Ccr7	Tgfb3
Cxcr2	Cd163	Elk1			Cd40	col2a1
Cxcr4	Gnas	Gnaq			Cfl1	
Ddit3	Gpr44	Hdac4			Csf1	
Il1rap	H2-Eb1	Hmgb2			Daxx	
Itgb2	Hsh2d	Hras1			Flt1	
Pdgfa	Ifi27l2a	Il5			Ifi44	
Ptgs1	Ifit2	Irf3			Irf7	
Retnla	Il1r1	Maff			Keap1	
Tgfb2	Il22	Mafg			Kng1	
Tlr2	Irf1	Mef2b			Mafk	
Tnf	Map3k5	Mx2			Map3k1	
Trem2	Nfkb1	Nlrp3			Masp1	
slc11a2	Shc1	Nod1			Mef2d	
	Stat1	Nr3c1			Mknk1	
	Stat3	Pparg			Mmp9	
	TIMP1	Prkcb			Myc	
	Tlr9	TIMP3			Nod2	
	leptin	nr4a2			Oas1a	
					Oas2	
					Oasl1	
					Plcb1	
					Ptger4	
					Ptgfr	
					Rela	
					Smad7	
					Stat2	
					Tcf4	
					Tgfbr1	
					Tnfaip3	
					Tollip	
					Traf2	
					adamst4	
					col10A1	
					mmp13	
					reck	
					slc39a14	
16	**21**	**21**	**2**	**3**	**39**	**4**

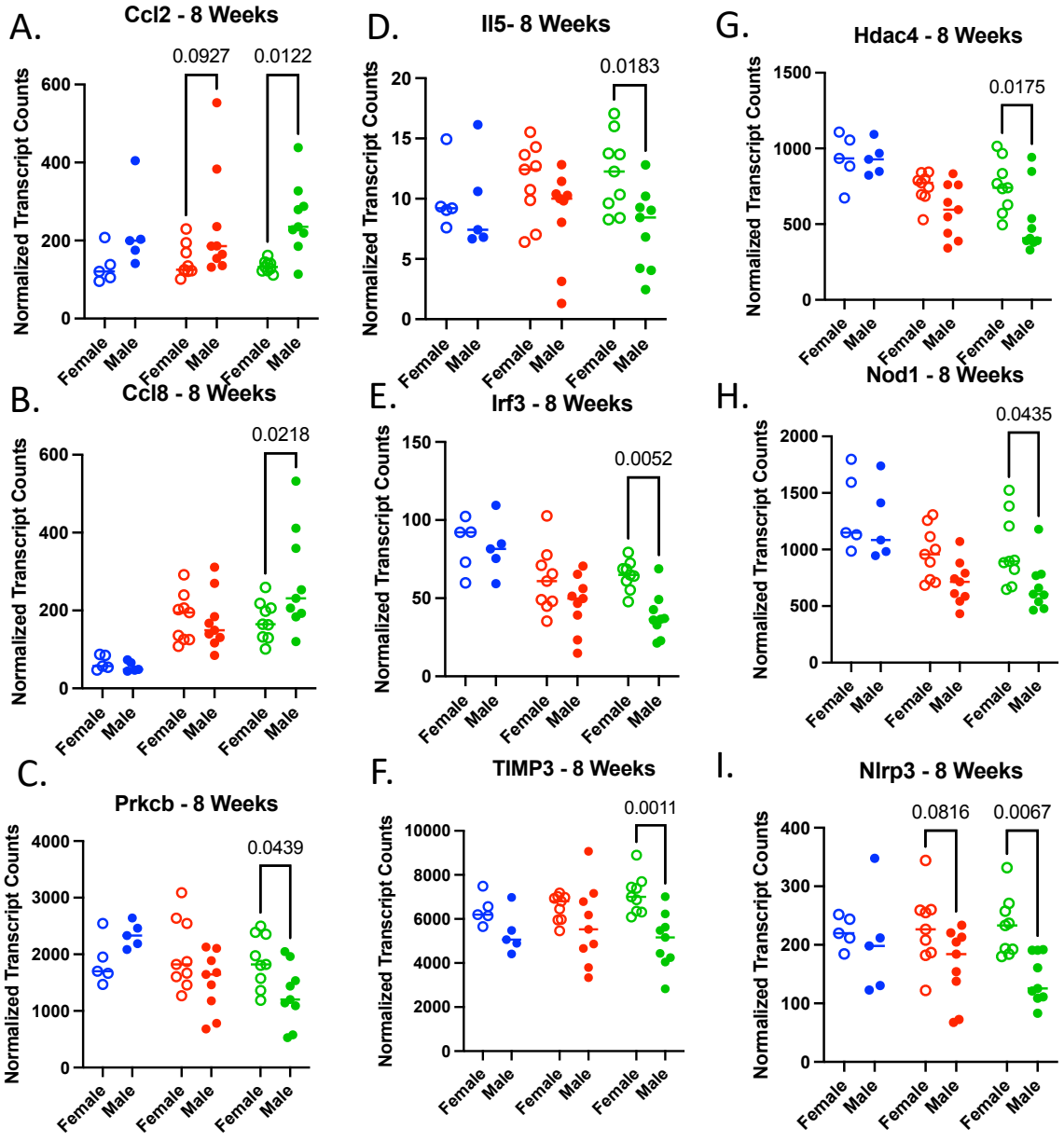

Figure 5.6: Normalized gene expression data showing significant sex differences at 4-weeks post-surgery in the naïve-compensatory DMM limb. Differences in naïve compensatory sham surgery limbs and naïve compensatory DMM surgery limbs for ease of reference. Genes shown include C-C Motif Chemokine Ligand 2 (Ccl2) **(A)**, C-C Motif Chemokine Ligand 8 (Ccl8) **(B)**, Protein kinase C beta type (Prkcb) **(C)**, Interleukin 5 (Il5) **(D)**, Interferon regulatory factor 3 (Irf3) **(E)**, TIMP metallopeptidase inhibitor 3 (TIMP3) **(F)**, Histone deacetylase 4 (Hdac4) **(G)**, Nucleotide Binding Oligomerization Domain Containing 1 (Nod1) **(H)**, and NLR family pyrin domain containing 3 (Nlrp3) **(I)**. Significance differences noted, with p values shown <0.1. NC - Naïve-compensatory (Blue); NC-SX - Naïve-compensatory Sham Surgery (Red); NC-DMM - Naïve-compensatory DMM Surgery (Green).

Table 5.4: Genes showing significant sex differences at 8-weeks post-surgery in the naïve-compensatory DMM limb aligned to Gene Ontology (GO) pathways.

GO-term	Description	Count in Network	Genes
GO:0050794	Regulation of cellular process	21 of 10932	Bcl6, Ccl2, Ccl8, Elk1, Gnaq, Hdac4, Hmgb2, Hras1, Il5, Irf3, Maff, Mafg, Mef2b, Mx2, Nlrp3, Nod1, Nr3c1, Pparg, Prkcb, TIMP3, nr4a2
GO:0065009	Regulation of molecular function	20 of 4379	Bcl6, Ccl2, Ccl8, Elk1, Gnaq, Hdac4, Hmgb2, Hras1, Il5, Irf3, Maff, Mafg, Mef2b, Nlrp3, Nod1, Nr3c1, Pparg, Prkcb, TIMP3, nr4a2
GO:0010604	Positive regulation of macromolecule metabolic process	18 of 3467	Bcl6, Ccl2, Ccl8, Elk1, Hdac4, Hmgb2, Hras1, Il5, Irf3, Maff, Mafg, Mef2b, Nlrp3, Nod1, Nr3c1, Pparg, Prkcb, nr4a2
GO:0006355	Regulation of transcription, dna-templated	16 of 2720	Bcl6, Elk1, Hdac4, Hmgb2, Hras1, Il5, Irf3, Maff, Mafg, Mef2b, Nlrp3, Nod1, Nr3c1, Pparg, Prkcb, nr4a2
GO:0048583	Regulation of response to stimulus	16 of 3651	Bcl6, Ccl2, Ccl8, Gnaq, Hdac4, Hmgb2, Hras1, Il5, Irf3, Nlrp3, Nod1, Nr3c1, Pparg, Prkcb, TIMP3, nr4a2

5.6 References

1. Glasson SS, Blanchet TJ, Morris EA. The surgical destabilization of the medial meniscus (DMM) model of osteoarthritis in the 129/SvEv mouse. *Osteoarthritis Cartilage*. Sep 2007;15(9):1061-9. doi:10.1016/j.joca.2007.03.006

2. Khella CM, Asgarian R, Horvath JM, Rolauffs B, Hart ML. An Evidence-Based Systematic Review of Human Knee Post-Traumatic Osteoarthritis (PTOA): Timeline of Clinical Presentation and Disease Markers, Comparison of Knee Joint PTOA Models and Early Disease Implications. *Int J Mol Sci*. Feb 17 2021;22(4)doi:10.3390/ijms22041996

3. Lohmander LS, Englund PM, Dahl LL, Roos EM. The long-term consequence of anterior cruciate ligament and meniscus injuries: osteoarthritis. *Am J Sports Med*. Oct 2007;35(10):1756-69. doi:10.1177/0363546507307396

4. Gelber AC, Hochberg MC, Mead LA, Wang NY, Wigley FM, Klag MJ. Joint injury in young adults and risk for subsequent knee and hip osteoarthritis. *Ann Intern Med*. Sep 05 2000;133(5):321-8. doi:10.7326/0003-4819-133-5-200009050-00007

5. March L, Smith EU, Hoy DG, et al. Burden of disability due to musculoskeletal (MSK) disorders. *Best Pract Res Clin Rheumatol*. Jun 2014;28(3):353-66. doi:10.1016/j.berh.2014.08.002

6. Christiansen BA, Anderson MJ, Lee CA, Williams JC, Yik JH, Haudenschild DR. Musculoskeletal changes following non-invasive knee injury using a novel mouse model of post-traumatic osteoarthritis. *Osteoarthritis Cartilage*. Jul 2012;20(7):773-82. doi:10.1016/j.joca.2012.04.014

7. Satkunananthan PB, Anderson MJ, De Jesus NM, Haudenschild DR, Ripplinger CM, Christiansen BA. In vivo fluorescence reflectance imaging of protease activity in a mouse model of post-traumatic osteoarthritis. *Osteoarthritis Cartilage*. Oct 2014;22(10):1461-9. doi:10.1016/j.joca.2014.07.011

8. Shakoor N, Block JA, Shott S, Case JP. Nonrandom evolution of end-stage osteoarthritis of the lower limbs. *Arthritis Rheum*. Dec 2002;46(12):3185-9. doi:10.1002/art.10649

9. Sayeed SA, Trousdale RT, Barnes SA, Kaufman KR, Pagnano MW. Joint arthroplasty within 10 years after primary charnley total hip arthroplasty. *Am J Orthop (Belle Mead NJ)*. Aug 2009;38(8):E141-3.

10. Husted H, Overgaard S, Laursen JO, et al. Need for bilateral arthroplasty for coxarthrosis. 1,477 replacements in 1,199 patients followed for 0-14 years. *Acta Orthop Scand*. Oct 1996;67(5):421-3. doi:10.3109/17453679608996660

11. Andriacchi TP, Mündermann A. The role of ambulatory mechanics in the initiation and progression of knee osteoarthritis. *Curr Opin Rheumatol*. Sep 2006;18(5):514-8. doi:10.1097/01.bor.0000240365.16842.4e

12. Wilson DR, McWalter EJ, Johnston JD. The measurement of joint mechanics and their role in osteoarthritis genesis and progression. *Rheum Dis Clin North Am*. Aug 2008;34(3):605-22. doi:10.1016/j.rdc.2008.05.002

13. Foucher KC, Wimmer MA. Contralateral hip and knee gait biomechanics are unchanged by total hip replacement for unilateral hip osteoarthritis. *Gait Posture*. Jan 2012;35(1):61-5. doi:10.1016/j.gaitpost.2011.08.006

14. Maly MR, Acker SM, Totterman S, et al. Knee adduction moment relates to medial femoral and tibial cartilage morphology in clinical knee osteoarthritis. *J Biomech*. Sep 18 2015;48(12):3495-501. doi:10.1016/j.jbiomech.2015.04.039

15. Aljehani MS, Christensen JC, Snyder-Mackler L, Crenshaw J, Brown A, Zeni JA. Knee biomechanics and contralateral knee osteoarthritis progression after total knee arthroplasty. *Gait Posture*. 01 2022;91:266-275. doi:10.1016/j.gaitpost.2021.10.020

16. Khella CM, Horvath JM, Asgarian R, Rolauffs B, Hart ML. Anti-Inflammatory Therapeutic Approaches to Prevent or Delay Post-Traumatic Osteoarthritis (PTOA) of the Knee Joint with a Focus on Sustained Delivery Approaches. *Int J Mol Sci*. Jul 27 2021;22(15)doi:10.3390/ijms22158005

17. Felson DT, Lawrence RC, Dieppe PA, et al. Osteoarthritis: new insights. Part 1: the disease and its risk factors. *Ann Intern Med*. Oct 17 2000;133(8):635-46. doi:10.7326/0003-4819-133-8-200010170-00016

18. Kim I, Kim HA, Seo YI, Song YW, Jeong JY, Kim DH. The prevalence of knee osteoarthritis in elderly community residents in Korea. *J Korean Med Sci*. Feb 2010;25(2):293-8. doi:10.3346/jkms.2010.25.2.293

19. Yoshimura N, Muraki S, Oka H, et al. Prevalence of knee osteoarthritis, lumbar spondylosis, and osteoporosis in Japanese men and women: the research on

osteoarthritis/osteoporosis against disability study. *J Bone Miner Metab*. 2009;27(5):620-8. doi:10.1007/s00774-009-0080-8

20. Zhang Y, Xu L, Nevitt MC, et al. Comparison of the prevalence of knee osteoarthritis between the elderly Chinese population in Beijing and whites in the United States: The Beijing Osteoarthritis Study. *Arthritis Rheum*. Sep 2001;44(9):2065-71. doi:10.1002/1529-0131(200109)44:9<2065::AID-ART356>3.0.CO;2-Z

21. Haller JM, McFadden M, Kubiak EN, Higgins TF. Inflammatory cytokine response following acute tibial plateau fracture. *J Bone Joint Surg Am*. Mar 18 2015;97(6):478-83. doi:10.2106/JBJS.N.00200

22. Haller JM, Swearingen CA, Partridge D, McFadden M, Thirunavukkarasu K, Higgins TF. Intraarticular Matrix Metalloproteinases and Aggrecan Degradation Are Elevated After Articular Fracture. *Clin Orthop Relat Res*. Oct 2015;473(10):3280-8. doi:10.1007/s11999-015-4441-4

23. Elsaid KA, Fleming BC, Oksendahl HL, et al. Decreased lubricin concentrations and markers of joint inflammation in the synovial fluid of patients with anterior cruciate ligament injury. *Arthritis Rheum*. Jun 2008;58(6):1707-15. doi:10.1002/art.23495

24. Swärd P, Frobell R, Englund M, Roos H, Struglics A. Cartilage and bone markers and inflammatory cytokines are increased in synovial fluid in the acute phase of knee injury (hemarthrosis)--a cross-sectional analysis. *Osteoarthritis Cartilage*. Nov 2012;20(11):1302-8. doi:10.1016/j.joca.2012.07.021

25. Bigoni M, Sacerdote P, Turati M, et al. Acute and late changes in intraarticular cytokine levels following anterior cruciate ligament injury. *J Orthop Res*. Feb 2013;31(2):315-21. doi:10.1002/jor.22208

26. Struglics A, Larsson S, Kumahashi N, Frobell R, Lohmander LS. Changes in Cytokines and Aggrecan ARGS Neoepitope in Synovial Fluid and Serum and in C-Terminal Crosslinking Telopeptide of Type II Collagen and N-Terminal Crosslinking Telopeptide of Type I Collagen in Urine Over Five Years After Anterior Cruciate Ligament Rupture: An Exploratory Analysis in the Knee Anterior Cruciate Ligament, Nonsurgical Versus Surgical Treatment Trial. *Arthritis Rheumatol*. Jul 2015;67(7):1816-25. doi:10.1002/art.39146

27. Lohmander LS, Atley LM, Pietka TA, Eyre DR. The release of crosslinked peptides from type II collagen into human synovial fluid is increased soon after joint

injury and in osteoarthritis. *Arthritis Rheum*. Nov 2003;48(11):3130-9. doi:10.1002/art.11326

28. Lohmander LS, Ionescu M, Jugessur H, Poole AR. Changes in joint cartilage aggrecan after knee injury and in osteoarthritis. *Arthritis Rheum*. Mar 1999;42(3):534-44. doi:10.1002/1529-0131(199904)42:3<534::AID-ANR19>3.0.CO;2-J

29. Loeser RF, Olex AL, McNulty MA, et al. Microarray analysis reveals age-related differences in gene expression during the development of osteoarthritis in mice. *Arthritis Rheum*. Mar 2012;64(3):705-17. doi:10.1002/art.33388

30. Ma HL, Blanchet TJ, Peluso D, Hopkins B, Morris EA, Glasson SS. Osteoarthritis severity is sex dependent in a surgical mouse model. *Osteoarthritis Cartilage*. Jun 2007;15(6):695-700. doi:10.1016/j.joca.2006.11.005

31. Hwang HS, Park IY, Hong JI, Kim JR, Kim HA. Comparison of joint degeneration and pain in male and female mice in DMM model of osteoarthritis. *Osteoarthritis Cartilage*. 05 2021;29(5):728-738. doi:10.1016/j.joca.2021.02.007

32. Kim I, Kim HA, Seo YI, et al. Tibiofemoral osteoarthritis affects quality of life and function in elderly Koreans, with women more adversely affected than men. *BMC Musculoskelet Disord*. Jun 22 2010;11:129. doi:10.1186/1471-2474-11-129

33. Ren G, Whittaker JL, Leonard C, et al. CCL22 is a biomarker of cartilage injury and plays a functional role in chondrocyte apoptosis. *Cytokine*. 03 2019;115:32-44. doi:10.1016/j.cyto.2018.11.030

34. Rapp M, Wintergerst MWM, Kunz WG, et al. CCL22 controls immunity by promoting regulatory T cell communication with dendritic cells in lymph nodes. *J Exp Med*. 05 2019;216(5):1170-1181. doi:10.1084/jem.20170277

35. Hirota T, Saeki H, Tomita K, et al. Variants of C-C motif chemokine 22 (CCL22) are associated with susceptibility to atopic dermatitis: case-control studies. *PLoS One*. 2011;6(11):e26987. doi:10.1371/journal.pone.0026987

36. Scheu S, Ali S, Ruland C, Arolt V, Alferink J. The C-C Chemokines CCL17 and CCL22 and Their Receptor CCR4 in CNS Autoimmunity. *Int J Mol Sci*. Nov 2017;18(11)doi:10.3390/ijms18112306

37. Johansson EK, Bergström A, Kull I, et al. Prevalence and characteristics of atopic dermatitis among young adult females and males-report from the Swedish population-based study BAMSE. *J Eur Acad Dermatol Venereol*. May 2022;36(5):698-704. doi:10.1111/jdv.17929

38. Walton C, King R, Rechtman L, et al. Rising prevalence of multiple sclerosis worldwide: Insights from the Atlas of MS, third edition. *Mult Scler*. 12 2020;26(14):1816-1821. doi:10.1177/1352458520970841

39. van Roon JA, Lafeber FP. Role of interleukin-7 in degenerative and inflammatory joint diseases. *Arthritis Res Ther*. 2008;10(2):107. doi:10.1186/ar2395

40. Hartgring SA, van Roon JA, Wenting-van Wijk M, et al. Elevated expression of interleukin-7 receptor in inflamed joints mediates interleukin-7-induced immune activation in rheumatoid arthritis. *Arthritis Rheum*. Sep 2009;60(9):2595-605. doi:10.1002/art.24754

41. McGarry T, Veale DJ, Gao W, Orr C, Fearon U, Connolly M. Toll-like receptor 2 (TLR2) induces migration and invasive mechanisms in rheumatoid arthritis. *Arthritis Res Ther*. Jun 09 2015;17:153. doi:10.1186/s13075-015-0664-8

42. Sigalov AB. Inhibition of TREM-2 Markedly Suppresses Joint Inflammation and Damage in Experimental Arthritis. *Int J Mol Sci*. Aug 09 2022;23(16)doi:10.3390/ijms23168857

43. Sambamurthy N, Nguyen V, Smalley R, et al. Chemokine receptor-7 (CCR7) deficiency leads to delayed development of joint damage and functional deficits in a murine model of osteoarthritis. *J Orthop Res*. 03 2018;36(3):864-875. doi:10.1002/jor.23671

44. Waszczykowski M, Fabiś-Strobin A, Bednarski I, Narbutt J, Fabiś J. Serum and synovial fluid concentrations of interleukin-18 and interleukin-20 in patients with osteoarthritis of the knee and their correlation with other markers of inflammation and turnover of joint cartilage. *Arch Med Sci*. 2022;18(2):448-458. doi:10.5114/aoms.2020.96717

45. Valdes AM, Loughlin J, Timms KM, et al. Genome-wide association scan identifies a prostaglandin-endoperoxide synthase 2 variant involved in risk of knee osteoarthritis. *Am J Hum Genet*. Jun 2008;82(6):1231-40. doi:10.1016/j.ajhg.2008.04.006

46. Loeser RF, Erickson EA, Long DL. Mitogen-activated protein kinases as therapeutic targets in osteoarthritis. *Curr Opin Rheumatol*. Sep 2008;20(5):581-6. doi:10.1097/BOR.0b013e3283090463

47. Wang S, Wang H, Liu W, Wei B. Identification of Key Genes and Pathways Associated with Sex Differences in Osteoarthritis Based on Bioinformatics Analysis. *Biomed Res Int*. 2019;2019:3482751. doi:10.1155/2019/3482751

48. Vega RB, Matsuda K, Oh J, et al. Histone deacetylase 4 controls chondrocyte hypertrophy during skeletogenesis. *Cell*. Nov 12 2004;119(4):555-66. doi:10.1016/j.cell.2004.10.024

49. Lu J, Sun Y, Ge Q, Teng H, Jiang Q. Histone deacetylase 4 alters cartilage homeostasis in human osteoarthritis. *BMC Musculoskelet Disord*. Dec 17 2014;15:438. doi:10.1186/1471-2474-15-438

50. Van Coillie E, Van Damme J, Opdenakker G. The MCP/eotaxin subfamily of CC chemokines. *Cytokine Growth Factor Rev*. Mar 1999;10(1):61-86. doi:10.1016/s1359-6101(99)00005-2

51. Ge B, Li J, Wei Z, Sun T, Song Y, Khan NU. Functional expression of CCL8 and its interaction with chemokine receptor CCR3. *BMC Immunol*. 12 28 2017;18(1):54. doi:10.1186/s12865-017-0237-5

52. Miotla Zarebska J, Chanalaris A, Driscoll C, et al. CCL2 and CCR2 regulate pain-related behaviour and early gene expression in post-traumatic murine osteoarthritis but contribute little to chondropathy. *Osteoarthritis Cartilage*. 03 2017;25(3):406-412. doi:10.1016/j.joca.2016.10.008

53. Wyatt LA, Nwosu LN, Wilson D, et al. Molecular expression patterns in the synovium and their association with advanced symptomatic knee osteoarthritis. *Osteoarthritis Cartilage*. 04 2019;27(4):667-675. doi:10.1016/j.joca.2018.12.012

Chapter 6: Conclusions

6.1 Summary

Post-traumatic osteoarthritis (PTOA) is a debilitating, degenerative condition that is characterized by clinical symptoms such as pain, swelling, and decreased range of motion of the knee or affected joint. Therefore, the development of clinically relevant models and creation of therapeutics that produce symptom and disease modifying effects are critically important. To further this research, the goals of this dissertation work was to develop and characterize a clinically relevant mouse PTOA anterior cruciate ligament (ACL) rupture model as well as, test therapeutics in pre-established PTOA mouse models.

To test this, Chapter 2 describes the development and characterization of a novel full non-invasive ACL rupture model in both male and female mice. Importantly, the described full ACL rupture model produces a rupture within the mid-substance of the ligament and demonstrates early PTOA progression by 14-days post-rupture. Additionally, we developed the first non-invasive partial ACL rupture model. As partial ACL ruptures account for 10-27% of total injuries clinically, and treatment of partial ACL rupture can differ from that of a full rupture, it is important to have a model to study and understand partial ACL ruptures and subsequent PTOA progression. Importantly, this clinically relevant model provides a unique way to study both full and partial mid-substance ACL ruptures in male and female mice and can be used to tease out potential mechanisms that could be utilized for therapeutic intervention.

Both Chapters 3 and 4 focus on potential PTOA therapeutic interventions in pre-established PTOA mouse models. Chapter 3 demonstrated that treatment with a toll-like receptor 4 (TLR4) systemic antagonist provided short term, but not long term, therapeutic effects in a cartilage defect mouse model. Following TLR4 antagonist treatment we saw pain modulation, decreased modified Mankin OA scores and decreased absolute RNA counts for key inflammatory genes up to 14-days post-injury. Additionally, Chapter 4 showed that removal of red blood cells from bone marrow aspirate concentrate (BMAC) improved the therapeutic potential of BMAC injections.

Finally, Chapter 5: (1) Identified transcriptional sex differences in knee joint tissue from naïve animals; and (2) Identified compensatory gene expression changes related to sex that are specific to animals receiving DMM surgery as compared to a naïve animal when taking into account surgery changes (i.e., sham surgery). These identified transcriptional sex differences may help us not only further our understanding of the compensatory limb following injury, but also help to identify future therapeutic treatments for PTOA.

6.2 Future Directions

The work described within this dissertation only just begins to look at the therapeutic treatments for PTOA. It is recommended that future therapeutic testing should be conducted in clinically relevant PTOA models, such as the aforementioned non-invasive full and partial ACL rupture models. Future work will focus on characterization of the partial ACL rupture model and characterization of longer timepoints of the full ACL rupture model.

Interestingly, Chapter 3 raised the possibility of producing a ‘cocktail’ or sequentially timed administration of antagonists and drugs for extended clinical improvement. Results from Chapters 3 and 4 leave the possibility that adding a TLR4 antagonist to BMAC injections may improve their therapeutic potential. Additionally, inflammatory transcripts that were modulated within the compensatory limb following PTOA induction, may give valuable insight to other antagonists to add to a therapeutic ‘cocktail’ for improved effect.

Lastly, Chapter 5 demonstrated sex differences within naïve limbs of mice at both 16- and 20- weeks of age. This reiterate the need for future studies to be conscious of inherent sex difference and biological differences between male and female animals and studies should be designed to reflect that. Additionally, this potentially implies a need for personalized medicine and therapeutics for the treatment of PTOA depending on genetic background and sex.

Overall, the work described in this dissertation has improved our understanding of the mouse knee joint during PTOA progression and potential therapeutics and targets for clinical treatment of PTOA.

Appendix: Supplemental Figures and Tables

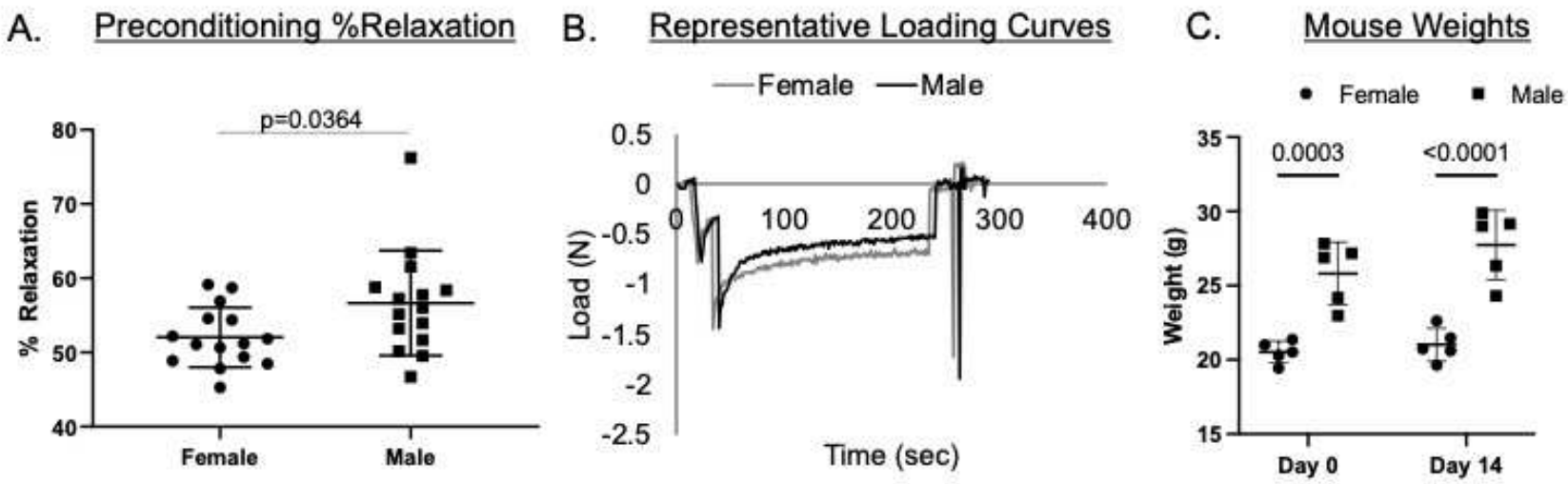

Supplemental Figure 2.1 (A) Comparison of percent relaxation during preconditioning for male and female mice. **(B)** Representative output loading curves for both female and male mice. *Percent relaxation was calculated as 1-(Load at 200 cycles/Peak Load).* **(C)** Mouse weights (in grams), at baseline (day 0) and day 14 post ACL rupture.

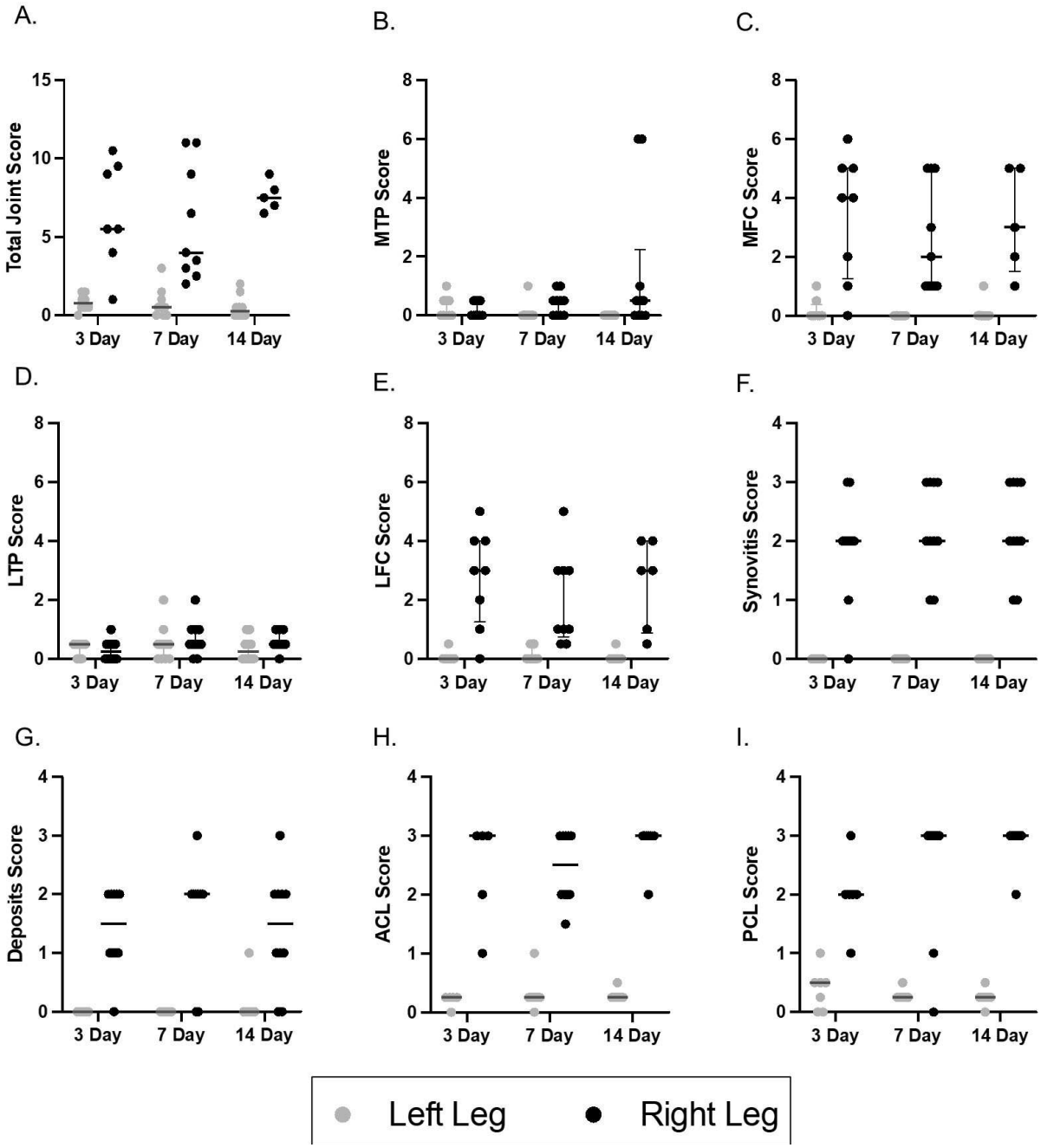

Supplemental Figure 2.2 Median modified OARSI histopathology scores for OA, following full ACL rupture on the right hind limb (black) of mice. Contralateral sham left limb scores (gray) included for reference. Medial Tibial Plateau (MTP), Medial Femoral Condyle (MFC), Lateral Tibial Plateau (LTP), Lateral Femoral Condyle (LFC)

Supplemental Table 2.2 Correlation of scored histopathology parameters to tibial displacement peak force during injury induction.

Parameter	R^2 value	p-value
Medial Tibial Plateau (MTP)	0.0001	0.9546
Medial Femoral Condyle (MFC)	0.0065	0.7206
Lateral Tibial Plateau (LTP)	0.0040	0.7498
Lateral Femoral Condyle (LFC)	0.0032	0.7983
Enthesophytes	0.0944	0.0987
Subchondral Bone	0.0773	0.1368
Synovitis	0.0168	0.4953
Blood	0.0084	0.6363
Deposits	0.0138	0.5364
ACL	0.0409	0.3549
PCL	0.1023	0.1820
Joint Capsule	0.0079	0.6396
Menisci	0.1211	0.0595

Supplemental Table 2.3 Table of MRI acquisition parameters

Sequence	T1_RARE-sag	RARE_PD_FS-cor	RARE_PD_FS-sag	T2_DIXON-cor	T2_DIXON-sag
FOV	40x40 mm	60x60 mm	40x40 mm	60x60 mm	40x40 mm
Slice Thickness	1.2 mm	1.2 mm	1.2 mm	1.2 mm	1.2 mm
Interslice Distance	0.3 mm	0.3 mm	0.3 mm	0.3 mm	0.3 mm
# Slices	28	16	28	16	28
Slice Orientation	sagittal	coronal	sagital	coronal	sagital
# Echoes	1	1	1	1	1
TR	788 ms	2600 ms	2600 ms	1234 ms	1780
TE	7.5 ms	32 ms	32 ms	24 ms	24 ms
Echo Spacing	7.5 ms	8.0 ms	8.0 ms	8.0 ms	8.0 ms
RARE Factor	2	8	8	8	8
# Averages	4	4	4	4	4
# Dummy Scans	3	1	1	1	1
Fat Suppression	yes	yes	yes	no	no
Fat Water Separation	no	no	no	yes	yes
In-plane Resolution	156x156 um	324x324 um	156x156 um	188x188 um	125x125 um
Matrix Size	256x256	256x256	256x256	320x320	320x320
Exc Pulse Flip Angle	90 degrees	90 degrees	90 degrees	90 degrees	90 degrees
Ref Pulse Flip Angle	180 degrees	180 degrees	180 degrees	180 degrees	180 degrees
Total Acquisition Time	06 minutes 43 seconds	05 minutes 32 seconds	05 minutes 32 seconds	6 minutes 34 seconds	8 minutes 22 seconds

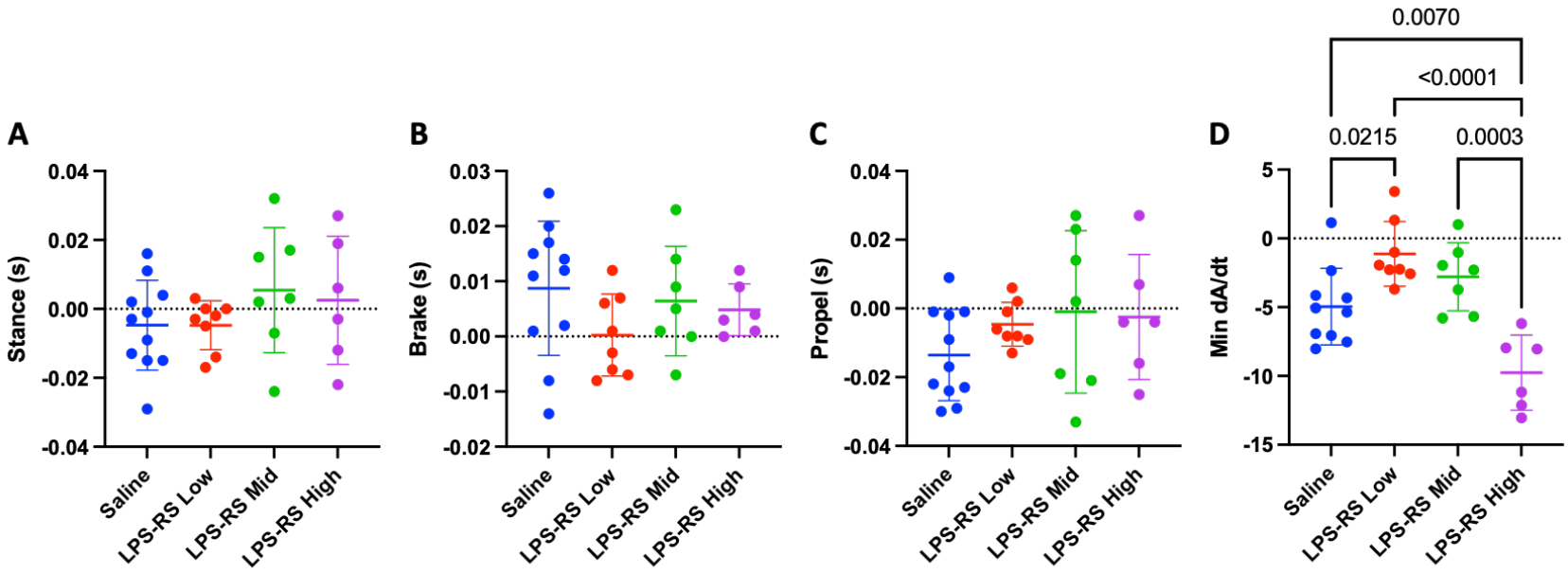

Supplemental Figure 3.1: Digigait controlled treadmill walking at 30cm/s at a 0-degree inclined/declined (flat). Parameters of interest have differences shown between groups after subtracting from baseline for stance (s) **(A)**, brake (s) **(B)**, propel (s) **(C)**, and Min dA/dt **(D)**. Sterile Saline treated animals are labeled in blue, with the published LPS-RS dose from the manuscript labeled as “low” (1ug LPS-RS 3x week) and coded in red. LPS-RS animals receiving a “mid” (1ug LPS-RS daily) dose are found in green and LPS-RS animals receiving a “high” (10ug LPS-RS 3x week) dose are in purple. Significant differences noted, with p-values shown <0.1

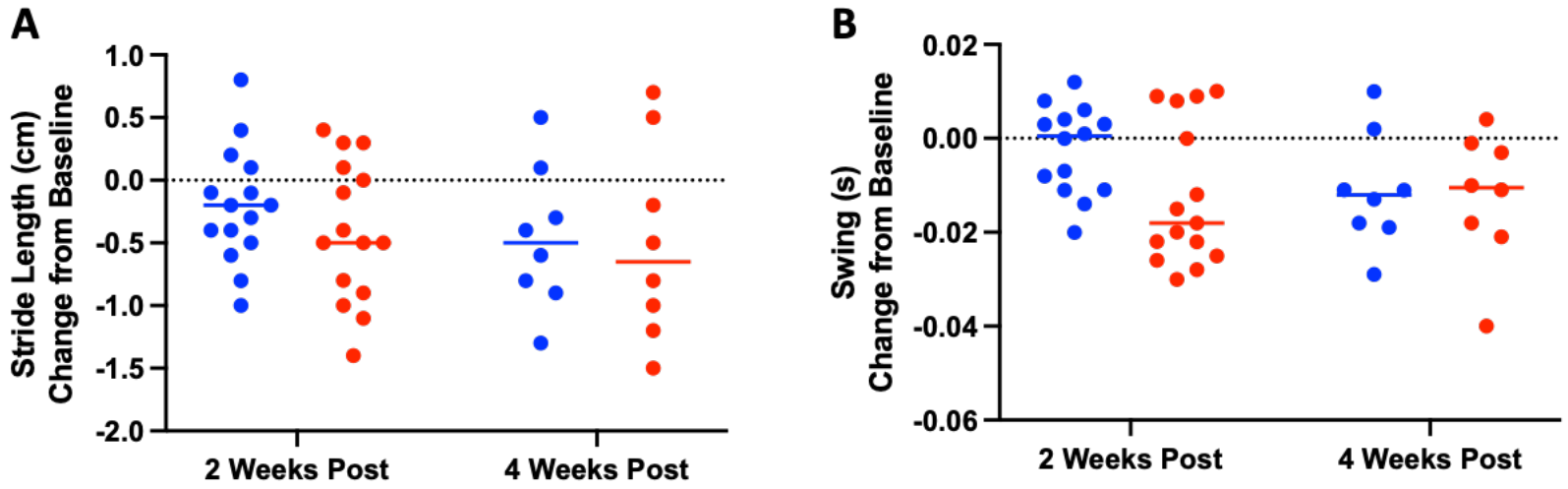

Supplemental Figure 3.2: Digigait controlled treadmill walking at 30cm/s at a 0-degree inclined/declined (flat). Parameters of interest have differences shown between groups after subtracting from baseline for Stride Length (cm) **(A)**, and swing (s) **(B)**. Sterile Saline treated animals are labeled in blue with LPS-RS treated animals labeled in red. Significant differences noted, with p-values shown <0.1.

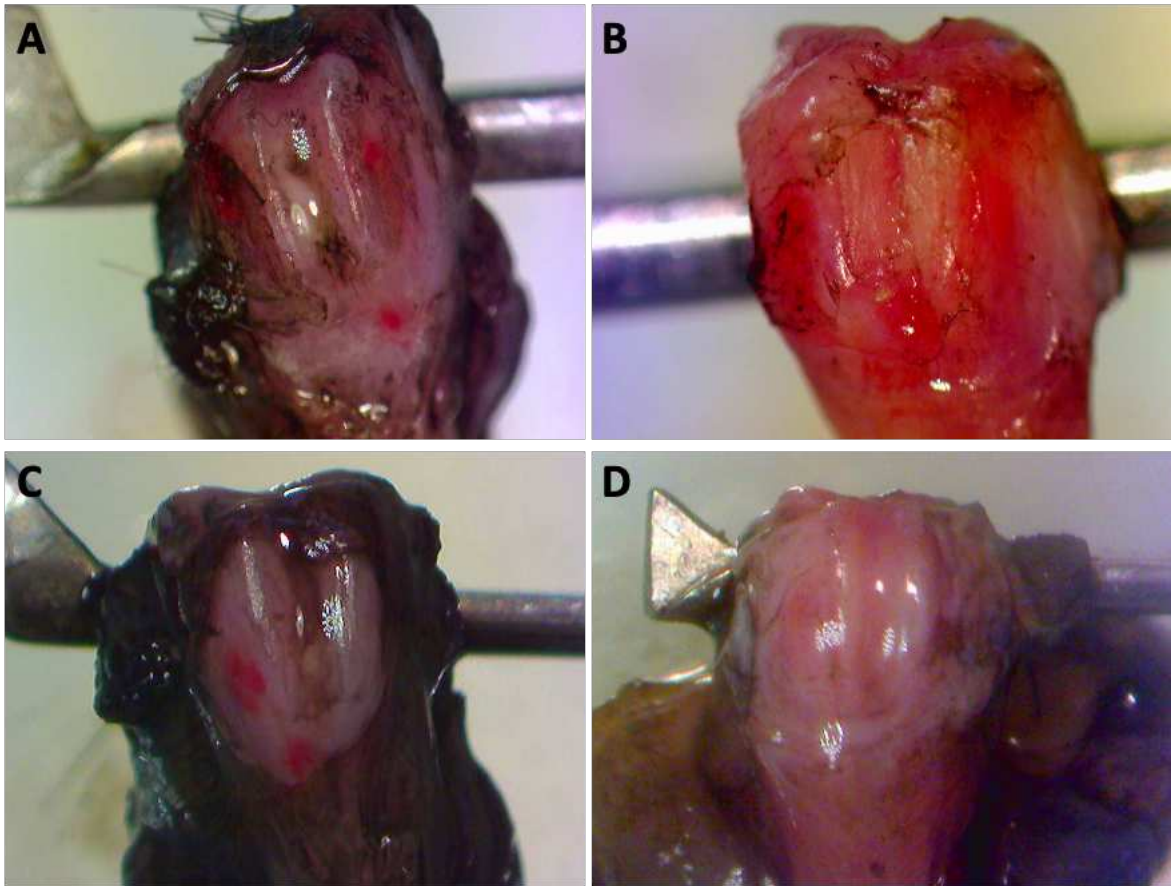

Supplemental Figure 3.3: Macroscopic imaging of femoral joint pathology stained with India ink from sterile saline injected animals (left) and TLR4 antagonist injected animals (right). Images of femoral condyles for visualization of damage to the patellofemoral groove. Representative image of animals two-weeks post-injury (top) treated with sterile saline **(A)** or LPS-RS **(B)**. Animals four-weeks post-injury (bottom) treated with sterile saline **(C)** or LPS-RS **(D)**.

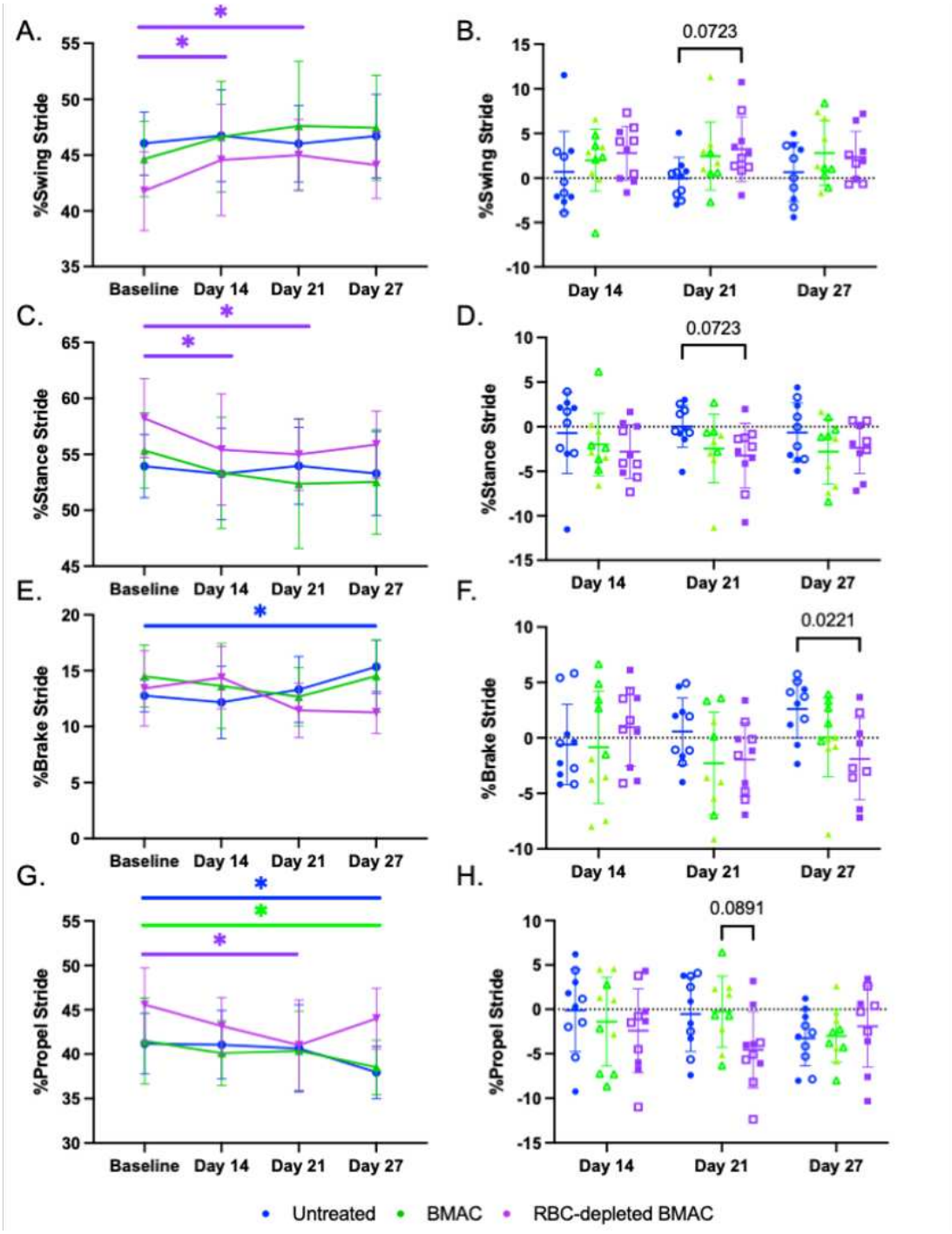

Supplemental Figure 4.1: Digigait controlled treadmill walking at 35cm/s on a flat horizontal surface. Parameters of interest are shown both overtime and between groups for %swing stride **(A, B)**, %stance stride **(C, D)**, %brake stride **(E, F)**, and %propel stride **(G, H)**. Filled in symbols indicate male animals and open symbols indicate female animals. Significant differences noted, with p value noted <0.1 and significant differences over time labeled (*p<0.05).

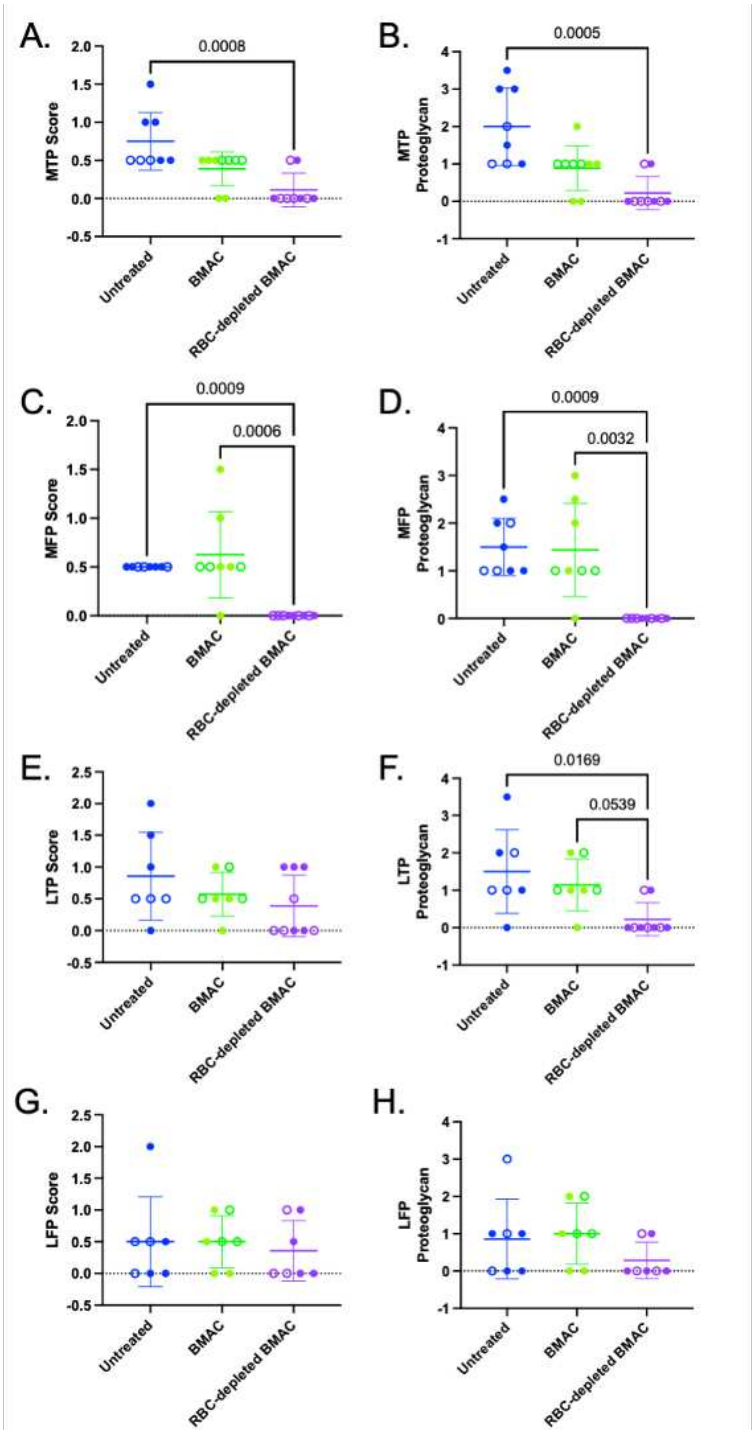

Supplemental Figure 4.2: OARSI histopathology scores following DMM surgery and treatment with untreated control (blue), BMAC (green), or RBC-depleted BMAC (purple). Medial Tibial Plateau (MTP), Medial Femoral Condyle (MFC), Lateral Tibial Plateau (LTP), Lateral Femoral Condyle (LFC). Filled in symbols indicate male animals and open symbols indicate female animals.

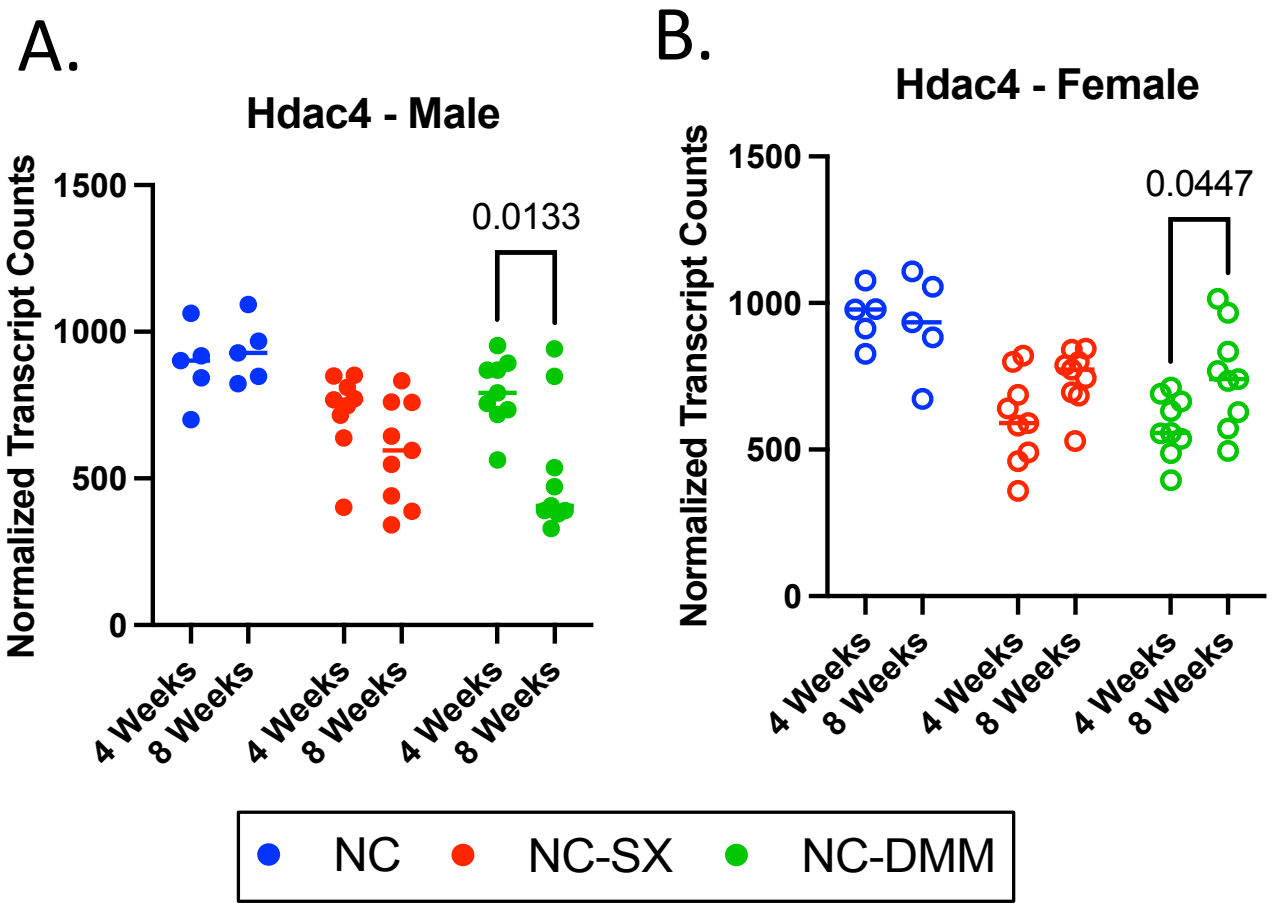

Supplemental Figure 5.1: Normalized gene expression data of Histone deacetylase 4 (Hdac4) stratified by timepoint and treatment group for male **(A)** and female **(B)** animals. Significance differences noted, with p values shown <0.1. NC - Naïve-compensatory (Blue); NC-SX - Naïve-compensatory Sham Surgery (Red); NC-DMM - Naïve-compensatory DMM Surgery (Green).